VRIJE UNIVERSITEIT

Experimental and Theoretical Studies in Optical Coherence Theory

ACADEMISCH PROEFSCHRIFT

ter verkrijging van de graad Doctor aan
de Vrije Universiteit Amsterdam,
op gezag van de rector magnificus
prof.dr. L.M. Bouter,
in het openbaar te verdedigen
ten overstaan van de promotiecommissie
van de faculteit der Exacte Wetenschappen
op maandag 4 april 2011 om 13.45 uur
in de aula van de universiteit,
De Boelelaan 1105

door

Thomas van Dijk

geboren te Enkhuizen

promotoren: prof.dr. T.D. Visser
prof.dr. W.M.G. Ubachs

Voor Laura

Netherlands Organisation for Scientific Research

This work was financially supported by a toptalent scholarship of NWO
'Nederlandse Organisatie voor Wetenschappelijk Onderzoek'

Contents

Chapter 1

Introduction

1.1 Historical introduction

Throughout history, people have been fascinated by the nature of light. A prime illustration is the use of mirrors. The first known man-made mirror, found in modern-day Turkey, dates from around 6200 BC. In the next three thousand years, Egyptians and Sumerians created metal mirrors, first from copper, then bronze, gold, and silver [Anderson, 2007]. The most famous account on their use in antiquity deals with Archimedes, who allegedly set up huge mirrors to set fire to the Roman fleet in the harbor of his native city Syracuse in 215–212 BC. However, it is now widely accepted that this is a myth. It was not until the sixth century AD that Anthemius described a specific arrangement of mirrors answering to Archimedes' purpose. He gave a quantitative description of the geometry of burning-mirrors which is based on the work of Diocles from the close of the third century BC [Knorr, 1983]. Greek philosophers discussed several theories on the nature of light. Euclid's written account on the laws of reflection (ca. 300 BC) is a prominent example.

Apart from mirrors, the use of lenses was also widespread in antiquity. Romans knew about the concept of magnification; for example Seneca mentions the use of a glass sphere filled with water to aid in reading fine writing [Sines and Sakellarakis, 1987]. Lenses made out of quartz and glass, dating as far back as 1400 BC, have been found in the Palace of Knossos.

The mentioned quantitative descriptions of reflection and the focusing of light by mirrors and lenses all use a geometric picture of light, i.e., light is assumed to consist of rays. This did not change until Huyghens proposed a different explanation for refraction and reflection of light, by assuming that light behaves as a wave. During his investigations, he explained the double refraction properties of calcite and, subsequently discovered polarization [Huyghens, 1690]. It is widely believed that such a calcite crystal was in fact the Sun stone mentioned in medieval sagas of the Vikings (ca. 700), which they allegedly used to navigate over the clouded

Atlantic ocean. This belief should however be taken with caution [Roslund and Beckman, 1994].

With Newton as a great champion of the corpuscular nature of light, the development of the wave theory was stifled for a long time. It was not until the beginning of the nineteenth century that Thomas Young took the first step that led to the acceptance of the wave character of light. He extended the existing theory by adding a new concept, the so-called principle of interference [Young, 1802, 1807]. He was thus able to explain the colored fringes of thin films, which were first described by Hooke [1665] and independently by Boyle [1738]. The combination of the principle of interference together with Huyghens principle enabled Fresnel to account for diffraction patterns arising from various obstacles and apertures [Fresnel, 1870]. Poisson however, objected that the theory predicted a bright spot in the center of the shadow of a circular disk. Challenged by this objection, Fresnel prompted Arago to perform the experiment and he indeed observed what is nowadays called the Poisson or Arago spot. Since the bright spot occurs in the geometrical shadow, only a wave theory can account for it. Fresnel also showed that light consists of two orthogonal vibrations, transverse to the direction of propagation. As a result almost the entire scientific community became convinced of the wave nature of light.

In the meantime research in electricity and magnetism was undertaken almost independently from optics. This effort culminated in the work of James Clerk Maxwell who was able to account for all the empirical knowledge on the subject by postulating a simple set of equations [Maxwell, 1873]. He established that light waves can be considered as electromagnetic waves propagating with a finite velocity. Maxwell's equations, together with the constitutive relations which describe the reaction of matter to electric and magnetic fields, form a proper physics-based model to describe all the phenomena connected with the propagation, diffraction and scattering of light.

With the constitutive relations in place, Maxwell's equations can be decoupled to give wave equations for both the magnetic and electric fields. These can be reduced to a set of Helmholtz equations if the fields are time-harmonic, i.e., the oscillate at a single frequency ω. The Helmholtz equations define a local relationship between the field at a given point and the source terms. The method of Green functions, which satisfy the relevant boundary conditions, can then be used to calculate the fields generated by the sources for every point in space.

Monochromatic wave fields are idealizations. They do not exist in nature. Every optical field has some randomness associated with it. These fluctuations can be small, as in the output of a well-stabilized laser, or large, as in the output of a thermal source. Statistical optics, or coherence theory, is the branch of physical optics that deals with the properties of these kinds of nondeterministic optical fields. Random fields can be characterized by correlation functions. Like the field itself, the correlation functions too obey a set of precise propagation laws [Wolf, 1954, 1955].

Recently is has become clear that polarization and coherence are both manifestations of field correlations. Whereas (scalar) coherence theory considers correlations of the field at two points, polarization is concerned with the correlation of two field components at a single point. This insight has lead to the recently formulated *unified theory of coherence and polarization of light* [Wolf, 2003b]. Both these two topics, coherence and polarization, are studied in this thesis.

After more than 300 years of study devoted to the wave nature of light, it was discovered in the mid-1970s that light fields have a fine structure smaller than the wavelength. This has lead to a new branch of optics, called singular optics [Nye and Berry, 1974; Nye, 1999]. It is concerned with the presence of singularities in a wavefield, as well as with the topology of the wavefield around the singular structures. For complex scalar fields the phase is singular at points were the field vanishes. In general, these zero-amplitude points lie on a line in space. The phase swirls around the line, creating a vortex structure. Such singularities can also occur in correlation functions, these so-called coherence vortices are discussed in later Chapters.

In the remainder of this introduction we describe the formalism that is used in this thesis. It consists of a brief summary of the mathematics of random processes, which we then apply to optical fields. We analyze Thomas Young's famous experiment [Young, 1802, 1807] within the context of coherence theory. We then study the role of correlation functions in the propagation of light. Next we broaden our scope to describe polarization. The state of polarization can be characterized by four numbers, the Stokes parameters [Stokes, 1852]. This representation is only valid if the field is confined to a two-dimensional plane, i.e., when the field is beam-like. In a more general setting, when the propagation direction is variable, the treatment is more involved [Hannay, 1998]. Here we restrict ourselves to the study of electromagnetic beams. After that some basic concepts in singular optics are introduced. The occurence of singular features in wave fields, polarization fields and coherence functions is discussed.

1.2 Elementary concepts

Before we turn our attention to coherence theory, i.e., a statistical description of optics, we briefly review the properties of random processes. Consider a random process $x(t)$, with t denoting the time. Every measurements of $x(t)$ will yield a different outcome, say: ${}^{(1)}x(t)$, ${}^{(2)}x(t)$, ${}^{(3)}x(t), \cdots$. The collection of all possible outcomes, or *realizations*, is known as the *ensemble* of $x(t)$. One can then define the ensemble average, or the expectation value, of a set of N realizations as,

$$\langle x(t) \rangle_{\mathrm{e}} = \lim_{N \to \infty} \frac{1}{N} \sum_{r=1}^{N} {}^{(r)}x(t), \tag{1.1}$$

where the angular brackets with the subscript e denotes the ensemble average. Equivalently, one may define the expectation of $x(t)$ by using the probability density $p_1(x, t)$. The quantity $p_1(x, t)\mathrm{d}x$ represents the probability that $x(t)$ will take on a value in the range $(x, x + \mathrm{d}x)$ at time t. The ensemble average is then given by the expression

$$\langle x(t)\rangle_{\mathrm{e}} = \int x p_1(x,t)\,\mathrm{d}x, \tag{1.2}$$

where the integration extends over all possible values of x. A random process is not fully described by the probability density $p_1(x,t)$. One also has to consider possible correlations between $x(t_1)$ and $x(t_2)$. Such correlations are characterized by the *joint probability density* $p_2(x_1, x_2, t_1, t_2)$. Clearly, the quantity $p_2(x_1, x_2, t_1, t_2)\mathrm{d}x_1\mathrm{d}x_2$ represents the probability that the variable x will take on a value in the range $x_1, x_1 + \mathrm{d}x_1$ at time t_1, and a value in the range $x_2, x_2 + \mathrm{d}x_2$ at time t_2. In a similar way one can define higher-order correlations that describe joint probabilities at three or more points in time, i.e., one can define an infinite number of probability densities

$$p_1(x,t),\ p_2(x_1,x_2,t_1,t_2),\ p_3(x_1,x_2,x_3,t_1,t_2,t_3),\ldots \tag{1.3}$$

The foregoing treatment is also applicable to a complex random process of t, say $z(t) = x(t) + \mathrm{i}y(t)$. The statistical properties of a complex process $z(t)$ are characterized by the sequence

$$p_1(z,t),\ p_2(z_1,z_2,t_1,t_2),\ p_3(z_1,z_2,z_3,t_1,t_2,t_3),\ldots \tag{1.4}$$

Where $p_1(z,t)\mathrm{d}^2z$ represents the probability that $z(t)$ will take on a value within the element $(x, x+\mathrm{d}x;\ y, y+\mathrm{d}y)$ at time t. Higher-order probability densities have similar meanings as explained in the case for real random processes. The average can be generalized to

$$\langle z(t)\rangle_{\mathrm{e}} = \int z p_1(z,t)\,\mathrm{d}^2 z, \tag{1.5}$$

where the integration extends over all possible values of z. The joint probability, p_2 allows us to define the ensemble average of the product $z(t_1)z(t_2)$, which is called the *autocorrelation function* $\Gamma(t_1, t_2)$

$$\Gamma(t_1,t_2) = \langle z^*(t_1)z(t_2)\rangle_{\mathrm{e}} = \iint z_1^* z_2 p_2(z_1,z_2,t_1,t_2)\,\mathrm{d}^2z_1\mathrm{d}^2z_2, \tag{1.6}$$

where the asterisks denotes the complex conjugate.

The statistical behavior of a random process often does not change with time. Such a process is called *statistically stationary.* Mathematically this means that the probability densities p_1, p_2, $p_3, \ldots$ are time-shift invariant,
i.e., $\langle z^*(t_1)z(t_2)\rangle_{\mathrm{e}} = \langle z^*(t_1+T)z(t_2+T)\rangle_{\mathrm{e}}$, for any value of T. Processes of which the statistics is only time-shift invariant up to second order are called *wide-sense stationary.* It is easy to show that the mean $\langle z(t)\rangle_{\mathrm{e}}$ is then independent of t and that the autocorrelation is a function only of the time difference $\tau = t_2 - t_1$, that is

$$\Gamma(\tau) = \langle z^*(t)z(t+\tau)\rangle_{\mathrm{e}}. \tag{1.7}$$

If the process is also *ergodic*, the ensemble average can be replaced by a time average [MANDEL AND WOLF, 1995]. From now on we will assume that all ensembles are both wide-sense stationary and ergodic. Consequently, the subscript e on the angular brackets can be omitted.

An important property of a stationary random process is its *spectral density* $S(\omega)$. This attribute provides a measure of the strength of the fluctuations for every specific Fourier component of $z(t)$. The Wiener-Khintchine-Einstein theorem [WIENER, 1930; KHINTCHINE, 1934; EINSTEIN, 1914] states that the autocorrelation function $\Gamma(\tau)$ forms a Fourier-transform pair with the spectral density $S(\omega)$ of that process, i.e.,

$$S(\omega) = \frac{1}{2\pi} \int_{-\infty}^{\infty} \Gamma(\tau) e^{\mathrm{i}\omega\tau}\, \mathrm{d}\tau. \tag{1.8}$$

This theorem can be generalized from a single random process $z(t)$ to a pair of random processes $z_1(t)$ and $z_2(t)$ which are jointly stationary, at least in the wide sense. That is, the cross-correlation between the two processes only depends on the time difference $\tau = t_2 - t_1$, i.e. $\Gamma_{12}(\tau) = \langle z_1^*(t) z_2(t+\tau)\rangle$. According to the generalized Wiener-Khintchine-Einstein theorem, the cross-spectral density $W_{12}(\omega)$ for the pair of processes is given by the formula

$$W_{12}(\omega) = \frac{1}{2\pi} \int_{-\infty}^{\infty} \Gamma_{12}(\tau) e^{\mathrm{i}\omega\tau}\, \mathrm{d}\tau. \tag{1.9}$$

1.3 Coherence theory

In optics the random processes $z_1(t)$ and $z_2(t)$ are typically optical fields. Let $V(\mathbf{r}, t)$ be a member of an ensemble $\{V(\mathbf{r}, t)\}$ representing a component of the fluctuating electric field, where $\mathbf{r}$ is the position vector of a point in space. Because the analytic signal representation is used, the field is complex-valued [MANDEL AND WOLF, 1995]. The cross-correlation function of the field is known as the *mutual coherence function*, which is defined as [MANDEL AND WOLF, 1995]

$$\Gamma(\mathbf{r}_1, \mathbf{r}_2, \tau) = \langle V^*(\mathbf{r}_1, t) V(\mathbf{r}_2, t+\tau)\rangle. \tag{1.10}$$

It is convenient to normalize the mutual coherence function by defining the *complex degree of coherence* as [ZERNIKE, 1938]

$$\gamma(\mathbf{r}_1, \mathbf{r}_2, \tau) = \frac{\Gamma(\mathbf{r}_1, \mathbf{r}_2, \tau)}{\sqrt{I(\mathbf{r}_1) I(\mathbf{r}_2)}}, \tag{1.11}$$

where

$$I(\mathbf{r}) = \Gamma(\mathbf{r}, \mathbf{r}, 0) \tag{1.12}$$

is the averaged intensity at position $\mathbf{r}$. The complex degree of coherence $\gamma(\mathbf{r}_1, \mathbf{r}_2, \tau)$ is a precise measure of the statistical similarity of the light vibrations at the positions $\mathbf{r}_1$ and $\mathbf{r}_2$ and can be shown to have a magnitude between zero and one.

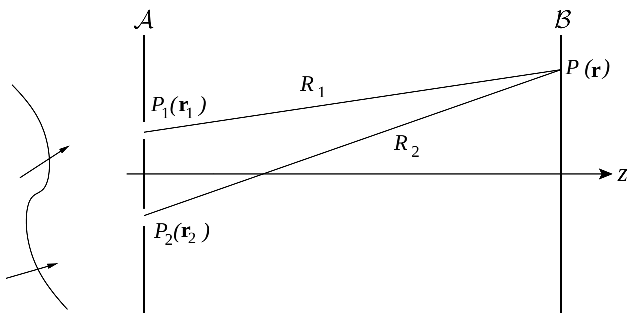

Figure 1.1: Young's interference experiment.

The extreme value one represents complete similarity of the light vibrations, i.e., the fields vibrate in unison. The other extreme value of zero represents the complete lack of correlation of the vibrations. The meaning of the complex degree of coherence can be elucidated by considering Young's double-slit experiment, illustrated in Fig. 1.1. The setup consists of an opaque screen $\mathcal{A}$, with two identical pinholes located at positions $\mathbf{r}_1$ and $\mathbf{r}_2$ which are illuminated by quasi monochromatic light. The ensuing interference pattern is observed on a second screen $\mathcal{B}$. Let $V(\mathbf{r}_1, t)$ and $V(\mathbf{r}_2, t)$ represent the light vibrations at the pinholes at time t and let R_1 and R_2 be the distance from the pinholes to the point of observation $P(\mathbf{r})$, $R_i = |\mathbf{r}_i - \mathbf{r}|$ with $i = 1, 2$. It can be shown that the averaged intensity at the observation point $P(\mathbf{r})$ equals

$$I(\mathbf{r}) = I^{(1)}(\mathbf{r}) + I^{(2)}(\mathbf{r}) + 2\mathrm{Re}\left\{\sqrt{I^{(1)}(\mathbf{r})}\sqrt{I^{(2)}(\mathbf{r})}\gamma\left[\mathbf{r}_1, \mathbf{r}_2, (R_2 - R_1)/c\right]\right\}, \quad (1.13)$$

where $I^{(1)}(\mathbf{r})$ is the averaged intensity at the point of observation when only the pinhole at position $\mathbf{r}_1$ is open. Similarly, if only the pinhole at $\mathbf{r}_2$ is open, the intensity at $\mathbf{r}$ equals $I^{(2)}(\mathbf{r})$. Looking at Eq. (1.13) we see that the average intensity at the observation point is not simply the sum of the two averaged intensities of the light from the two pinholes. It differs from it by a term dependent on the complex degree of coherence. If $\mathrm{Re}[\gamma(\mathbf{r}_1, \mathbf{r}_2, \tau)] \neq 0$ the light emanating from the pinholes will interfere. A measure of the quality of the pattern, or contrast of the fringes is provided by the so-called *visibility* $\mathcal{V}(\mathbf{r})$, defined as

$$\mathcal{V}(\mathbf{r}) \equiv \frac{I_{\max}(\mathbf{r}) - I_{\min}(\mathbf{r})}{I_{\max}(\mathbf{r}) + I_{\min}(\mathbf{r})}, \quad (1.14)$$

where $I_{\max}$ and $I_{\min}$ are the maximum and the minimum values of the averaged intensity in the immediate neighborhood of $\mathbf{r}$. For the case that the intensity of the light at the two pinholes is equal, it is readily shown that

$$\mathcal{V}(\mathbf{r}) = |\gamma(\mathbf{r}_1, \mathbf{r}_2, \tau)|. \quad (1.15)$$

When $|\gamma(\mathbf{r}_1, \mathbf{r}_2, \tau)| = 1$ the light at the two pinholes is called fully coherent, resulting in a fringe pattern with maximal (i.e. unity) sharpness. When $|\gamma(\mathbf{r}_1, \mathbf{r}_2, \tau)| = 0$ the field at the two positions in completely incoherent and there will be no visible interference pattern. For intermediate values of $|\gamma(\mathbf{r}_1, \mathbf{r}_2, \tau)|$ the light is called partially coherent. Hence we conclude that the degree of statistical similarity of the light at the two pinholes is directly related to the, easily measurable, visibility of the interference pattern.

For many applications it is more convenient to work in the space-frequency domain. To do so we formally represent $V(\mathbf{r}, t)$ as a Fourier integral

$$V(\mathbf{r}, t) = \int_0^\infty \widetilde{V}(\mathbf{r}, \omega) e^{-\mathrm{i}\omega t}\, \mathrm{d}\omega. \tag{1.16}$$

This is more complicated than it might seem because $V(\mathbf{r}, t)$ is a random function and does not tend zero as $t \to \pm\infty$. The *cross-spectral density* function of the light fluctuations at two points $\mathbf{r}_1$ and $\mathbf{r}_2$ is then heuristically described by

$$\langle \widetilde{V}^*(\mathbf{r}_1, \omega) \widetilde{V}(\mathbf{r}_2, \omega') \rangle = W(\mathbf{r}_1, \mathbf{r}_2, \omega) \delta(\omega - \omega'). \tag{1.17}$$

According to the generalized Wiener-Khintchine-Einstein theorem Eq. (1.9), the mutual coherence function and the cross-spectral density function form a Fourier transform pair. It is possible to consider the cross-spectral density function to be the ensemble average of a collection of strictly monochromatic wave functions $\{U(\mathbf{r}, \omega) e^{-\mathrm{i}\omega t}\}$, i.e. $W(\mathbf{r}_1, \mathbf{r}_2, \omega) = \langle U^*(\mathbf{r}_1, \omega) U(\mathbf{r}_2, \omega) \rangle$. It is emphasized that the ensemble of temporal fields $\{V(\mathbf{r}, t)\}$ and the collection of frequency-domain fields are not related by a Fourier transform. A normalized version of $W(\mathbf{r}_1, \mathbf{r}_2, \omega)$, *the spectral degree of coherence*, is given by the expression

$$\mu(\mathbf{r}_1, \mathbf{r}_2, \omega) = \frac{W(\mathbf{r}_1, \mathbf{r}_2, \omega)}{\sqrt{S(\mathbf{r}_1, \omega) S(\mathbf{r}_2, \omega)}}, \tag{1.18}$$

where

$$S(\mathbf{r}, \omega) = W(\mathbf{r}, \mathbf{r}, \omega) \tag{1.19}$$

is the spectral density at position $\mathbf{r}$. It can be shown that the spectral degree of coherence is bounded in absolute value by zero and unity, i.e., [Mandel and Wolf, 1995]

$$0 \leq |\mu(\mathbf{r}_1, \mathbf{r}_2, \omega)| \leq 1. \tag{1.20}$$

Let us again consider Young's double slit experiment, but now in the space-frequency domain. This time the light does not have to be quasi-monochromatic, and instead of considering the averaged intensity in the observation plane we will consider the spectral density of the light. We may represent the field at the pinholes by ensembles of frequency-dependent realizations $\{U(\mathbf{r}_1, \omega)\}$ and $\{U(\mathbf{r}_2, \omega)\}$. The resulting spectral density in the plane of observation is

$$\begin{aligned} S(\mathbf{r}, \omega) &= S^{(1)}(\mathbf{r}, \omega) + S^{(2)}(\mathbf{r}, \omega) \\ &\quad + 2\sqrt{S^{(1)}(\mathbf{r}, \omega)}\sqrt{S^{(2)}(\mathbf{r}, \omega)} \mathrm{Re}\left[\mu(\mathbf{r}_1, \mathbf{r}_2, \omega) e^{-\mathrm{i}\omega(R_1 - R_2)/c}\right]. \end{aligned} \tag{1.21}$$

The first term, $S^{(1)}(\mathbf{r},\omega)$, is the spectral density of the light that reaches the point of observation when only the pinhole at $\mathbf{r}_1$ is open. Similarly the second term on the right-hand side of Eq. (1.21) represents the spectral density of the light that reaches the point of observation from the second pinhole at $\mathbf{r}_2$ alone. This so-called *spectral interference law* shows that in general the resulting spectral density is not just the sum of the spectral densities $S^{(1)}(\mathbf{r},\omega)$ and $S^{(2)}(\mathbf{r},\omega)$, but differs from it by a term that depend on the spectral degree of coherence $\mu(\mathbf{r}_1,\mathbf{r}_2,\omega)$ of the light at the two pinholes. That is, it depends on the statistical similarity of the vibrations at frequency ω. This is an example of *correlation-induced spectral changes* [Wolf and James, 1996]. Eq. (1.13) shows that the averaged intensity may be modulated when two quasi-monochromatic light beams are superimposed, the spectral interference law shows that the spectrum may change appreciably when two broad-band beams are superimposed.

1.4 Propagation of correlation functions

In free space each member $V(\mathbf{r},t)$ of the ensemble of wavefields satisfies the wave equation

$$\left(\nabla^2 - \frac{1}{c^2}\frac{\partial^2}{\partial t^2},\right) V(\mathbf{r},t) = 0 \tag{1.22}$$

where c is the speed of light in vacuum. From this it follows that the mutual coherence function in free space also satisfies the two wave equations, namely [Wolf, 1955]

$$\begin{aligned}\left(\nabla_1^2 - \frac{1}{c^2}\frac{\partial^2}{\partial \tau^2}\right)\Gamma(\mathbf{r}_1,\mathbf{r}_2,\tau) = 0,\\ \left(\nabla_2^2 - \frac{1}{c^2}\frac{\partial^2}{\partial \tau^2}\right)\Gamma(\mathbf{r}_1,\mathbf{r}_2,\tau) = 0,\end{aligned} \tag{1.23}$$

where ∇_1^2 and ∇_2^2 denote the Laplace operator acting on $\mathbf{r}_1$ and $\mathbf{r}_2$, respectively. We see that not only the field but also the mutual coherence function obeys precise propagation laws, that is, it has a wave-like character. From the Wiener-Khintchine-Einstein theorem it immediately follows that the cross-spectral density satisfies the two Helmholtz equations

$$\begin{aligned}\left(\nabla_1^2 + k^2\right) W(\mathbf{r}_1,\mathbf{r}_2,\omega) = 0,\\ \left(\nabla_2^2 + k^2\right) W(\mathbf{r}_1,\mathbf{r}_2,\omega) = 0,\end{aligned} \tag{1.24}$$

so this correlation function too behaves as a wave. As a consequence these correlation functions may in general change on propagation, even on propagation through free space. Hence all the properties of the wavefield, that is the degree of coherence or the spectrum of the field, that are derived from the correlation function may also chance. As an example, consider a planar secondary stochastic source located in the plane $z = 0$, that radiates into the half-space $z > 0$, as illustrated in Fig. 1.2. Such a source may be an opening in an opaque screen for example. The cross-spectral density function of the field at a pair of points in the source plane can be expressed in the form

$$W^{(0)}(\mathbf{r}_1', \mathbf{r}_2', \omega) = \langle U^{(*)}(x_1', y_1', 0, \omega) U(x_2', y_2', 0, \omega) \rangle, \tag{1.25}$$

where the superscript 0 indicates that we are dealing with properties of the field in the source plane. By applying the first *Rayleigh diffraction formula* [Mandel and Wolf, 1995] we obtain the cross-spectral density function of the light at any pairs of points $\mathbf{r}_1$ and $\mathbf{r}_2$ in terms of the cross-spectral density function in the plane $z = 0$, namely

$$\begin{aligned} W(\mathbf{r}_1, \mathbf{r}_2, \omega) &= \frac{1}{(2\pi)^2} \iint_{z=0} W^{(0)}(\mathbf{r}_1', \mathbf{r}_2', \omega) \left[\frac{\partial}{\partial z_1} \left(\frac{e^{-\mathrm{i}kR_1}}{R_1} \right) \right] \\ &\times \left[\frac{\partial}{\partial z_2} \left(\frac{e^{\mathrm{i}kR_2}}{R_2} \right) \right] \mathrm{d}^2 r_1' \mathrm{d}^2 r_2', \end{aligned} \tag{1.26}$$

where $R_1 = |\mathbf{r}_1 - \mathbf{r}_1'|$, $R_2 = |\mathbf{r}_2 - \mathbf{r}_2'|$ and $\partial/\partial z_1$, $\partial/\partial z_2$ indicate differentiation along the positive z-direction. For pairs of points that are many wavelengths away from the source plane Eq. (1.26) reduces to [Mandel and Wolf, 1995]

$$W(\mathbf{r}_1, \mathbf{r}_2, \omega) \approx \left(\frac{k}{2\pi} \right) \iint_{(z=0)} W^{(0)}(\mathbf{r}_1', \mathbf{r}_2', \omega) \frac{e^{\mathrm{i}k(R_2 - R_1)}}{R_1 R_2} \cos\theta_1 \cos\theta_2 \, \mathrm{d}^2 r_1' \mathrm{d}^2 r_2', \tag{1.27}$$

where θ_1 and θ_2 are the angles the lines R_1 and R_2 make with the positive z-axis (Fig. 1.2). According to Eq. (1.26) the cross-spectral density function generally changes on propagation, even through free space. As the cross-spectral density changes, the spectral density, given by Eq. (1.19) will also change, just like the coherence properties, that is to the ability of the light to produce interference fringes. This is the reason why an incoherent source like the Sun emits light that is able to produce interference fringes when observed on Earth [Verdet, 1865].

1.5 Electromagnetic beams

Thus far we have treated optical fields as scalar fields, i.e. we have ignored their polarization properties which arise from their vector nature. The concept of coherence can be generalized to describe stochastic electromagnetic beams. We assume that the beam propagates from the plane $z = 0$ into the half-space $z > 0$ close to the z-axis. If the beam width is larger than the wavelength of the optical field, it is justified to use the paraxial limit in which the z-components of the fields can be ignored [Carter, 1974]. As before we will assume that the fluctuation of the electric and the magnetic field vectors are characterized by ensembles which are

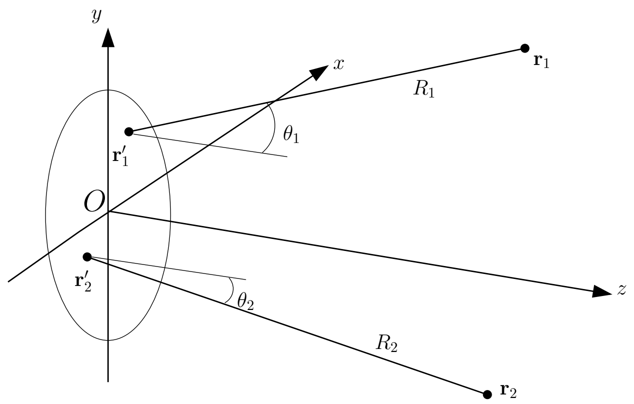

Figure 1.2: Illustrating the notation for propagation of the cross-spectral density from the source plane into the half space $z > 0$.

statistically stationary, at least in the wide sense. The coherence and the polarization properties of the beam, up to second order, can be described by the *electric cross-spectral density matrix*, which is given by the expression

$$\mathbf{W}(\mathbf{r}_1, \mathbf{r}_2, \omega) = \begin{pmatrix} W_{xx}(\mathbf{r}_1, \mathbf{r}_2, \omega) & W_{xy}(\mathbf{r}_1, \mathbf{r}_2, \omega) \\ W_{yx}(\mathbf{r}_1, \mathbf{r}_2, \omega) & W_{yy}(\mathbf{r}_1, \mathbf{r}_2, \omega) \end{pmatrix}, \tag{1.28}$$

where

$$W_{ij}(\mathbf{r}_1, \mathbf{r}_2, \omega) = \langle E_i^*(\mathbf{r}_1, \omega) E_j(\mathbf{r}_2, \omega)\rangle, \quad (i, y = x, y). \tag{1.29}$$

Here E_x and E_y are the components of the electric field of a typical member of the ensemble that represents the field. Analogous to the scalar case we examine the coherence properties of this beam by studying Young's double-slit experiment. Consider then a stochastic electromagnetic beam, propagating along the z-axis, which is incident on an opaque screen with the two pinholes located symmetrically around the z-axis (see Fig. 1.1). The spectral density $S(\mathbf{r}, \omega)$ of the field at a point $\mathbf{r}$ in the observation plane, i.e., the averaged electric density is defined as

$$S(\mathbf{r}, \omega) = \langle \mathbf{E}^*(\mathbf{r}, \omega) \cdot \mathbf{E}(\mathbf{r}, \omega)\rangle = \mathrm{Tr}\mathbf{W}(\mathbf{r}, \mathbf{r}, \omega), \tag{1.30}$$

where Tr denotes the trace. For the spectral density at a point in the observation plane an expression of the same form as the spectral interference law for scalar wavefields (Eq. 1.21) is found to read

$$\begin{aligned} S(\mathbf{r}, \omega) = {} & S^{(1)}(\mathbf{r}, \omega) + S^{(2)}(\mathbf{r}, \omega) + \\ & + 2\sqrt{S^{(1)}(\mathbf{r}, \omega)}\sqrt{S^{(2)}(\mathbf{r}, \omega)} \mathrm{Re}\left[\mu(\mathbf{r}_1, \mathbf{r}_2, \omega) e^{-\omega(R_1 - R_2)/c}\right]. \end{aligned} \tag{1.31}$$

The only difference with the scalar interference law is that the spectral degree of coherence $\mu(\mathbf{r}_1, \mathbf{r}_2, \omega)$ is now defined as

$$\mu(\mathbf{r}_1, \mathbf{r}_2, \omega) = \frac{\mathrm{Tr}\mathbf{W}(\mathbf{r}_1, \mathbf{r}_2, \omega)}{\sqrt{S(\mathbf{r}_1, \omega)}\sqrt{S(\mathbf{r}_2, \omega)}}. \tag{1.32}$$

The electric cross-spectral density matrix of a beam in the source plane (see Fig. 1.2) is defined as

$$\mathbf{W}^{(0)}(\boldsymbol{\rho}_1, \boldsymbol{\rho}_2, \omega) = \begin{pmatrix} W_{xx}^{(0)}(\boldsymbol{\rho}_1, \boldsymbol{\rho}_2, \omega) & W_{xy}^{(0)}(\boldsymbol{\rho}_1, \boldsymbol{\rho}_2, \omega) \\ W_{yx}^{(0)}(\boldsymbol{\rho}_1, \boldsymbol{\rho}_2, \omega) & W_{yy}^{(0)}(\boldsymbol{\rho}_1, \boldsymbol{\rho}_2, \omega) \end{pmatrix}, \tag{1.33}$$

where

$$W_{ij}^{(0)}(\boldsymbol{\rho}_1, \boldsymbol{\rho}_2, \omega) = \langle E_i^{*(0)}(\boldsymbol{\rho}_1, \omega) E_j^{(0)}(\boldsymbol{\rho}_2, \omega)\rangle, \quad (i, y = x, y). \tag{1.34}$$

Because the field is beam-like, we may use the paraxial approximation to describe its propagation. Consequently, the electric field components in any transverse plane $z > 0$ are given by the equation

$$E_i(\mathbf{r}, \omega) = \int_{z'=0} E_i^{(0)}(\boldsymbol{\rho}', 0, \omega) G(\boldsymbol{\rho} - \boldsymbol{\rho}', z, \omega)\, \mathrm{d}^2\rho', \quad i = x, y, \tag{1.35}$$

where G denotes the Green's function for paraxial propagation from the point $(\boldsymbol{\rho}', 0)$ in the source plane to the field point $(\boldsymbol{\rho}, z)$, viz.,

$$G(\boldsymbol{\rho} - \boldsymbol{\rho}', z, \omega) = -\frac{\mathrm{i}k}{2\pi z} \exp(\mathrm{i}kz) \exp\left[\mathrm{i}k|\boldsymbol{\rho} - \boldsymbol{\rho}'|^2/2z\right]. \tag{1.36}$$

On substituting from Eq. (1.35) into Eq. (1.29) it is found the that the electric cross-spectral density matrix of the beam at a pair of points in a transverse plane $z > 0$ is given by the formula [Wolf, 2003a]

$$\begin{aligned} \mathbf{W}(\mathbf{r}_1, \mathbf{r}_2, \omega) \quad &= \quad \iint_{(z=0)} \mathbf{W}^{(0)}(\boldsymbol{\rho}_1', \boldsymbol{\rho}_2', \omega) \\ &\quad \times K(\boldsymbol{\rho}_1 - \boldsymbol{\rho}_1', \boldsymbol{\rho}_2 - \boldsymbol{\rho}_2', z, \omega)\, \mathrm{d}^2\rho_1' \mathrm{d}^2\rho_2', \end{aligned} \tag{1.37}$$

where

$$K(\boldsymbol{\rho}_1 - \boldsymbol{\rho}_1', \boldsymbol{\rho}_2 - \boldsymbol{\rho}_2', z, \omega) = G^*(\boldsymbol{\rho}_1 - \boldsymbol{\rho}_1', z, \omega) G(\boldsymbol{\rho}_2 - \boldsymbol{\rho}_2', z, \omega). \tag{1.38}$$

Expression (1.37) shows that from knowledge of the cross-spectral density matrix across the plane $z = 0$, one can determine this matrix everywhere in the half-space $z > 0$. Just as in the scalar case, all the fundamental properties of the field such as the spectrum, spectral degree of coherence and as we shall see shortly, all polarization properties, can be determined from the (propagated) electric cross-spectral density matrix.

Whereas scalar coherence theory considers correlations of the field at two points, polarization is concerned with the correlation of two field components at a single point. A beam is said to be completely polarized if the the electric field components, E_x and E_y, are fully correlated. If they are completely uncorrelated the beam is unpolarized. In the completely polarized case the end point of the electric field vector moves on an ellipse with time, and the field is said to be elliptically polarized. The ellipse may be traversed in two possible senses. Looking into the direction from the source, we call the polarization right-handed if the electric vector traverses the ellipse in clockwise manner. In the opposite case we call the polarization left-handed. Two special degenerate cases of an ellipse are a circle and a straight line, in which case the light is circularly or linearly polarized, respectively.

The polarization properties of the beam at a point $\mathbf{r}$ can be deduced from the cross-spectral density matrix evaluated at identical points in space $\mathbf{r}_1 = \mathbf{r}_2 = \mathbf{r}$, i.e. from $\mathbf{W}(\mathbf{r}, \mathbf{r}, \omega)$. It is possible to decompose the beam into two parts, one which is completely polarized and the other completely unpolarized. The ratio of the intensity of the polarized part of the beam and its total intensity is called the *spectral degree of polarization* and is given by the formula

$$\mathcal{P}(\mathbf{r}, \omega) = \sqrt{1 - \frac{4\,\mathrm{Det}\mathbf{W}(\mathbf{r}, \mathbf{r}, \omega)}{[\mathrm{Tr}\mathbf{W}(\mathbf{r}, \mathbf{r}, \omega)]^2}}, \tag{1.39}$$

where Det denotes the determinant. It can be shown that the spectral degree of polarization is a non-negative number bounded by zero and unity, i.e. $0 \leq \mathcal{P}(\mathbf{r}, \omega) \leq 1$. If the light is completely polarized $\mathcal{P}$ equals unity. The light is said to be unpolarized when $\mathcal{P} = 0$. For intermediate values the light is said to be partially polarized. It is to be noted that the decomposition of a beam in a polarized and an unpolarized part is a local operation. That is, although the field at a single point can be written as the sum of completely polarized and a unpolarized part, this does not hold true for the beam as a whole [Korotkova and Wolf, 2005]. The polarization properties of the beam consist of the degree of polarization of the beam and the state of polarization of its polarized part. To specify the latter it is convenient to use the spectral *Stokes parameters.* These can be expressed in terms of the elements of the cross-spectral density matrix, viz.,

$$\begin{aligned}
S_0(\mathbf{r}, \omega) &= W_{xx}(\mathbf{r}, \mathbf{r}, \omega) + W_{yy}(\mathbf{r}, \mathbf{r}, \omega), \\
S_1(\mathbf{r}, \omega) &= W_{xx}(\mathbf{r}, \mathbf{r}, \omega) - W_{yy}(\mathbf{r}, \mathbf{r}, \omega), \\
S_2(\mathbf{r}, \omega) &= W_{xy}(\mathbf{r}, \mathbf{r}, \omega) + W_{yx}(\mathbf{r}, \mathbf{r}, \omega), \\
S_3(\mathbf{r}, \omega) &= \mathrm{i}\left[W_{yx}(\mathbf{r}, \mathbf{r}, \omega) - W_{xy}(\mathbf{r}, \mathbf{r}, \omega)\right].
\end{aligned} \tag{1.40}$$

It is seen from Eq. (1.40) that, in general, the Stokes parameters depend on position, a fact that is not always recognized in the literature. The Stokes parameters are not independent but are related by the inequality

$$S_0^2(\mathbf{r}, \omega) \geq S_1^2(\mathbf{r}, \omega) + S_2^2(\mathbf{r}, \omega) + S_3^2(\mathbf{r}, \omega). \tag{1.41}$$

For a fully polarized beam the equality sign in Eq. (1.41) holds, whereas for a completely unpolarized beam $S_1(\mathbf{r},\omega) = S_2(\mathbf{r},\omega) = S_3(\mathbf{r},\omega) = 0$. Let us now decompose a given beam into an unpolarized and a polarized portion using the Stokes representation. If we denote the set of four Stokes parameters by $\mathbf{s}(\mathbf{r},\omega)$, then the required decomposition is [Born and Wolf, 1999]

$$\mathbf{s}(\mathbf{r},\omega) = \mathbf{s}^{(u)}(\mathbf{r},\omega) + \mathbf{s}^{(p)}(\mathbf{r},\omega), \tag{1.42}$$

where

$$\begin{aligned} \mathbf{s}^{(u)}(\mathbf{r},\omega) &= S_0(\mathbf{r},\omega) - \sqrt{S_1^2(\mathbf{r},\omega) + S_2^2(\mathbf{r},\omega) + S_3^2(\mathbf{r},\omega)}, 0, 0, 0, \\ \mathbf{s}^{(p)}(\mathbf{r},\omega) &= \sqrt{S_1^2(\mathbf{r},\omega) + S_2^2(\mathbf{r},\omega) + S_3^2(\mathbf{r},\omega)}, S_1(\mathbf{r},\omega), S_2(\mathbf{r},\omega), S_3(\mathbf{r},\omega). \end{aligned} \tag{1.43}$$

Here $\mathbf{s}^{(u)}(\mathbf{r},\omega)$ represents the unpolarized part and $\mathbf{s}^{(p)}(\mathbf{r},\omega)$ the polarized part of the beam. Hence, in terms of the spectral Stokes parameters, the degree of polarization reads

$$\mathcal{P}(\mathbf{r},\omega) = \frac{\sqrt{S_1^2(\mathbf{r},\omega) + S_2^2(\mathbf{r},\omega) + S_3^2(\mathbf{r},\omega)}}{S_0(\mathbf{r},\omega)}. \tag{1.44}$$

The state of polarization of the fully polarized part of the beam can be represented geometrically. We normalize the Stokes parameters of the fully polarized part of the beam by dividing them by the intensity of the polarized part, i.e., by $I_{\mathrm{pol}}(\mathbf{r},\omega) = [S_1^2(\mathbf{r},\omega) + S_2^2(\mathbf{r},\omega) + S_3^2(\mathbf{r},\omega)]^{1/2}$. These normalized Stokes parameters $s_1(\mathbf{r},\omega) = S_1(\mathbf{r},\omega)/I_{\mathrm{pol}}(\mathbf{r},\omega)$, $s_2(\mathbf{r},\omega) = S_2(\mathbf{r},\omega)/I_{\mathrm{pol}}(\mathbf{r},\omega)$ and $s_3(\mathbf{r},\omega) = S_3(\mathbf{r},\omega)/I_{\mathrm{pol}}(\mathbf{r},\omega)$ may be represented as a point on the *Poincaré sphere* (see Fig. 1.3). Every possible state of a fully polarized beam corresponds to a point on the Poincaré sphere. On the north pole $[s_1(\mathbf{r},\omega) = s_2(\mathbf{r},\omega) = 0, s_3(\mathbf{r},\omega) = 1]$ the polarization is right-handed circular. The polarization for all points on the northern hemisphere is right-handed, and left-handed for all points on the southern hemisphere. At the south pole the polarization is circular and left-handed. For points on the equator $[s_3(\mathbf{r},\omega) = 0]$, the polarization is linear. For all other points the polarization is elliptical.

From Eq. (1.37) it is seen that the cross-spectral density matrix generally changes on propagation, even if the beam propagates through free space. Since the cross-spectral density matrix changes, all the quantities that are determined by it, that is, the spectral density, the spectral degree of coherence, the spectral degree of polarization, and the Stokes parameters also change on propagation. Such changes of the polarization properties have been reported in several publications [James, 1994; Wolf, 2003a; Korotkova and Wolf, 2005; Korotkova et al., 2008].

The coherence properties of a beam are described only by the diagonal elements of the electric cross-spectral density matrix (1.28) whereas the state of polarization depends also on the off-diagonal elements. The fact that a beam is completely spatially coherent does not impose any conditions on the state of polarization. A field that is spatially fully coherent can be completely unpolarized at the same time [Ponomarenko and Wolf, 2003].

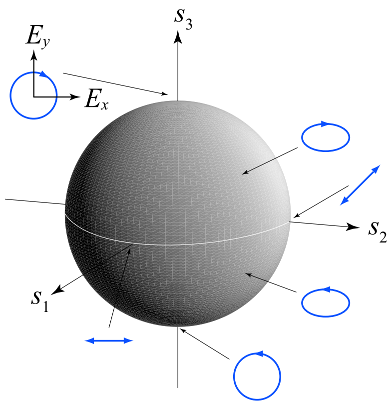

Figure 1.3: The Poincaré sphere with Cartesian axes (s_1, s_2, s_3).

1.6 Singular optics

Every monochromatic wavefield can be characterized by a phase and an amplitude. At points where the amplitude vanishes the phase is undefined or singular. Such a *phase singularity* can be observed in many physical systems. In optics it was shown that they occur in the energy flow of a convergent beam in the focal plane [Boivin et al., 1967] or at the edge of a perfectly reflecting half-plane screen [Braunbek and Laukien, 1952]. The systematic study of optical phase singularities initiated by Nye and Berry [1974] resulted in a new branch of optics called Singular Optics [Nye, 1999; Soskin and Vasnetsov, 2001]. We now briefly mention the main concepts of this sub-discipline.

Consider a complex scalar field $U(\mathbf{r})$ and write it as

$$U(\mathbf{r}) = A(\mathbf{r})e^{\mathrm{i}\phi(\mathbf{r})}. \tag{1.45}$$

A phase singularity arises at points where the field amplitude $A(\mathbf{r})$ is zero and hence the phase $\phi(\mathbf{r})$ is undefined, where

$$\mathrm{Re}[U(\mathbf{r})] = 0, \tag{1.46}$$
$$\mathrm{Im}[U(\mathbf{r})] = 0. \tag{1.47}$$

In three dimensions these two conditions generically have solutions in the form of lines. In a plane they will be isolated points. Around these points the phase of the field will typically have a vortex structure. Another topological feature of a field are its stationary points. Here the phase is well defined but the gradient of the field, $\nabla\phi(\mathbf{r})$ vanishes. These points correspond to a minimum, a maximum or a saddle point of the phase. The topological charge s of the singular and stationary points, is defined by the relation

$$s = \frac{1}{2\pi}\oint_C \nabla\phi(\mathbf{r}) \cdot \mathrm{d}\mathbf{r}, \tag{1.48}$$

where C is a closed path that encircles the feature once in a anticlockwise manner. Because the phase of the field at a fixed position is defined modulo 2π, s has an integer value, i.e., $s = 0, \pm 1, \pm 2, \ldots$. These vortices are referred to as positive or negative depending on the sign of the topological charge. In principle phase singularities can have a arbitrary topological charge. However most phase singularities with charges unequal to ± 1 are unstable with respect to pertubations and will decay in phase singularities with charges equal to ± 1. The charge of a given singularity is independent of the choice of the enclosing path C. The topological charge of a phase saddle, maximum or minimum is always zero.

It is also possible to define the topological charge of the phase singularities of the vector field $\nabla\phi(\mathbf{r})$, this quantity is called the *topological index* t [Nye et al., 1988]. It can be shown that both for a positive and a negative vortex $t = 1$, this also true for phase singularities with a larger topological charge. For a saddlepoint $t = -1$ and for a phase maximum or minimum $t = 1$.

Both the topological charge and index are conserved quantities of the field. Therefore they can not simply disappear under smooth variation of relevant system parameters [Nye and Berry, 1974]. The only way a phase singularity can disappear is if it annihilates with another phase singularity such that the total topological charge and index are conserved. Likewise, a phase singularity can only be created together with an other singularity such that the sum of their topological charge and index is zero. For example, the creation of a phase singularity with $s = 1$ and $t = 1$, a positive vortex, typically occurs with the creation of a negative vortex with $s = -1$ and $t = 1$ and two phase saddles each with $s = 0$, and $t = -1$.

In this section we have thus far regarded light as a scalar disturbance. To account for polarization consider again an electromagnetic beam. At every point in space the end point of the electric vector of a fully polarized beam traces out an ellipse over time. This polarization ellipse is characterized by three parameters describing its eccentricity, orientation and handedness. So-called C points, where the orientation of the ellipse is undefined hence the polarization is purely circular and L lines, where the polarization is linear and therefore the handedness is undefined are singulatities of this field. It can be shown that a perfect interference fringe in a polarized beam is unstable and will always split up in C and L lines [Nye and Berry, 1974; Visser and Schoonover, 2008]. So any phase singularity predicted in a scalar theory has a finer polarization structure associated with it.

Until now we have discussed phase singularities of fields that depend on one spatial coordinate. However the spectral degree of coherence, which is a function of two spatial variables $\mathbf{r}_1$ and $\mathbf{r}_2$, can also exhibit zeros. At pairs of points where the spectral degree of coherence vanishes, the phase is undefined and exhibits a singular behavior [Gbur and Visser, 2003b]. If this happens the field is said to have a *coherence singularity.* If the light at the two points $\mathbf{r}_1$ and $\mathbf{r}_2$ were to be combined in a Young double-slit experiment it would yield an interference pattern with no spatial modulation.

1.7 Outline of this thesis

The influence of the state of coherence on the focal intensity distribution of a converging partially coherent field is investigated in Chapter 2. The commonly held belief is that reducing the coherence length of a partially coherent beam will smear out the intensity distribution. It is shown however that, on changing the coherence length, far more drastic changes can be obtained. Specifically when a Bessel-correlated beam is focused it is shown that it is possible to continuously change from a maximum of intensity at focus to a minimum by altering the coherence length. The predicted coherence shaping of the intensity may be a promising novel technique for optical manipulation.

In Chapter 3 it is shown that on propagation of a partially coherent *vortex beam* a coherence singularity gradually develops. It is found that this coherence singularity in the far zone can unfold into a doublet of singularities.

In Chapter 4 the topology of coherence singularities in the far zone, of a broad class of partially coherent sources is analyzed. It is found that the coherence singularities form a two-dimensional surface. Specifically, for a partially coherent vortex beam, the geometry of its coherence singularities can be associated with different kinds of conic sections.

The subject of Chapter 5 is an experiment, where it is shown that polarization changes in a monochromatic light beam are accompanied by a phase change, a *Pancharatnam-Berry phase*. The origin of the phase is geometric (i.e. not dynamic) and it can have a linear, nonlinear or singular dependence on the orientation angle of polarization elements. A novel setup is presented together with experimental results that confirm these three types of behavior.

The Pancharatnam-Berry phase is also the subject of Chapter 6. It is known that for a cyclic change of the state of polarization of a monochromatic beam, the beam acquires a geometric phase. This Pancharatnam-Berry phase has a geometric interpretation that is connected to the Poincaré sphere. In this Chapter it is shown that such a geometric interpretation also exist for the *Pancharatnam connection*, i.e., the criterion according to which two beams with different states of polarization are said to be in phase.

The seventh Chapter gives a description of partially coherent light scattering on a homogeneous sphere, so-called *Mie-scattering*. In the usual description of Mie-scattering it is assumed that the incident field is spatially fully coherent. In practice, the field will often be partially coherent. In this Chapter the *partial waves expansion method* is generalized to this situation. The influence of the degree of coherence of the incident field on the scattered field is examined. It is found that the angular distribution of the scattered energy depends strongly on the coherence length.

Chapter 2

Shaping the focal intensity distribution using spatial coherence

This Chapter is based on the following publication:

- T. van Dijk, G. Gbur and T.D. Visser "Shaping the focal intensity distribution using spatial coherence",
  J. Opt. Soc. Am. A, vol. 25, pp. 575–581 (2008).

Abstract
The intensity and the state of coherence are examined in the focal region of a converging, partially coherent wave field. In particular, Bessel-correlated fields are studied in detail. It is found that it is possible to change the intensity distribution and even to produce a local minimum of intensity at the geometrical focus by altering the coherence length. It is also shown that, even though the original field is partially coherent, in the focal region there are pairs of points at which the field is fully correlated, and pairs of points at which the field is completely incoherent. The relevance of this work to applications such as optical trapping and beam shaping is discussed[1].

[1]The behavior predicted in this paper has recently been observed experimentally [Raghunathan et al., 2011].

2.1 Introduction

Although light encountered under many practical circumstances is partially coherent, the intensity near focus of such wavefields has been studied in relatively few cases [Lu et al., 1995; Wang et al., 1997; Friberg et al., 2001; Visser et al., 2002; Wang and Lu, 2006]. The correlation properties of focused partially coherent fields have been examined by Fischer and Visser [2004]; Rao and Pu [2007], where it was shown that the correlation function exhibits phase singularities. In a recent study [Gbur and Visser, 2003a] it was suggested that the state of coherence of a field may be used to tailor the shape of the intensity distribution in the focal region. More specifically, it was shown that a minimum of intensity may occur at the geometrical focus.

In the present paper we explore converging, Bessel-correlated fields in more detail. Three-dimensional plots of the intensity distribution, in which the transition from a maximum of intensity to a minimum of intensity at the focal point can be seen, are presented. Also, the state of coherence of the field near focus is examined. It is found that there exist pairs of points at which the field is fully coherent and pairs at which the field is completely uncorrelated.

2.2 Focusing of partially coherent light

Consider first a converging, monochromatic field of frequency ω that emanates from a circular aperture with radius a in a plane screen (see Fig. 2.1). The origin O of the coordinate system is taken at the geometrical focus. The field at a point $Q(\mathbf{r}')$ on the wavefront A which fills the aperture is denoted by $U^{(0)}(\mathbf{r}', \omega)$. The field at an observation point $P(\mathbf{r})$ in the focal region is, according to the Huygens-Fresnel principle and within the paraxial approximation, given by the expression [Born and Wolf, 1999, Chap. 8.8]

$$U(\mathbf{r}, \omega) = -\frac{\mathrm{i}}{\lambda} \int_A U^{(0)}(\mathbf{r}', \omega) \frac{e^{\mathrm{i}ks}}{s} \,\mathrm{d}^2 r', \tag{2.1}$$

where $s = |\mathbf{r} - \mathbf{r}'|$ denotes the distance QP, λ is the wavelength of the field, and we have suppressed a time-dependent factor $\exp(-\mathrm{i}\omega t)$.

For a partially coherent wave, instead of just the field, one also has to consider the *cross-spectral density function* of the field at two points $Q(\mathbf{r}'_1)$ and $Q(\mathbf{r}'_2)$, namely,

$$W^{(0)}(\mathbf{r}'_1, \mathbf{r}'_2, \omega) = \langle U^*(\mathbf{r}'_1, \omega) U(\mathbf{r}'_2, \omega) \rangle, \tag{2.2}$$

where the angular brackets denote an ensemble average, and the superscript "(0)" indicates fields in the aperture. This definition, and others related to coherence theory in the space-frequency domain, are discussed in Mandel and Wolf [1995, Chapters 4 and 5]. On substituting from Eq. (2.1) into Eq. (2.2) we obtain for the cross-spectral density function in the focal region the formula

$$W(\mathbf{r}_1, \mathbf{r}_2, \omega) = \frac{1}{\lambda^2} \iint_A W^{(0)}(\mathbf{r}_1', \mathbf{r}_2', \omega) \frac{e^{\mathrm{i}k(s_2 - s_1)}}{s_1 s_2} \, \mathrm{d}^2 r_1' \mathrm{d}^2 r_2'. \tag{2.3}$$

The distances s_1 and s_2 are given by the expressions

$$s_1 = |\mathbf{r}_1 - \mathbf{r}_1'|, \tag{2.4}$$

$$s_2 = |\mathbf{r}_2 - \mathbf{r}_2'|. \tag{2.5}$$

If the Fresnel-number of the focusing geometry is large compared to unity, i.e. if $N \equiv a^2/\lambda f \gg 1$, with f the radius of curvature of the field, then the distances s_1 and s_2 may be approximated by the expressions

$$s_1 \approx f - \mathbf{q}_1' \cdot \mathbf{r}_1, \tag{2.6}$$

$$s_2 \approx f - \mathbf{q}_2' \cdot \mathbf{r}_2, \tag{2.7}$$

where $\mathbf{q}_1'$ and $\mathbf{q}_2'$ are unit vectors in the directions $O\mathbf{r}_1'$ and $O\mathbf{r}_2'$, respectively. The factors s_1 and s_2 in the denominator of Eq. (2.3) may be approximated by f, hence we obtain the expression

$$W(\mathbf{r}_1, \mathbf{r}_2, \omega) = \frac{1}{(\lambda f)^2} \iint_A W^{(0)}(\mathbf{r}_1', \mathbf{r}_2', \omega) e^{\mathrm{i}k(\mathbf{q}_1' \cdot \mathbf{r}_1 - \mathbf{q}_2' \cdot \mathbf{r}_2)} \, \mathrm{d}^2 r_1' \mathrm{d}^2 r_2'. \tag{2.8}$$

The *spectral density* of the focused field at a point of observation $P(\mathbf{r})$ in the focal region is given by the 'diagonal elements' of the cross-spectral density function, i.e.

$$S(\mathbf{r}, \omega) = W(\mathbf{r}, \mathbf{r}, \omega). \tag{2.9}$$

From Eqs. (2.9) and (2.8) it follows that

$$S(\mathbf{r}, \omega) = \frac{1}{(\lambda f)^2} \iint_A W^{(0)}(\mathbf{r}_1', \mathbf{r}_2', \omega) e^{\mathrm{i}k(\mathbf{q}_1' - \mathbf{q}_2') \cdot \mathbf{r}} \, \mathrm{d}^2 r_1' \mathrm{d}^2 r_2'. \tag{2.10}$$

A normalized measure of the field correlations is given by the *spectral degree of coherence*, which is defined as

$$\mu(\mathbf{r}_1, \mathbf{r}_2, \omega) \equiv \frac{W(\mathbf{r}_1, \mathbf{r}_2, \omega)}{[S(\mathbf{r}_1, \omega) S(\mathbf{r}_2, \omega)]^{1/2}}. \tag{2.11}$$

It may be shown that $0 \leq |\mu(\mathbf{r}_1, \mathbf{r}_2, \omega)| \leq 1$. The upper bound represents complete coherence of the field fluctuations at $\mathbf{r}_1$ and $\mathbf{r}_2$, whereas the lower bound represents complete incoherence. For all intermediate values the field is said to be partially coherent.

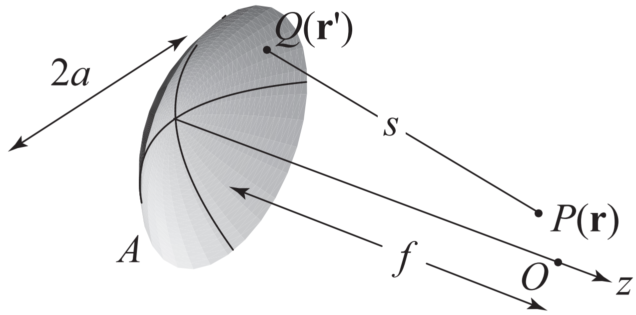

Figure 2.1: Illustrating the notation.

2.3 Gaussian Schell-model fields

We now briefly review the focusing of a *Gaussian Schell-model* field with a uniform spectral density. Such a field is characterized by a cross-spectral density function of the form

$$W^{(0)}(\boldsymbol{\rho}_1, \boldsymbol{\rho}_2, \omega) = S^{(0)}(\omega) e^{-(\boldsymbol{\rho}_2 - \boldsymbol{\rho}_1)^2/2\sigma_g^2}, \tag{2.12}$$

where $S^{(0)}(\omega)$ is the spectral density and σ_g a measure of the coherence length of the field in the aperture. Furthermore, $\boldsymbol{\rho} = (x, y)$ is the two-dimensional transverse vector that specifies the position of a point in the aperture plane. It was shown in Visser et al. [2002] that the maximum of intensity always occurs at the geometrical focus, irrespective of the value of σ_g. Furthermore, the spectral density distribution was found to be symmetric about the focal plane and about the axis of propagation. On decreasing σ_g, the maximum spectral density decreases, and the secondary maxima and minima gradually disappear. In the coherent limit (*i.e.*, $\sigma_g \to \infty$) the classical result [Linfoot and Wolf, 1956] is retrieved.

The coherence properties of a focused Gaussian Schell-model field were examined in [Fischer and Visser, 2004]. It was shown that the coherence length can be either larger or smaller than the width of the spectral density distribution. In addition, the spectral degree of coherence was found to possess *phase singularities*.

2.4 J_0-correlated fields

J_0-correlated fields with a constant spectral density are characterized by a cross-spectral density function of the form

$$W^{(0)}(\mathbf{r}_1', \mathbf{r}_2', \omega) = S^{(0)}(\omega) J_0(\beta|\mathbf{r}_2' - \mathbf{r}_1'|), \tag{2.13}$$

where J_0 denotes the Bessel function of the first kind of zeroth order. The correlation length is roughly given by β^{-1}. In [Gbur and Visser, 2003a] it was shown that the occurrence of a maximum of intensity at the geometrical focus is related to the positive definiteness of the cross-spectral density. Since the cross-spectral density function of Eq. (2.13) takes on negative values, another kind of behavior may now be possible. In this Section we analyze the effect of the state of coherence on the three-dimensional spectral density distribution near focus. The cross-spectral density of the focused field is, according to Eq. (2.8), given by

$$W(\mathbf{r}_1, \mathbf{r}_2, \omega) = \frac{1}{(\lambda f)^2} \iint_A S^{(0)}(\omega) J_0(\beta|\mathbf{r}_2' - \mathbf{r}_1'|) e^{\mathrm{i}k(\mathbf{q}_1' \cdot \mathbf{r}_1 - \mathbf{q}_2' \cdot \mathbf{r}_2)} \, \mathrm{d}^2 r_1' \mathrm{d}^2 r_2'. \quad (2.14)$$

We use scaled polar coordinates to write

$$\mathbf{r}_i' = (a\rho_i \cos\phi_i, a\rho_i \sin\phi_i, z_i) \quad (i = 1, 2). \quad (2.15)$$

The spectral density is normalized to its value at the geometrical focus for a spatially fully coherent wave, i.e.

$$S_{\mathrm{coh}} = \lim_{\beta \to 0} W(\mathbf{r}_1 = \mathbf{r}_2 = 0, \omega) = \frac{a^4 \pi^2 S^{(0)}(\omega)}{\lambda^2 f^2}. \quad (2.16)$$

To specify the position of an observation point we use the dimensionless Lommel variables which are defined as

$$u = k \left(\frac{a}{f}\right)^2 z, \quad (2.17)$$

$$v = k \left(\frac{a}{f}\right) \rho = k \left(\frac{a}{f}\right) \sqrt{x^2 + y^2}. \quad (2.18)$$

The expression for the normalized spectral density distribution is thus given by

$$\begin{aligned} S_{\mathrm{norm}}(u, v, \omega) &= \frac{S(u, v, \omega)}{S_{\mathrm{coh}}} \\ &= \frac{1}{\pi^2} \int_0^{2\pi} \int_0^1 \int_0^{2\pi} \int_0^1 J_0 \left\{ \beta a \left[\rho_1^2 + \rho_2^2 - 2\rho_1\rho_2 \cos(\phi_1 - \phi_2) \right]^{1/2} \right\} \\ &\quad \times \cos[v(\rho_1 \cos\phi_1 - \rho_2 \cos\phi_2) + u(\rho_1^2 - \rho_2^2)/2] \\ &\quad \times \rho_1 \rho_2 \, \mathrm{d}\rho_1 \mathrm{d}\phi_1 \mathrm{d}\rho_2 \mathrm{d}\phi_2. \end{aligned} \quad (2.19)$$

It can be shown that this distribution is symmetric about the plane $u = 0$ and the line $v = 0$. To reduce this four-dimensional integral to a sum of two-dimensional integrals we use a coherent mode expansion, as described in Appendix A.

The contours and three-dimensional images of the spectral density of a converging J_0-correlated Schell-model field are shown for several values of the coherence length β^{-1} in Figs. 2.2–2.4. When this length is significantly larger than the aperture size a, the intensity pattern of the field in the focal region approaches that of the coherent case of LINFOOT AND WOLF [1956]. This is illustrated in Fig. 2.2 where $(\beta a)^{-1} = 2$. This quantity is a measure of the effective coherence of the field in the aperture.

When the correlation length is decreased, a local minimum appears at the geometrical focus. This is shown in Fig. 2.3 for which $(\beta a)^{-1} = 0.35$. An intensity minimum can be seen at $u = v = 0$. Also, the overall intensity has decreased.

Fig. 2.4 shows the intensity pattern for the case when $(\beta a)^{-1} = 0.25$. The minimum at the geometrical focus is now deeper, the focal spot is broadened, and the overall intensity has decreased even further.

The behavior of the cross-spectral density function of the field in the aperture for the cases mentioned above is shown in Fig. 2.5. The spectral degree of coherence is plotted as a function of $\rho = |\mathbf{r}_2 - \mathbf{r}_1|$. It is to be noted that for the two cases in which the spectral density has a local minimum at the geometrical focus, the spectral degree of coherence also takes on negative values.

2.5 Spatial correlation properties

We next turn our attention to the spectral degree of coherence in the focal region of a J_0-correlated Schell model field. We first look at pairs of points on the z-axis, i.e.,

$$\begin{aligned} \mathbf{r}_1 &= (0, 0, z_1), & (2.20) \\ \mathbf{r}_2 &= (0, 0, z_2). & (2.21) \end{aligned}$$

On using cylindrical coordinates ρ and ϕ and the expressions in [Fischer and Visser, 2004] we obtain

$$\begin{aligned} \mathbf{q}'_1 \cdot \mathbf{r}_1 &\approx -z_1(1 - \rho_1^2/2f^2), & (2.22) \\ \mathbf{q}'_2 \cdot \mathbf{r}_2 &\approx -z_2(1 - \rho_2^2/2f^2). & (2.23) \end{aligned}$$

Substituting these approximations in Eq. (2.14), we obtain for the cross-spectral density the expression

$$\begin{aligned} W(0, 0, z_1; 0, 0, z_2; \omega) = {} & \frac{1}{(\lambda f)^2} \int_0^{2\pi} \int_0^{a} \int_0^{2\pi} \int_0^{a} S^{(0)}(\omega) \\ & \times J_0 \left\{ \beta \left[\rho_1^2 + \rho_2^2 - 2\rho_1\rho_2 \cos(\phi_1 - \phi_2) \right]^{1/2} \right\} \\ & \times e^{ik[-z_1(1-\rho_1^2/2f^2)+z_2(1-\rho_2^2/2f^2)]} \rho_1 \rho_2 \\ & \times \, \mathrm{d}\phi_1 \mathrm{d}\rho_1 \mathrm{d}\phi_2 \mathrm{d}\rho_2. \qquad (2.24) \end{aligned}$$

As shown in Appendix A, the coherent mode expansion for J_0 reads

$$\begin{aligned} J_0 \left\{ \beta \left[\rho_1^2 + \rho_2^2 - 2\rho_1\rho_2 \cos(\phi_1 - \phi_2) \right]^{1/2} \right\} = {} & J_0(\beta\rho_1) J_0(\beta\rho_2) \\ & + \sum_{n=1}^{\infty} 2 \left[J_n(\beta\rho_1) J_n(\beta\rho_2) \cos[n(\phi_1 - \phi_2)] \right]. \qquad (2.25) \end{aligned}$$

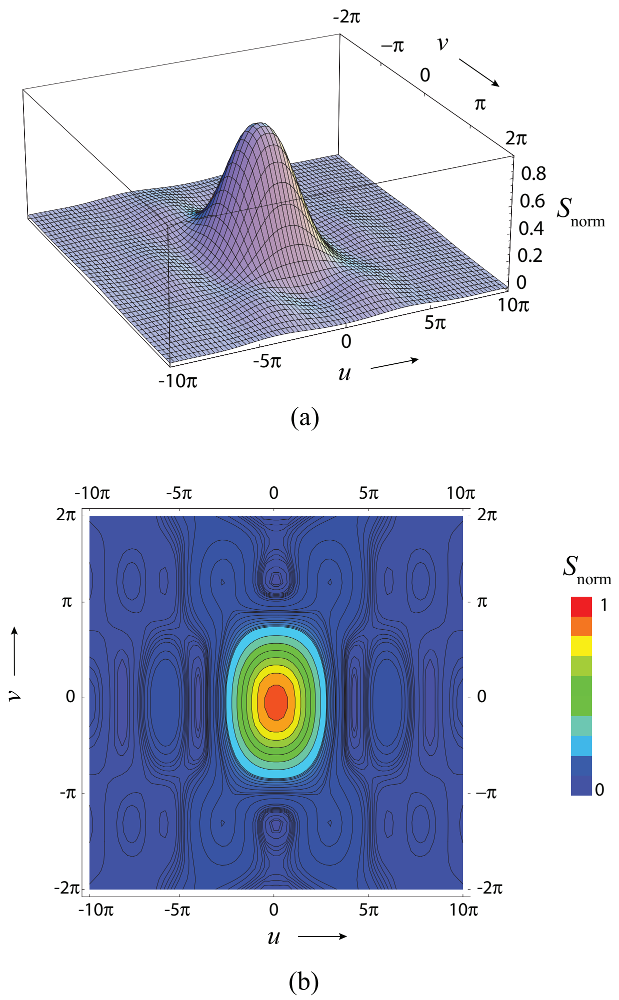

Figure 2.2: The three-dimensional normalized spectral density distribution (a) and its contours (b) for the case $\beta^{-1} = 0.02$ m, $a = 0.01$ m and hence $(\beta a)^{-1} = 2.00$. In this example $\lambda = 500$ nm, and $f = 2$ m.

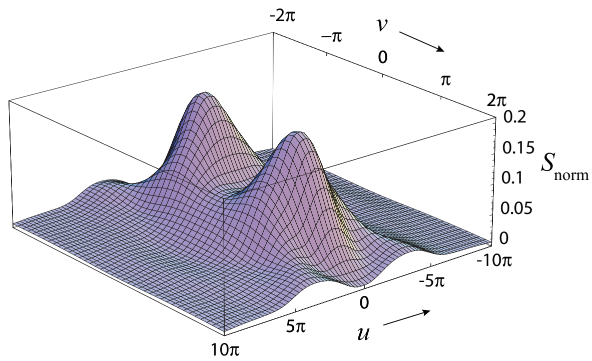

(a)

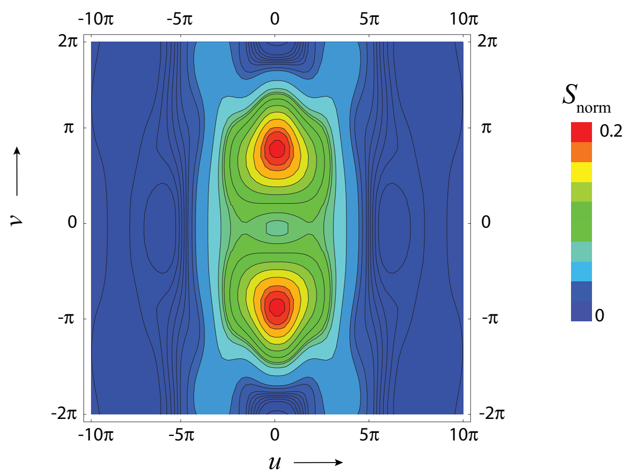

(b)

Figure 2.3: The three-dimensional normalized spectral density distribution (a) and its contours (b) for the case $\beta^{-1} = 3.5 \times 10^{-3}$ m, $a = 0.01$ m and hence $(\beta a)^{-1} = 0.35$. The other parameters are the same as those of Fig. 2.2.

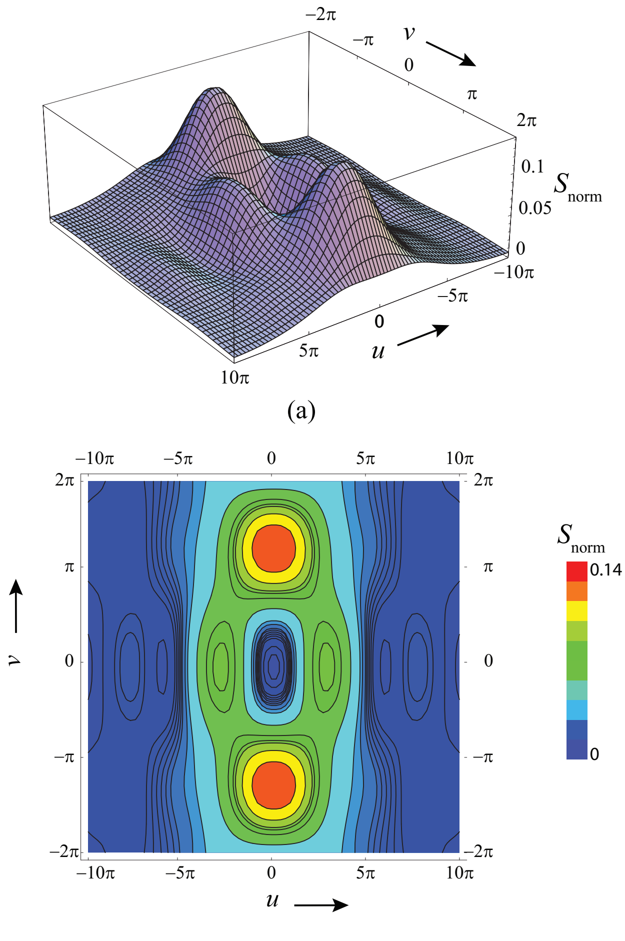

(b)

Figure 2.4: The three-dimensional normalized spectral density distribution (a) and its contours (b) for the case $\beta^{-1} = 2.5 \times 10^{-3}$ m, $a = 0.01$ m and hence $(\beta a)^{-1} = 0.25$. The other parameters are the same as those of Fig. 2.2.

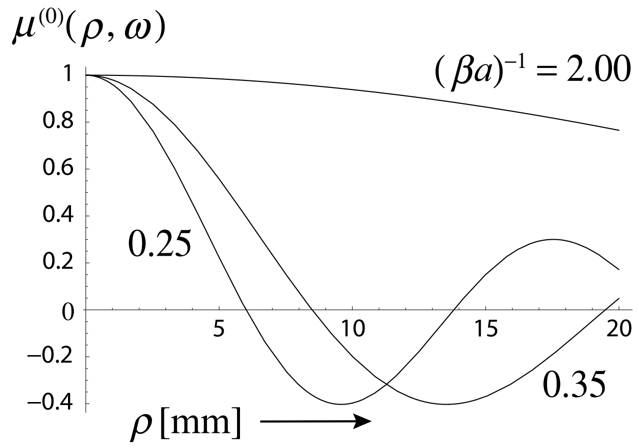

Figure 2.5: The spectral degree of coherence of the field in the aperture $\mu^{(0)}(\boldsymbol{\rho},\omega)$ for three different values of $(\beta a)^{-1}$, as discussed in the text. In this example $\lambda = 500$ nm, $a = 0.01$ m, and $f = 2$ m.

It is to be noted that in the expression for the cross-spectral density, Eq. (2.24), the angular dependence resides exclusively in the correlation function, hence after integration over ϕ_1 and ϕ_2 only the zeroth-order term of Eq. (2.25) remains. We therefore find that

$$W(0,0,z_1;0,0,z_2;\omega) = f^*(0,0,z_1;\omega)f(0,0,z_2;\omega), \tag{2.26}$$

with

$$f(0,0,z;\omega) = \frac{k}{f}\int_0^a J_0(\beta\rho)e^{\mathrm{i}kz(1-\rho^2/2f^2)}\rho\,\mathrm{d}\rho. \tag{2.27}$$

From this result and Eq. (2.11) it readily follows that

$$|\mu(0,0,z_1;0,0,z_2;\omega)| = 1. \tag{2.28}$$

This implies that the field is fully coherent for all pairs of points along the z-axis, even though the field in the aperture is partially coherent. This surprising effect can be understood by noticing that only a single coherent mode comes into play.

Next we examine pairs of points that lie in the focal plane. One point is taken to be at the geometrical focus O. Due to the rotational invariance of the system we may assume, without loss of generality, that the second point lies on the x-axis. Hence we consider pairs of points for which

$$\mathbf{r}_1 = (0,0,0), \tag{2.29}$$
$$\mathbf{r}_2 = (x,0,0). \tag{2.30}$$

The cross-spectral density, Eq. (2.14), then yields

$$\begin{aligned} W(0,0,0;x,0,0;\omega) &= \frac{1}{(\lambda f)^2}\int_0^{2\pi}\int_0^a\int_0^{2\pi}\int_0^a S^{(0)}(\omega) \\ &\times J_0\left\{\beta\left[\rho_1^2+\rho_2^2-2\rho_1\rho_2\cos(\phi_1-\phi_2)\right]^{1/2}\right\} \\ &\times e^{-\mathrm{i}k(\rho_2 x\cos\phi_2)/f}\rho_1\rho_2\,\mathrm{d}\phi_1\mathrm{d}\rho_1\mathrm{d}\phi_2\mathrm{d}\rho_2. \end{aligned} \tag{2.31}$$

on using the coherent mode expansion of J_0 and integrating over ϕ_1, again a single term remains, i.e.,

$$\begin{aligned} W(0,0,0;x,0,0;\omega) &= \frac{2\pi}{(\lambda f)^2}\int_0^a\int_0^{2\pi}\int_0^a S^{(0)}(\omega)J_0(\beta\rho_1)J_0(\beta\rho_2) \\ &\times\cos\left(k\frac{\rho_2 x}{f}\cos\phi_2\right)\rho_1\rho_2\,\mathrm{d}\rho_1\mathrm{d}\phi_2\mathrm{d}\rho_2. \end{aligned} \tag{2.32}$$

It is to be noted that this expression is real-valued.

In order to obtain the spectral degree of coherence we use the facts that

$$S(0,0,0;\omega) = \left(\frac{k}{f}\right)^2\int_0^a\int_0^a J_0(\beta\rho_1)J_0(\beta\rho_2)\rho_1\rho_2\,\mathrm{d}\rho_1\mathrm{d}\rho_2, \tag{2.33}$$

and

$$\begin{aligned} S(x,0,0;\omega) &= \frac{1}{(\lambda f)^2}\int_0^{2\pi}\int_0^a\int_0^{2\pi}\int_0^a S^{(0)}(\omega) \\ &\times J_0\left\{\beta\left[\rho_1^2+\rho_2^2-2\rho_1\rho_2\cos(\phi_1-\phi_2)\right]^{1/2}\right\} \\ &\times\cos[kx(\rho_1\cos\phi_1-\rho_2\cos\phi_2)/f]\rho_1\rho_2 \\ &\times\mathrm{d}\phi_1\mathrm{d}\rho_1\mathrm{d}\phi_2\mathrm{d}\rho_2. \end{aligned} \tag{2.34}$$

Examples of the spectral degree of coherence $\mu(0,0,0;x,0,0;\omega)$ are depicted in Figs. 2.6 and 2.7 for selected values of the coherence parameter $(\beta a)^{-1}$. For comparison's sake the normalized spectral density is also shown. In Fig. 6(a) two regions can be distinguished, regions where the fields are approximately co-phasal [i.e., $\mu(0,0,0;x,0,0;\omega)\approx 1$] and regions where the fields have opposite phases [i.e., $\mu(0,0,0;x,0,0;\omega)\approx -1$]. In between these two regions the spectral degree of coherence exhibits *phase singularities* [i.e., $\mu(0,0,0;x,0,0;\omega)=0$]. The latter points coincide with approximate zeros of the field.

When the coherence parameter is decreased, the overall intensity gets lower. This is shown in Fig. 2.6(b) for which $(\beta a)^{-1}=0.35$. An intensity minimum now occurs at the geometrical focus. The spectral degree of coherence still possesses a phase singularity, however its position no longer coincides with a zero of the field.

On further decreasing the coherence, the spectral density at focus almost gets zero. This is shown in Fig. 2.7(a) for which $(\beta a)^{-1}=0.25$. The spectral density

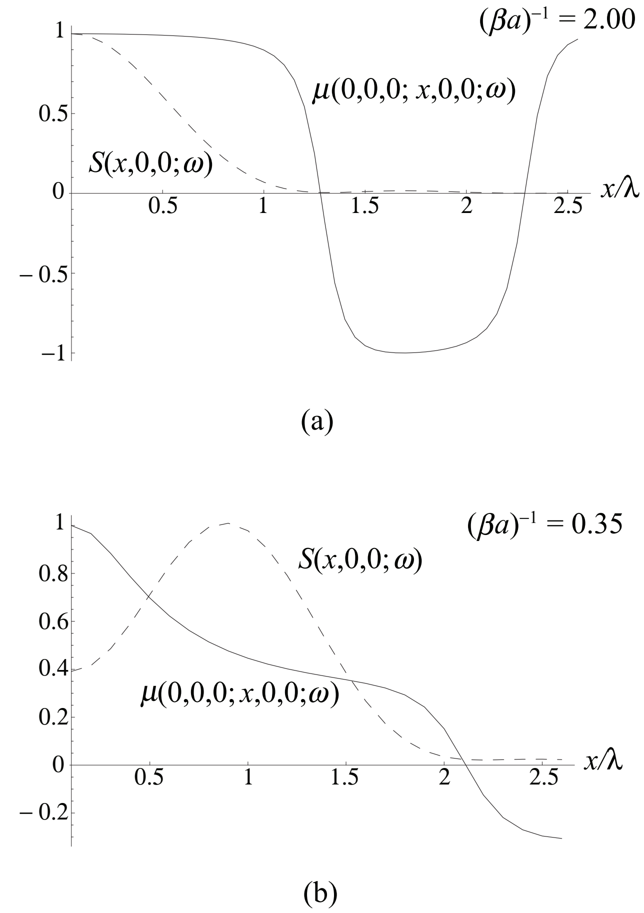

Figure 2.6: Spectral degree of coherence $\mu(0,0,0;x,0,0;\omega)$ (solid line) and the spectral density $S(x,0,0,\omega)$ normalized to its maximum value (dashed line), for the case (a): $(\beta a)^{-1} = 2$ and (b): $(\beta a)^{-1} = 0.35$. In this example $\lambda = 0.6328$ μm, $a = 0.01$ m, and $f = 0.02$ m.

rises again if the correlation parameter is decreased further, as can been seen in Fig. 2.7(b). In all cases the spectral degree of coherence exhibits phase singularities.

2.6 Other correlation functions

In this Section we examine the spectral density in the focal plane for other Bessel-correlated fields. In particular we consider a cross-spectral density function of the

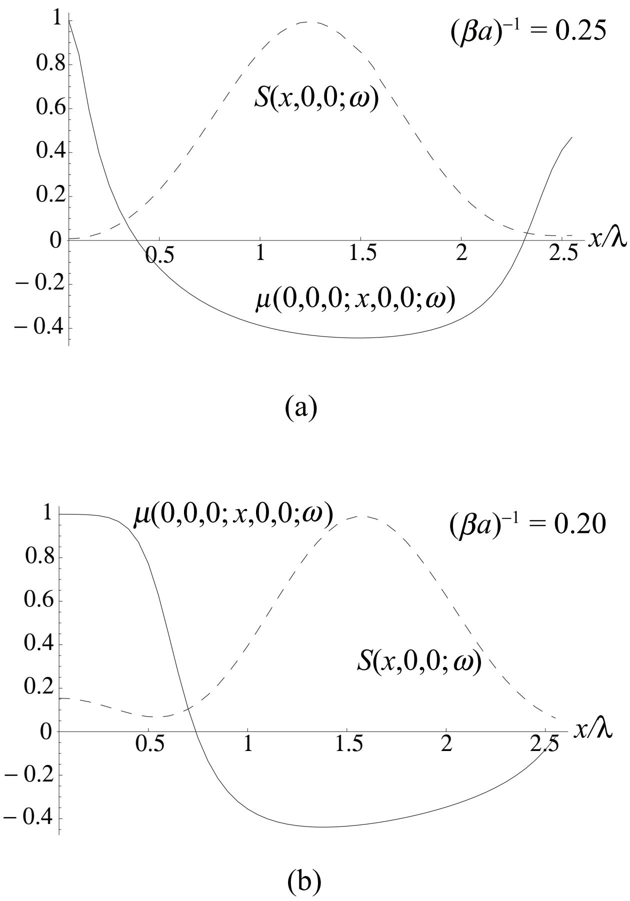

Figure 2.7: Spectral degree of coherence $\mu(0,0,0;x,0,0;\omega)$ (solid line) and the spectral density $S(x,0,0,\omega)$ normalized to its maximum value (dashed line), for the case (a): $(\beta a)^{-1} = 0.25$ and (b): $(\beta a)^{-1} = 0.2$. In this example $\lambda = 0.6328$ μm, $a = 0.01$ m, and $f = 0.02$ m.

form (see Section 5.3 of [Mandel and Wolf, 1995])

$$W_n^{(0)}(\boldsymbol{\rho}_1, \boldsymbol{\rho}_2, \omega) = S^{(0)}(\omega) 2^{n/2} \Gamma\left(1 + \frac{n}{2}\right) \frac{J_{n/2}(\beta|\boldsymbol{\rho}_2 - \boldsymbol{\rho}_1|)}{(\beta|\boldsymbol{\rho}_2 - \boldsymbol{\rho}_1|)^{n/2}}, \tag{2.35}$$

where $J_{n/2}$ is a Bessel function of the first kind and Γ is the gamma function. The case $n = 0$ was discussed in the previous Sections.

Let us denote a position in the focal plane with the vector $(\boldsymbol{\rho}, 0)$. The spectral density is then given by the expression

$$S_n(\boldsymbol{\rho}, 0, \omega) = \frac{1}{(\lambda f)^2} \int_A \int_A W_n^{(0)}(\boldsymbol{\rho}_1, \boldsymbol{\rho}_2, \omega) e^{-\mathrm{i}k(\boldsymbol{\rho}_2 - \boldsymbol{\rho}_1)\cdot\boldsymbol{\rho}/f} \, \mathrm{d}^2\rho_1 \mathrm{d}^2\rho_2. \tag{2.36}$$

This can be simplified to [Foley, 1991]

$$S_n(\boldsymbol{\rho}, 0, \omega) = 2\left(\frac{ka^2}{f}\right)^2 \int_0^1 C(b) W_n^{(0)}(2a\beta b) J_0\left(\frac{2ka\rho b}{f}\right) b \, \mathrm{d}b, \tag{2.37}$$

where

$$C(b) = (2/\pi)\left[\arccos(b) - b(1 - b^2)^{1/2}\right]. \tag{2.38}$$

As before the spectral density is normalized to its value for a fully coherent field at the geometrical focus. The normalized spectral density is thus given by the formula

$$\frac{S_n(\boldsymbol{\rho}, 0, \omega)}{S_{\text{coh}}} = \frac{8}{S^{(0)}(\omega)} \int_0^1 C(b) W_n^{(0)}(2a\beta b) J_0\left(\frac{2ka\rho b}{f}\right) b \, \mathrm{d}b, \tag{2.39}$$

An example is shown Fig. 2.8 for the case $n = 2$ and $(\beta a)^{-1} = 0.13$. It is seen that the spectral density now has a flat-topped profile. Fields with such a $J_1(x)/x$ correlation can be synthesized by placing a circular incoherent source in the first focal plane of a converging lens [Wolf and James, 1996].

2.7 Conclusions

We have investigated the behavior of selected Bessel-correlated, focused fields. It is observed that J_0-correlated fields produce a tunable, local minimum of intensity within a high-intensity shell of light. This observation suggests that such beams might be useful in a number of optical manipulation applications. In particular, it is well-appreciated that optical trapping of high-index particles requires high intensity at focus, while the trapping of low index particles requires low intensity at focus. The J_0 focusing configuration allows one to construct a system which can continuously switch between these two trapping conditions [Gahagan and Swartzlander, 1999].

It is also observed that $J_1(x)/x$ correlated fields result in a flat-top intensity distribution at. Such an intensity distribution could be useful in applications where a uniform intensity spot is required, such as lithography.

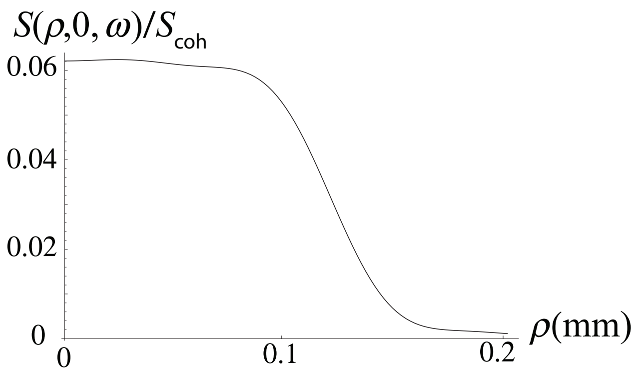

Figure 2.8: Normalized spectral density, Eq. (2.39), in the focal plane for the case $(\beta a)^{-1} = 0.13$. In this example $\lambda = 500$ nm, $a = 0.01$ m, $n = 2$, and $f = 2$ m.

These intensity distributions, and others, can be roughly predicted using straightforward Fourier optics. The image which appears in the focal plane is essentially the Fourier transform of the aperture-truncated correlation function in the lens plane. This correlation function can in turn be generated by an incoherent source whose aperture is given by the Fourier transform of the correlation function. One such example is using an annular incoherent source to produce a J_0-correlated field at the lens. The detailed three-dimensional structure of the light field in the focal region, however, requires a numerical solution of the diffraction problem.

It is important to note that this method of generating the necessary correlations is by no means unique. Any technique which produces the desired Bessel-correlation in the lens plane will result in the same intensity distribution at focus. For instance, one could use a coherent laser field transmitted through a rotating ground-glass plate with the desired correlations.

This coherence shaping of the intensity distribution at focus holds promise as a new technique for optical manipulation (c.f. Ref. [Arlt and Padgett, 2000]).

Appendix A: Coherent-mode expansion of a J_0-correlated field

Following Gori et al. [1987], we use the coherent mode expansion for the cross-spectral density function given by Eq. (2.13) to evaluate expression (2.19). Since it belongs to the Hilbert-Schmidt class, it can be expressed in the form [Wolf, 1982]

$$W^{(0)}(\boldsymbol{\rho}_1, \boldsymbol{\rho}_2, \omega) = \sum_n \lambda_n(\omega)\psi_n^*(\boldsymbol{\rho}_1, \omega)\psi_n(\boldsymbol{\rho}_2, \omega). \tag{A.1}$$

Here $\psi_n(\boldsymbol{\rho},\omega)$ are the orthonormal eigenfunctions and $\lambda_n(\omega)$ the eigenvalues of the integral equation

$$\int_D W^{(0)}(\boldsymbol{\rho}_1,\boldsymbol{\rho}_2,\omega)\psi_n(\boldsymbol{r}_1,\omega)\,\mathrm{d}^2\rho_1 = \lambda_n(\omega)\psi_n(\boldsymbol{\rho}_2,\omega), \tag{A.2}$$

where the integral extends over the aperture plane D. We rewrite the expansion (A.1) as

$$W^{(0)}(\boldsymbol{\rho}_1,\boldsymbol{\rho}_2,\omega) = \sum_n \lambda_n(\omega)W_n(\boldsymbol{\rho}_1,\boldsymbol{\rho}_2,\omega), \tag{A.3}$$

where $W_n(\boldsymbol{\rho}_1,\boldsymbol{\rho}_2,\omega) = \psi_n^*(\boldsymbol{\rho}_1,\omega)\psi_n(\boldsymbol{\rho}_2,\omega)$. The spectral degree of coherence corresponding to a single term W_n, is clearly uni-modular. Hence the expansion in Eq. (A.3) represents the cross-spectral density as a superposition of fully coherent modes.

In the case of a J_0-correlated field the expression for the eigenfunctions $\psi_n(\boldsymbol{\rho},\omega)$ reads [Gori et al., 1987]

$$\psi_n(\rho,\phi) = C_n\sqrt{S^{(0)}(\omega)}\left[a_nJ_n(\beta\rho)e^{-\mathrm{i}n\phi} + b_nJ_{-n}(\beta\rho)e^{\mathrm{i}n\phi}\right], \tag{A.4}$$

where C_n is a suitable normalization factor and the ratio a_n/b_n is arbitrary. On substituting from Eq. (A.4) into Eq. (A.2) and using Neumann's addition theorem

$$J_0\left\{\beta\left[\rho_1^2+\rho_2^2-2\rho_1\rho_2\cos(\phi_1-\phi_2)\right]^{1/2}\right\} = \sum_{k=-\infty}^{\infty} J_k(\beta\rho_1)J_k(\beta\rho_2)e^{\mathrm{i}k(\phi_1-\phi_2)}, \tag{A.5}$$

we find that the eigenvalues λ_n are given by the formulas

$$\lambda_n = \pi a^2 S^{(0)}(\omega)[J_n^2(\beta a) - J_{n-1}(\beta a)J_{n+1}(\beta a)], \quad (n=0,1,2,\ldots). \tag{A.6}$$

To ensure that all the functions $\psi_n(\boldsymbol{\rho},\omega)$ are orthonormal, we may choose

$$C_n = \frac{1}{\sqrt{\lambda_n}}, \quad (n=0,1,2,\ldots). \tag{A.7}$$

This choice implies that

$$(a_0+b_0)^2 = 1 \tag{A.8}$$
$$a_n^2+b_n^2 = 1, \quad (n=1,2,3,\ldots). \tag{A.9}$$

Hence we find a twofold degeneracy for the eigenfunctions ψ_n, except for the case that $n=0$. We thus obtain the expansion

$$J_0\left\{\beta\left[\rho_1^2+\rho_2^2-2\rho_1\rho_2\cos(\phi_1-\phi_2)\right]^{1/2}\right\} = J_0(\beta\rho_1)J_0(\beta\rho_2) + \sum_{n=1}^{\infty} 2\left\{J_n(\beta\rho_1)J_n(\beta\rho_2)\cos[n(\phi_1-\phi_2)]\right\}, \tag{A.10}$$

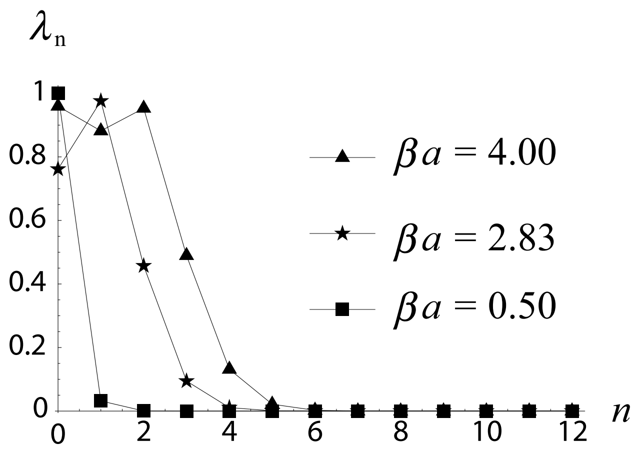

Figure 2.9: Eigenvalues λ_n versus n for a J_0-correlated field with a uniform spectral density across the plane of the aperture. Only the points corresponding to integer values of n are meaningful, the connecting lines are drawn to aid the eye.

where we have used the fact that the functions J_n and J_{-n} are related by [Arfken and Weber, 2001]

$$J_{-n}(x) = (-1)^n J_n(x) \quad (n \in \mathbb{N}). \tag{A.11}$$

The behavior of the eigenvalues λ_n versus n is shown in Fig. 2.9. Although the decreasing behavior of the eigenvalues is not strictly monotone it can be seen that as soon n exceeds βa the eigenvalues become very small. In other words only those modes whose index n is smaller than βa contribute effectively to the cross-spectral density.

Chapter 3

The evolution of singularities in a partially coherent vortex beam

This Chapter is based on the following publication:

- T. van Dijk and T.D. Visser "Evolution of singularities in a partially coherent beam",
  J. Opt. Soc. Am. A, vol. 26, pp. 741–744 (2009).

Abstract
We study the evolution of phase singularities and coherence singularities in a Laguerre-Gauss beam that is rendered partially coherent by letting it pass through a spatial light modulator. The original beam has an on-axis minimum of intensity–a phase singularity–that transforms into a maximum of the far-field intensity. In contrast, although the original beam has no coherence singularities, such singularities are found to develop as the beam propagates. This disappearance of one kind of singularity and the gradual appearance of another is illustrated with numerical examples.

3.1 Introduction

Singular optics [Nye, 1999; Soskin and Vasnetsov, 2001], the study of topological features of optical fields, has expanded in scope from phase singularities and polarization singularities [Berry and Dennis, 2001; Freund et al., 2002; Schoonover and Visser, 2006] to coherence singularities. The latter kind occurs when the field at a certain frequency at one point is completely uncorrelated with the field at another point, at the same frequency [Schouten et al., 2003a; Fischer and Visser, 2004; Gbur and Visser, 2006; Visser and Schoonover, 2008]. Coherence singularities affect one of the most basic properties of a wave field, namely its ability to produce interference patterns.

Vortex beams (sometimes called 'dark core beams' or 'doughnut beams') have an on-axis zero of intensity, i.e., a phase singularity [Yin et al., 2003]. They are widely used for the guiding of atomic beams [Wang et al., 2005], the trapping of cold atomic clouds [Kuga et al., 1997], and as optical tweezers for low-index particles [Gahagan and Swartzlander, 1999]. In addition, their relative insensitivity to atmospheric turbulence makes them candidates for optical communication [Gbur and Tyson, 2008]. The coherence properties of certain types of vortex beams have been studied by Ponomarenko [2001]; Bogatyryova et al. [2003]. Theoretical and experimental studies of correlations in the time-domain were reported by Palacios et al. [2004]; Swartzlander and Schmit [2004]; Maleev and Swartzlander [2008].

It is the aim of this paper to deepen the understanding of the not yet completely clarified interplay between intensity zeros (phase singularities) and coherence singularities. We study a new type of beam, namely a partially coherent Laguerre-Gauss beam (LG). Such a beam may be produced by letting a monochromatic, and hence fully coherent, single mode of frequency ω pass through a phase screen [Andrews and Phillips, 2005; Goodman, 2000], leaving its amplitude unchanged. In the case of a LG_1^0 mode propagating along the z-axis, the field incident on the phase screen is given by the expression [Siegman, 1986, Sec. 16.4]

$$U^{(\mathrm{inc})}(\boldsymbol{\rho}, \omega) = A \exp(\mathrm{i}\phi) \rho \exp(-\rho^2/4\sigma_S^2), \tag{3.1}$$

with A a constant, σ_S the effective source width, and $\boldsymbol{\rho} = \rho(\cos\phi, \sin\phi)$ a two-dimensional vector that represents a position in the plane perpendicular to the z-axis. The action of the phase screen is twofold: it imprints a deterministic phase $-\phi$ onto the beam, and in addition it randomizes the phase with a Gaussian correlation function. This can be achieved by means of a Spatial Light Modulator (SLM). By averaging over different realizations of the SLM a beam with the prescribed statistical behavior is obtained [Dayton et al., 1998].

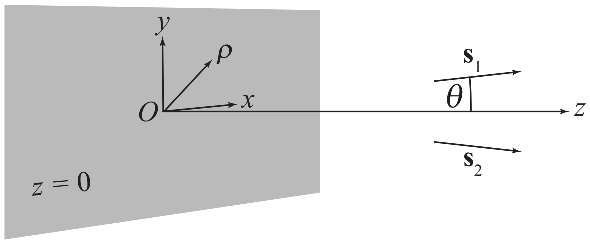

Figure 3.1: Illustrating the notation.

3.2 Partially coherent sources

In the space-frequency domain, the statistical properties of a source may be characterized by its cross-spectral density function [Mandel and Wolf, 1995]

$$W^{(0)}(\boldsymbol{\rho}_1, \boldsymbol{\rho}_2, \omega) = \langle U^{(0)*}(\boldsymbol{\rho}_1, \omega) U^{(0)}(\boldsymbol{\rho}_2, \omega) \rangle, \tag{3.2}$$

where the asterisk denotes complex conjugation and the angular brackets indicate an ensemble average. The superscript (0) indicates positions in the secondary source plane ($z = 0$) immediately behind the SLM (see Fig. 3.1). The spectral degree of coherence is the normalized version of the cross-spectral density, viz.

$$\mu^{(0)}(\boldsymbol{\rho}_1, \boldsymbol{\rho}_2, \omega) = \frac{W^{(0)}(\boldsymbol{\rho}_1, \boldsymbol{\rho}_2, \omega)}{\sqrt{S^{(0)}(\boldsymbol{\rho}_1, \omega) S^{(0)}(\boldsymbol{\rho}_2, \omega)}}, \tag{3.3}$$

with

$$S^{(0)}(\boldsymbol{\rho}, \omega) = W^{(0)}(\boldsymbol{\rho}, \boldsymbol{\rho}, \omega) = A^2 \rho^2 \exp(-\rho^2/2\sigma_S^2) \tag{3.4}$$

the spectral density (or 'intensity at frequency ω'). The spectral degree of coherence caused by the SLM is homogeneous and Gaussian, i.e.

$$\mu^{(0)}(\boldsymbol{\rho}_1, \boldsymbol{\rho}_2, \omega) = \mu^{(0)}(\boldsymbol{\rho}_2 - \boldsymbol{\rho}_1, \omega) = \exp[-(\rho_2 - \rho_1)^2/2\sigma_\mu^2], \tag{3.5}$$

with σ_μ the effective coherence length of the secondary source. On substituting from Eqs. (3.4) and (3.5) into Eq. (3.3) we find that the cross-spectral density takes the form

$$W^{(0)}(\boldsymbol{\rho}_1, \boldsymbol{\rho}_2, \omega) = A^2 \rho_1 \rho_2 \exp[-(\rho_1^2 + \rho_2^2)/4\sigma_S^2] \exp[-(\rho_2 - \rho_1)^2/2\sigma_\mu^2]. \tag{3.6}$$

We notice that Eq. (3.4) indicates the presence of an on-axis phase singularity in the source plane, i.e. $S^{(0)}(\boldsymbol{\rho} = 0, \omega) = 0$. Coherence singularities occur when the phase of the spectral degree of coherence is undefined, i.e., when $\mu^{(0)}(\boldsymbol{\rho}_1, \boldsymbol{\rho}_2, \omega) = 0$. In that case, the combination of the fields at $\boldsymbol{\rho}_1$ and $\boldsymbol{\rho}_2$ in a Young's type experiment yields an interference pattern without spatial modulation. Eq. (3.5) implies that no such singularities exist in the source plane.

3.3 Quasi-homogeneous sources

A source is said to be quasi-homogeneous if its spectral degree of coherence $\mu^{(0)}(\boldsymbol{\rho}', \omega)$ varies much more rapidly with $\boldsymbol{\rho}'$ than its spectral density $S^{(0)}(\boldsymbol{\rho}, \omega)$ varies with $\boldsymbol{\rho}$. In that case the radiant intensity (defined as r^2 times the far-field spectral density) and the spectral degree of coherence of the field in the far zone are related to the same properties in the source plane by the reciprocity relations [Mandel and Wolf, 1995, Sec. 5.3.2]

$$J(\mathbf{s}, \omega) = (2\pi k)^2 \tilde{S}^{(0)}(0, \omega) \tilde{\mu}^{(0)}(k\mathbf{s}_\perp, \omega) \cos^2\theta, \tag{3.7}$$

$$\mu^{(\infty)}(r_1\mathbf{s}_1, r_2\mathbf{s}_2, \omega) = \tilde{S}^{(0)}\left[k(\mathbf{s}_{2\perp} - \mathbf{s}_{1\perp}), \omega\right] \exp[\mathrm{i}k(r_2 - r_1)] / \tilde{S}^{(0)}(0, \omega), \tag{3.8}$$

with the two-dimensional Fourier transforms given by the expressions

$$\tilde{S}^{(0)}(\mathbf{f}, \omega) = \frac{1}{(2\pi)^2} \int S^{(0)}(\boldsymbol{\rho}, \omega)\, e^{-\mathrm{i}\mathbf{f}\cdot\boldsymbol{\rho}}\, \mathrm{d}^2\rho, \tag{3.9}$$

$$\tilde{\mu}^{(0)}(\mathbf{f}, \omega) = \frac{1}{(2\pi)^2} \int \mu^{(0)}(\boldsymbol{\rho}, \omega)\, e^{-\mathrm{i}\mathbf{f}\cdot\boldsymbol{\rho}}\, \mathrm{d}^2\rho. \tag{3.10}$$

Here $k = 2\pi/\lambda$ is the wavenumber associated frequency ω, $\mathbf{s}_\perp$ is the projection of the unit direction vector $\mathbf{s}$ onto the xy-plane, and θ is the angle which the $\mathbf{s}$-direction makes with the z-axis (see Fig. 3.1). The superscript (∞) indicates points in the far zone.

3.4 A partially coherent Laguerre-Gauss source

To analyse a partially coherent source that generates a Laguerre-Gauss beam we substitute from Eqs. (3.4) and (3.5) into Eqs. (3.9) and (3.10) while using the theorem for Fourier transforms of derivatives, and find that

$$\tilde{S}^{(0)}(\mathbf{f}, \omega) = \left(2 - f^2\sigma_S^2\right) \sigma_S^4 A^2 \exp\left(-f^2\sigma_S^2/2\right)/2\pi, \tag{3.11}$$

$$\tilde{\mu}^{(0)}(\mathbf{f}, \omega) = \sigma_\mu^2 \exp(-f^2\sigma_\mu^2/2)/2\pi. \tag{3.12}$$

On choosing the two observation points to be symmetrically positioned with respect to the z-axis, i.e., $r_1 = r_2 = r$, and $\mathbf{s}_{2\perp} = -\mathbf{s}_{1\perp} = (\sin\theta, 0)$, we obtain the formulas

$$J(\mathbf{s}, \omega) = 2k^2\sigma_S^4\sigma_\mu^2 A^2 \cos^2\theta \exp(-k^2\sigma_\mu^2 \sin^2\theta/2), \tag{3.13}$$

$$\mu^{(\infty)}(r\mathbf{s}_1, r\mathbf{s}_2, \omega) = \left[1 - 2k^2\sigma_S^2 \sin^2\theta\right] \exp(-2k^2\sigma_S^2 \sin^2\theta). \tag{3.14}$$

These last two results indicate that the character of the field singularities changes as the beam propagates: Eq. (3.13) shows that the on-axis intensity, a phase singularity in the source plane, transforms into a maximum of the far zone radiant intensity; and Eq. (3.14) implies that, in contrast to the source plane, there are pairs of points in the far zone at which the field is completely uncorrelated. Coherence singularities, i.e. $\mu^{(\infty)}(r\mathbf{s}_1, r\mathbf{s}_2, \omega) = 0$, occur at observation points for which the term between square brackets in Eq. (3.14) vanishes. This happens for observation angles θ_{CS} such that

$$\sin\theta_{CS} = \left(2k^2\sigma_S^2\right)^{-1/2}. \tag{3.15}$$

It is to be noted that this behavior is quite different from that of the class of partially coherent vortex beams described earlier [Ponomarenko, 2001; Bogatyryova et al., 2003]. Those beams, being an incoherent superposition of Laguerre-Gauss modes, retain their on-axis phase singularity on propagation. We mention in passing that Eq. (3.13) implies that in order for the field to be beam-like the source has to satisfy the condition

$$k^2\sigma_\mu^2/2 \gg 1. \tag{3.16}$$

The reciprocity relations (3.7) and (3.8) describe the connection between the field in the source plane and that in the far-zone. However, they do not describe how the initial on-axis phase singularity changes on propagation, or how the coherence singularity comes into existence. In order to investigate this, we study the propagation of the cross-spectral density function to an arbitrary transverse plane. We have [Mandel and Wolf, 1995, Sec. 5.6.3]

$$\begin{aligned} W(\boldsymbol{\rho}_1, \boldsymbol{\rho}_2, z, \omega) = & \iint\limits_{(z=0)} W^{(0)}(\boldsymbol{\rho}'_1, \boldsymbol{\rho}'_2, \omega) \\ & \times\, G^*(\boldsymbol{\rho}_1, \boldsymbol{\rho}'_1, z, \omega) G(\boldsymbol{\rho}_2, \boldsymbol{\rho}'_2, z, \omega)\, \mathrm{d}^2\rho'_1 \mathrm{d}^2\rho'_2, \end{aligned} \tag{3.17}$$

with the paraxial Green's function given by the expression

$$G(\boldsymbol{\rho}, \boldsymbol{\rho}', z, \omega) = -\frac{\mathrm{i}k}{2\pi z}\exp(\mathrm{i}kz)\exp[\mathrm{i}k(\boldsymbol{\rho} - \boldsymbol{\rho}')^2/2z]. \tag{3.18}$$

On substituting from Eqs. (3.6) into Eq. (3.18) we obtain after some calculations for the on-axis spectral density the formula

$$S(\boldsymbol{\rho} = 0, z, \omega) = W(\boldsymbol{\rho}_1 = 0, \boldsymbol{\rho}_2 = 0, z, \omega) \tag{3.19}$$

$$\begin{aligned} = & \left(\frac{kA}{z}\right)^2 \int_0^\infty \int_0^\infty \rho_1'^2 \rho_2'^2 \exp(-\rho_1'^2/2\sigma_+^2)\exp(-\rho_2'^2/2\sigma_-^2) \\ & \times I_0(\rho'_1\rho'_2/\sigma_\mu^2)\, \mathrm{d}\rho'_1 \mathrm{d}\rho'_2, \end{aligned} \tag{3.20}$$

with $I_0(x)$ the modified Bessel function of the first kind of order zero, and

$$\frac{1}{2\sigma_\pm^2} = \frac{1}{4\sigma_S^2} + \frac{1}{2\sigma_\mu^2} \pm \frac{\mathrm{i}k}{2z}. \tag{3.21}$$

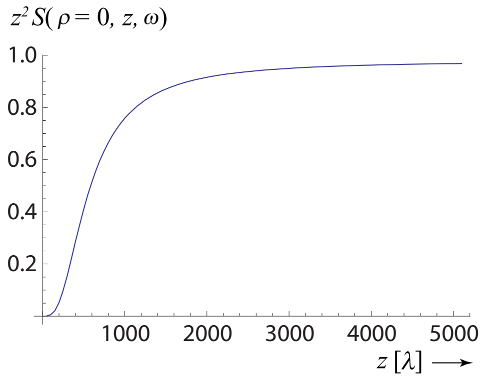

Figure 3.2: The scaled on-axis spectral density $z^2 S(\boldsymbol{\rho} = 0, z, \omega)$, calculated from Eq. (3.20), normalized by the radiant intensity in the forward direction $J[\mathbf{s} = (0, 0, 1), \omega]$. In this example $\sigma_S = 15\lambda$ and $\sigma_\mu = 4\lambda$.

Equation (3.20) can be integrated numerically for $z \gg \lambda$. An illustration of the behavior of the scaled on-axis spectral density $z^2 S(\boldsymbol{\rho} = 0, z, \omega)$ is shown in Fig. 3.2, with the limiting value given by Eq. (3.4) added. It is seen that on propagation the phase singularity immediately evolves into a finite-valued intensity that gradually rises towards its asymptotic value, namely that of the radiant intensity in the forward direction $J[\mathbf{s} = (0, 0, 1), \omega]$, as given by Eq. (3.13).

In Fig. 3.3 the spectral density $S(\boldsymbol{\rho}, z, \omega)$ is shown for several cross-sections of the beam. As can be seen, the on-axis spectral density (initially a phase singularity) gradually rises and changes from being a minimum in the source plane to being a maximum in the far field.

The evolution of the coherence singularity is depicted in Fig. 3.4. There the behavior of $|\mu(\boldsymbol{\rho}, z, -\boldsymbol{\rho}, z, \omega)|$ is shown shown for pairs of points on the lines of observation $\arctan(\boldsymbol{\rho}/z) = \theta_{CS}$, the angle defined by Eq. (3.15), i.e., the two lines on which a correlation singularity occurs in the far zone. The modulus of the spectral degree of coherence gradually decreases as the beam propagates and eventually becomes zero, meaning that the two points form a coherence singularity.

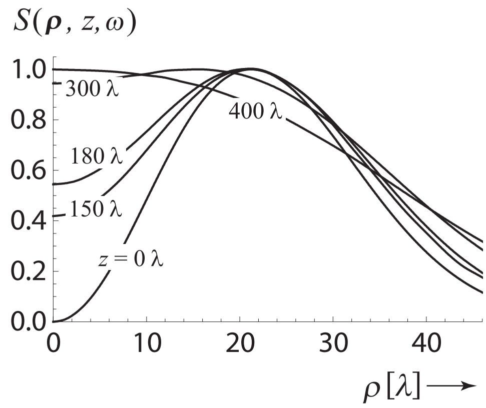

Figure 3.3: The normalized spectral density $S(\boldsymbol{\rho}, z, \omega)$, calculated from Eq. (3.18), in several cross-sections of the beam. In this example $\sigma_S = 15\lambda$ and $\sigma_\mu = 4\lambda$.

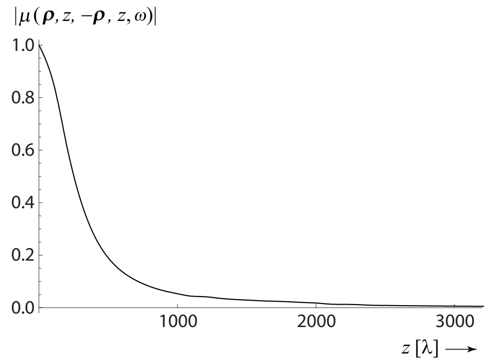

Figure 3.4: Evolution of the modulus of the spectral degree of coherence, as calculated from Eq. (3.18), along the two directions of observation at which a coherence singularity occurs in the far field. In this example $\sigma_S = 15\lambda$ and $\sigma_\mu = 4\lambda$.

3.5 The far-zone state of coherence

The behavior of the far-zone state of coherence is further analyzed by considering the spectral degree of coherence of two observation points that lie on a circle which is centered around the z-axis [see Fig. 3.5(a)]. One point is kept fixed, whereas the other point is moved around the circle, i.e., we choose

$$\mathbf{s_{1\perp}} = (\sin\theta, 0), \tag{3.22}$$

$$\mathbf{s_{2\perp}} = (\sin\theta\cos\phi, \sin\theta\sin\phi), \tag{3.23}$$

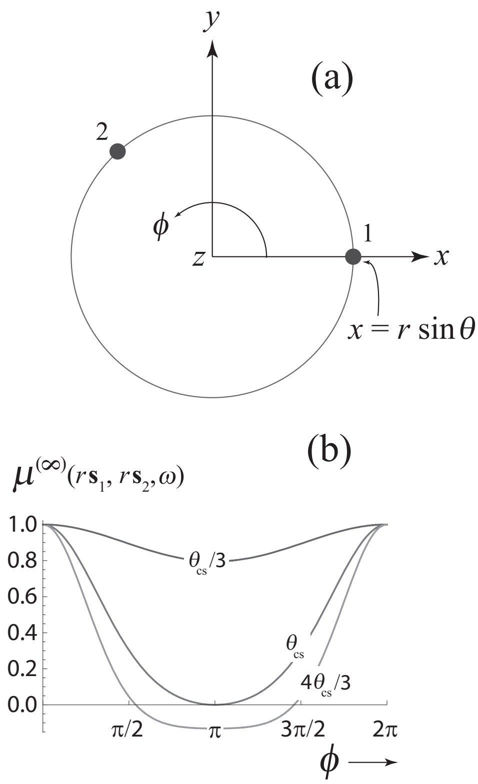

Figure 3.5: (a): The position of two far-zone observation points (blue dots) on a circle centered around the z-axis. (b) The spectral degree of coherence of the field at the two points as a function of the angle ϕ for three values of θ. In this example $\sigma_S = 15\lambda$ and $\sigma_\mu = 4\lambda$.

and study the dependence of the spectral degree of coherence as a function of the angle ϕ. We now obtain from Eq. (3.8) the expression

$$\begin{aligned}\mu^{(\infty)}(r\mathbf{s}_1, r\mathbf{s}_2, \omega) &= \left[1 - 2k^2\sigma_S^2 \sin^2\theta \sin^2(\phi/2)\right] \\ &\quad \times \exp\left[-2k^2\sigma_S^2 \sin^2\theta \sin^2(\phi/2)\right]. \end{aligned} \tag{3.24}$$

Eq. (3.24) shows that the spectral degree of coherence in this case is real-valued. For small circles, for which the angle $\theta < \theta_{CS}$, $\mu^{(\infty)}(r\mathbf{s}_1, r\mathbf{s}_2, \omega)$ is always positive and no coherence singularities occur (see Fig. 3.5(b)). If $\theta = \theta_{CS}$, there is precisely one zero of the spectral degree of coherence, and the two points that lie diagonally opposite each other on the circle ($\phi = \pi$) form a correlation singularity. When θ is further increased two zeros occur, i.e., the singularity unfolds into a doublet.

3.6 Conclusions

We have analyzed the behavior a partially coherent Laguerre-Gauss beam and found a new kind of behavior of its singularities. The initial on-axis phase singularity evolves into a maximum of the radiant intensity. In contrast, a coherence singularity gradually develops as the beam propagates. As the angle between two far-field observation points is increased, this singularity unfolds into a doublet.

Chapter 4

Coherence singularities in the far field generated by partially coherent sources

This Chapter is based on the following publication:

- T. van Dijk, H.F. Schouten and T.D. Visser "Coherence singularities in the far field generated by partially coherent sources", Phys. Rev. A, vol. 79, 033805 (2009).

Abstract
We analyze the coherence singularities that occur in the far field that is generated by a broad class of partially coherent sources. It is shown that for rotationally symmetric, planar, quasi-homogeneous sources the coherence singularities form a two-dimensional surface in a reduced three-dimensional space. We illustrate our results by studying the topology of the coherence singularity of a partially coherent vortex beam. We find that the geometry of the phase singularity can be associated with conic sections such as ellipses, lines and hyperbolas.

4.1 Introduction

There is a growing interest in the structure of wave fields in the vicinity of points where certain field parameters are undefined, or 'singular'. This has given rise to the new sub-discipline of *singular optics*. [Nye, 1999; Soskin and Vasnetsov, 2001] In the past few years, many different types of singular behavior have been identified. For example, *phase singularities* occur at positions where the field amplitude vanishes, and hence the phase is undefined. [Nye and Berry, 1974] *Polarization singularities* arise at locations where the field is circularly or linearly polarized. [Berry and Dennis, 2001; Dennis, 2002; Freund et al., 2002; Mokhun et al., 2002; Freund, 2002; Soskin et al., 2003; Schoonover and Visser, 2006] There either the orientation angle of the polarization ellipse or its handedness is undefined. Also the *Poynting vector* can exhibit singular behavior at points where its modulus is zero, and hence its orientation is undefined. [Boivin et al., 1967] Topological reaction of such singularities were studied in [Schouten et al., 2003b, 2004]

Optical coherence theory [Wolf, 2007] deals with the statistical properties of light fields. In this theory, correlation functions play a central role. [Schouten and Visser, 2008] A form of singular behavior that is slightly more abstract than those mentioned above, occurs in two-point correlation functions. At pairs of points at which the field (at a particular frequency) is completely uncorrelated, the phase of the correlation function is singular. [Schouten et al., 2003a; Fischer and Visser, 2004; Palacios et al., 2004; Swartzlander and Schmit, 2004; Wang et al., 2006; Maleev and Swartzlander, 2008] When the field at two such points is combined in an interference experiment, no fringes are produced. These *coherence singularities* are points in six-dimensional space. Their relationship to other types of singularities has only recently been clarified. [Gbur et al., 2004; Flossmann et al., 2005, 2006; Gbur and Visser, 2006; Visser and Schoonover, 2008]

Thusfar, only one study has been devoted to the description of the multi-dimensional structure of a specific coherence singularity, namely that of a vortex beam propagating through turbulence. [Gbur and Swartzlander, 2008] In the present article, we analyze the more general case of coherence singularities in the far zone of the field generated by a broad class of partially coherent sources. These *quasi-homogeneous sources* are often encountered in practice. We analyze the generic structure of the coherence singularities and also discuss the practical case of a rotationally symmetric source. We illustrate our results by applying them to a recently described, new type of 'dark core' or vortex beam. For this beam all different cross-sections of the singularity are shown to be conic sections in a suitable coordinate system.

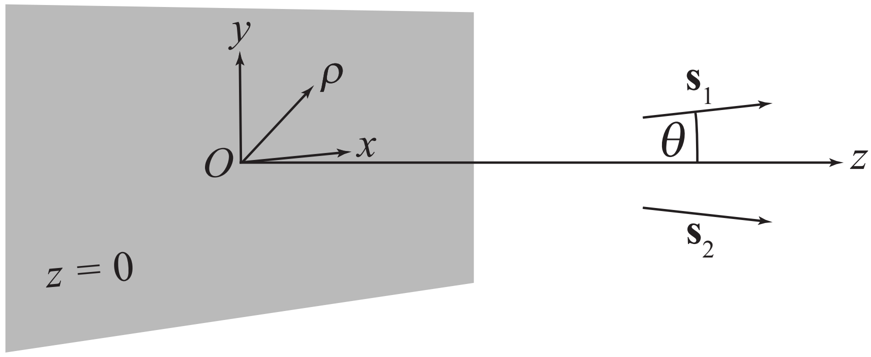

Figure 4.1: Illustrating the notation.

4.2 Partially coherent sources

Consider a partially coherent, planar, secondary source, situated in the plane $z = 0$, that emits radiation into the half-space $z > 0$ (see Fig. 4.1). In the space-frequency domain, the source is characterized by its *cross-spectral density function* [Wolf, 2007]

$$W^{(0)}(\boldsymbol{\rho}_1, \boldsymbol{\rho}_2, \omega) = \langle U^{(0)*}(\boldsymbol{\rho}_1, \omega) U^{(0)}(\boldsymbol{\rho}_2, \omega)\rangle. \tag{4.1}$$

Here $U^{(0)}(\boldsymbol{\rho}, \omega)$ represents the source field at frequency ω at position $\boldsymbol{\rho} = (x, y)$, the asterisk indicates complex conjugation, and the angled brackets denote an ensemble average. The *spectral degree of coherence* is the normalized form of the cross-spectral density, i.e.,

$$\mu^{(0)}(\boldsymbol{\rho}_1, \boldsymbol{\rho}_2, \omega) = \frac{W^{(0)}(\boldsymbol{\rho}_1, \boldsymbol{\rho}_2, \omega)}{\sqrt{S^{(0)}(\boldsymbol{\rho}_1, \omega) S^{(0)}(\boldsymbol{\rho}_2, \omega)}}, \tag{4.2}$$

with

$$S^{(0)}(\boldsymbol{\rho}, \omega) = W^{(0)}(\boldsymbol{\rho}, \boldsymbol{\rho}, \omega), \tag{4.3}$$

the *spectral density* (or 'intensity at frequency ω') of the source. For *Schell-model* sources [Wolf, 2007] the spectral degree of coherence only depends on position through the difference $\boldsymbol{\rho}_1 - \boldsymbol{\rho}_2$, i.e.,

$$\mu^{(0)}(\boldsymbol{\rho}_1, \boldsymbol{\rho}_2, \omega) = \mu^{(0)}(\boldsymbol{\rho}_1 - \boldsymbol{\rho}_2, \omega). \tag{4.4}$$

The field in an arbitrary transverse plane $z > 0$ is given by the expression

$$U(\boldsymbol{\rho}, z, \omega) = \int\limits_{(z=0)} U^{(0)}(\boldsymbol{\rho}', \omega) G(\boldsymbol{\rho} - \boldsymbol{\rho}', z, \omega)\, \mathrm{d}^2\rho', \tag{4.5}$$

where $G(\boldsymbol{\rho} - \boldsymbol{\rho}', z, \omega)$ is an appropriate free-space Green's function [WOLF, 2007, Sec. 5.2]. On substituting from Eq. (4.5) in Eq. (4.1), while interchanging the order of integration and ensemble averaging, it follows that the cross-spectral density at two arbitrary points $(\boldsymbol{\rho}_1, z_1)$ and $(\boldsymbol{\rho}_2, z_2)$ satisfies the equation

$$\begin{aligned} W(\boldsymbol{\rho}_1, z_1, \boldsymbol{\rho}_2, z_2, \omega) = & \iint_{(z=0)} W^{(0)}(\boldsymbol{\rho}_1', \boldsymbol{\rho}_2', \omega) G^*(\boldsymbol{\rho}_1 - \boldsymbol{\rho}_1', z_1, \omega) \\ & \times G(\boldsymbol{\rho}_2 - \boldsymbol{\rho}_2', z_2, \omega)\, \mathrm{d}^2\rho_1' \mathrm{d}^2\rho_2'. \end{aligned} \tag{4.6}$$

The spectral density and the spectral degree of coherence at arbitrary points are given by formulas that are quite similar to Eqs. (4.2) and (4.3), viz.,

$$\mu(\boldsymbol{\rho}_1, z_1, \boldsymbol{\rho}_2, z_2, \omega) = \frac{W(\boldsymbol{\rho}_1, z_1, \boldsymbol{\rho}_2, z_2, \omega)}{\sqrt{S(\boldsymbol{\rho}_1, z_1, \omega) S(\boldsymbol{\rho}_2, z_2, \omega)}}, \tag{4.7}$$

and

$$S(\boldsymbol{\rho}, z, \omega) = W(\boldsymbol{\rho}, z, \boldsymbol{\rho}, z, \omega). \tag{4.8}$$

Coherence singularities are phase singularities of the spectral degree of coherence, they occur at pairs of points at which the field at frequency ω is completely uncorrelated, i.e.,

$$\mu(\boldsymbol{\rho}_1, z_1, \boldsymbol{\rho}_2, z_2, \omega) = 0. \tag{4.9}$$

4.3 Quasi-homogeneous sources

An important sub-class of Schell-model sources is formed by so-called quasi-homogeneous sources. [WOLF, 2007] For such sources the spectral density $S^{(0)}(\boldsymbol{\rho}, \omega)$ varies much more slowly with $\boldsymbol{\rho}$ than the spectral degree of coherence $\mu^{(0)}(\boldsymbol{\rho}', \omega)$ varies with $\boldsymbol{\rho}'$. This behavior, that often occurs in practice, is sketched in Fig. 4.2.

For quasi-homogeneous sources the field in the source plane and the field in the far zone are related by two *reciprocity relations*, namely

$$S^{(\infty)}(\mathbf{s}, \omega) = (2\pi k)^2 \tilde{S}^{(0)}(0, \omega) \tilde{\mu}^{(0)}(k\mathbf{s}_\perp, \omega) \cos^2\theta / r^2, \tag{4.10}$$

$$\mu^{(\infty)}(r_1\mathbf{s}_1, r_2\mathbf{s}_2, \omega) = \frac{\tilde{S}^{(0)}\,[k(\mathbf{s}_{2\perp} - \mathbf{s}_{1\perp}), \omega]}{\tilde{S}^{(0)}(0, \omega)} \exp[\mathrm{i}k(r_2 - r_1)], \tag{4.11}$$

with the two-dimensional spatial Fourier transforms given by the expressions

$$\tilde{S}^{(0)}(\mathbf{f}, \omega) = \frac{1}{(2\pi)^2} \int S^{(0)}(\boldsymbol{\rho}, \omega)\, e^{-\mathrm{i}\mathbf{f}\cdot\boldsymbol{\rho}}\, \mathrm{d}^2\rho, \tag{4.12}$$

$$\tilde{\mu}^{(0)}(\mathbf{f}, \omega) = \frac{1}{(2\pi)^2} \int \mu^{(0)}(\boldsymbol{\rho}, \omega)\, e^{-\mathrm{i}\mathbf{f}\cdot\boldsymbol{\rho}}\, \mathrm{d}^2\rho. \tag{4.13}$$

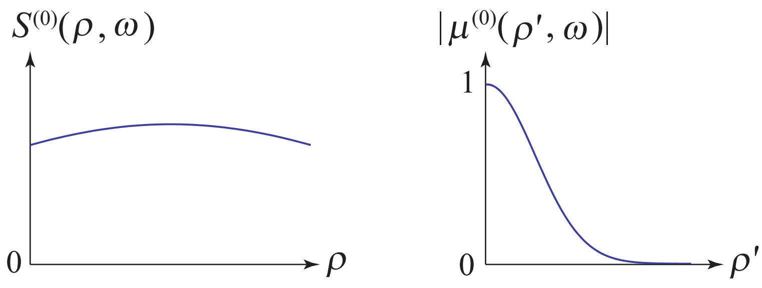

Figure 4.2: Illustrating the concept of quasi-homogeneity.

In these formulas $k = \omega/c$ is the wavenumber associated with frequency ω, c being the speed of light in vacuum, $\mathbf{s}_\perp$ is the projection of the unit direction vector $\mathbf{s}$ onto the xy-plane, and θ is the angle that the $\mathbf{s}$-direction makes with the z-axis (see Fig. 4.1). The superscript (∞) indicates points in the far zone. Equation (4.10) states that the far-field spectral density of a planar, secondary, quasi-homogeneous source is proportional to the Fourier transform of its spectral degree of coherence. Equation (4.11) expresses that the far-field spectral degree of coherence of such a source is, apart from a geometrical factor, given by the Fourier transform of its spectral density.

Even though Eq. (4.11) is quite general, it allows us to draw several conclusions. First, the far-field spectral degree of coherence depends on the spectral density of the source, but is independent of its spectral degree of coherence. Second, the dependence of the far-field spectral degree of coherence on the two distances r_1 and r_2 enters only through the factor $\exp[\mathrm{i}k(r_2 - r_1)]$. This means that coherence singularities occur along certain pairs of observation directions $\mathbf{s}_1 = (\sin\theta_1\cos\phi_1, \sin\theta_1\sin\phi_1, \cos\theta_1)$ and $\mathbf{s}_2 = (\sin\theta_2\cos\phi_2, \sin\theta_2\sin\phi_2, \cos\theta_2)$ for which the prefactor in Eq. (4.11) vanishes. Since $\tilde{S}^{(0)}(0,\omega)$ is both finite and real, this yields the two constraints

$$\Re\left\{\tilde{S}^{(0)}\left[k(\mathbf{s}_{2\perp} - \mathbf{s}_{1\perp}),\omega\right]\right\} = 0, \tag{4.14}$$

$$\Im\left\{\tilde{S}^{(0)}\left[k(\mathbf{s}_{2\perp} - \mathbf{s}_{1\perp}),\omega\right]\right\} = 0, \tag{4.15}$$

where $\Re$ and $\Im$ denote the real and imaginary part, respectively. These two conditions imply that generically (i.e., when they are independent and commensurate), the coherence singularities form a two-dimensional surface in the four-dimensional $(\theta_1, \phi_1, \theta_2, \phi_2)$-space.

Let us next consider the specialized case of a source whose spectral density is mirror-symmetric with respect to both the x- and the y-axis. In that case the factor $\tilde{S}^{(0)}[k(\mathbf{s}_{2\perp} - \mathbf{s}_{1\perp}],\omega)$ that appears in Eq. (4.11) is real-valued for all values of its spatial argument, [BRACEWELL, 1965, Ch. 2] and hence condition (4.15) is lifted. This means that the coherence singularity is a three-dimensional volume in $(\theta_1, \phi_1, \theta_2, \phi_2)$-space. Furthermore, if the spectral density of the source is rotationally symmetric, the spectral degree of coherence in the far zone depends on the observation angles ϕ_1 and ϕ_2 only through their difference $\phi_2 - \phi_1$. We therefore conclude that for planar, secondary, rotationally symmetric, quasi-homogeneous sources the coherence singularities are two-dimensional surfaces in the reduced $(\theta_1, \theta_2, \phi_2 - \phi_1)$-space. An example of such a source is examined in the next Section.

4.4 A partially coherent Laguerre-Gauss source

We illustrate our results thusfar with the analysis of a partially coherent source that generates a Laguerre-Gauss beam. [VAN DIJK ET AL., 2008] For this source we have

$$S^{(0)}(\boldsymbol{\rho}, \omega) \;=\; A^2 \rho^2 \exp(-\rho^2/2\sigma_S^2), \tag{4.16}$$

$$\mu^{(0)}(\boldsymbol{\rho}_2 - \boldsymbol{\rho}_1, \omega) \;=\; \exp[-(\rho_2 - \rho_1)^2/2\sigma_\mu^2], \tag{4.17}$$

with A a real number, $\rho = |\boldsymbol{\rho}|$, and σ_S and σ_μ the effective width of the spectral density and of the spectral degree of coherence, respectively. If $\sigma_\mu \ll \sigma_S$ the source is quasi-homogeneous. Since

$$\tilde{S}^{(0)}(\mathbf{f}, \omega) \;=\; \left(2 - f^2\sigma_S^2\right) \sigma_S^4 A^2 \exp\left(-f^2\sigma_S^2/2\right)/2\pi, \tag{4.18}$$

application of the reciprocity relation (4.11) yields

$$\begin{aligned} \mu^{(\infty)}(r_1\mathbf{s}_1, r_2\mathbf{s}_2, \omega) \;=\; & \left[1 - k^2(\mathbf{s}_{2\perp} - \mathbf{s}_{1\perp})^2\sigma_S^2/2\right] \exp\left[-k^2(\mathbf{s}_{2\perp} - \mathbf{s}_{1\perp})^2\sigma_S^2/2\right] \\ & \times \exp\left[\mathrm{i}k(r_2 - r_1)\right]. \end{aligned} \tag{4.19}$$

Because

$$(\mathbf{s}_{2\perp} - \mathbf{s}_{1\perp})^2 = \sin^2\theta_1 + \sin^2\theta_2 - 2\sin\theta_1\sin\theta_2\cos(\phi_1 - \phi_2), \tag{4.20}$$

it follows from Eq. (4.19) that coherence singularities occur for those values of θ_1, ϕ_1, θ_2, and ϕ_2 for which

$$\sin^2\theta_1 + \sin^2\theta_2 - 2\sin\theta_1\sin\theta_2\cos(\phi_1 - \phi_2) = 2/k^2\sigma_S^2. \tag{4.21}$$

As remarked at the end of the previous Section, the dependence of the spectral degree of coherence on the two angles ϕ_1 and ϕ_2 is through their difference $\phi_1 - \phi_2$. From now on we set, without loss of generality, $\phi_2 = 0$.

An example of the topology of the coherence singularity is shown in Fig. 4.3, from which it can be seen that it forms a saddle-like surface. Let us consider the $\theta_1 = \theta_2$ cross-section. For small values of these two angles, there is no value of ϕ_1

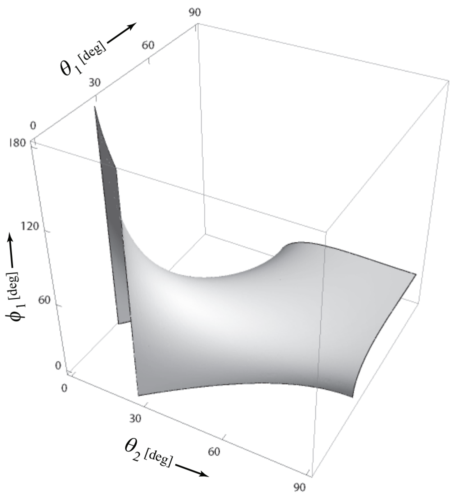

Figure 4.3: A two-dimensional coherence singularity in $(\theta_1, \theta_2, \phi_1)$-space. In this example $k^2\sigma_S^2 = 10$.

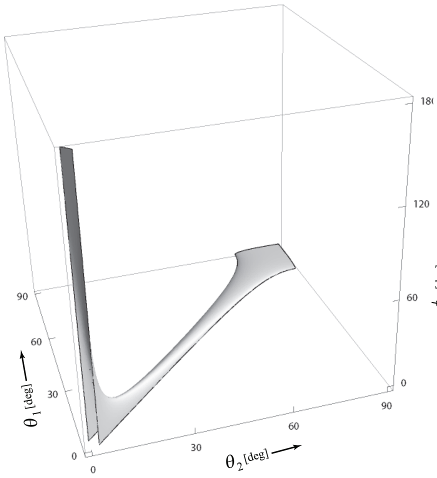

Figure 4.4: A two-dimensional coherence singularity in $(\theta_1, \theta_2, \phi_1)$-space. In this example $k^2\sigma_S^2 = 1000$.

that corresponds with a point on the surface, i.e., there exist no pairs of points at which the field is completely uncorrelated. When the angles are gradually increased to a critical value $\theta_1 = \theta_2 = \theta_c$ a coherence singularity occurs at $\phi_1 = 180°$. [van Dijk et al., 2008] For larger values $(\theta_1 = \theta_2 > \theta_c)$ a value of $\phi_1 < 180°$ corresponds to a point on the surface. Since Eq. (4.21) shows a dependence of the singularity on $\cos\phi_1$, this means that the initial singularity has unfolded into two pairs of singularities, one for ϕ_1 and one for $-\phi_1$. It is to noted that in this example $k^2\sigma_S^2 = 10$ for illustrative purposes. In Fig. 4.4 the more realistic value of 1000 was used. It can be seen that the topological features of the coherence singularity remain unchanged.

4.5 Conic sections

In order to study the coherence singularity depicted in Fig. 4.3 in more detail, it is instructive to re-write Eq. (4.21) in the form

$$x^2 + y^2 + 2xyz + G = 0, \tag{4.22}$$

where

$$
\begin{aligned}
x &= \sin\theta_1, && (4.23)\\
y &= \sin\theta_2, && (4.24)\\
z &= -\cos\phi_1, && (4.25)\\
G &= -2/k^2\sigma_S^2. && (4.26)
\end{aligned}
$$

Although Eq. (4.22) is *not* a quadratic surface in (x, y, z)-space, both the horizontal and the vertical cross-sections of the coherence singularity are quadratic curves. Horizontal cross-sections (i.e., fixing the value of z and hence of ϕ_1) are conic sections in (x, y)-space [Beyer, 1980]; since x and y are limited to the interval $[0, 1]$, only parts of these conic sections are realized. More specifically, if $z = -1$ the cross-section takes the form of two parallel lines. On increasing z it becomes an ellipse (with a circle as a special case when $z = 0$), and finally, for $z = 1$, it becomes two parallel lines again (only one of which lies in the physical domain of x and y). Various cross-sections of the coherence singularity are shown in Fig. 4.5 for selected values of z. Because of the interchangeable roles of x and y in Eq. (4.22), the cross-sections are symmetric about the line $x = y$.

According to Eq. (4.22) vertical cross-sections of the coherence singularities (e.g., fixing the value of y and hence of θ_2) are conic sections in (x, z)-space; since $0 \le x \le 1$ and $-1 \le z \le 1$, only parts of these conic sections are realized. More specifically, if $y = 0$ the cross-section has the form of two parallel lines (only one of which lies in the physical domain of x and z). On increasing y it becomes a branch of a hyperbola, two intersecting lines and again a branch of a hyperbola. This is illustrated in Fig. 4.6. This concludes our identification of various cross-section of the coherence singularity with a variety of conic curves.

4.6 Conclusions

We have analyzed the topology of coherence singularities that occur in the far field generated by quasi-homogeneous sources. As a specific example we examined the coherence singularity of a partially coherent vortex beam. Its cross-sections were found to be different kinds of conic sections in a modified coordinate system.

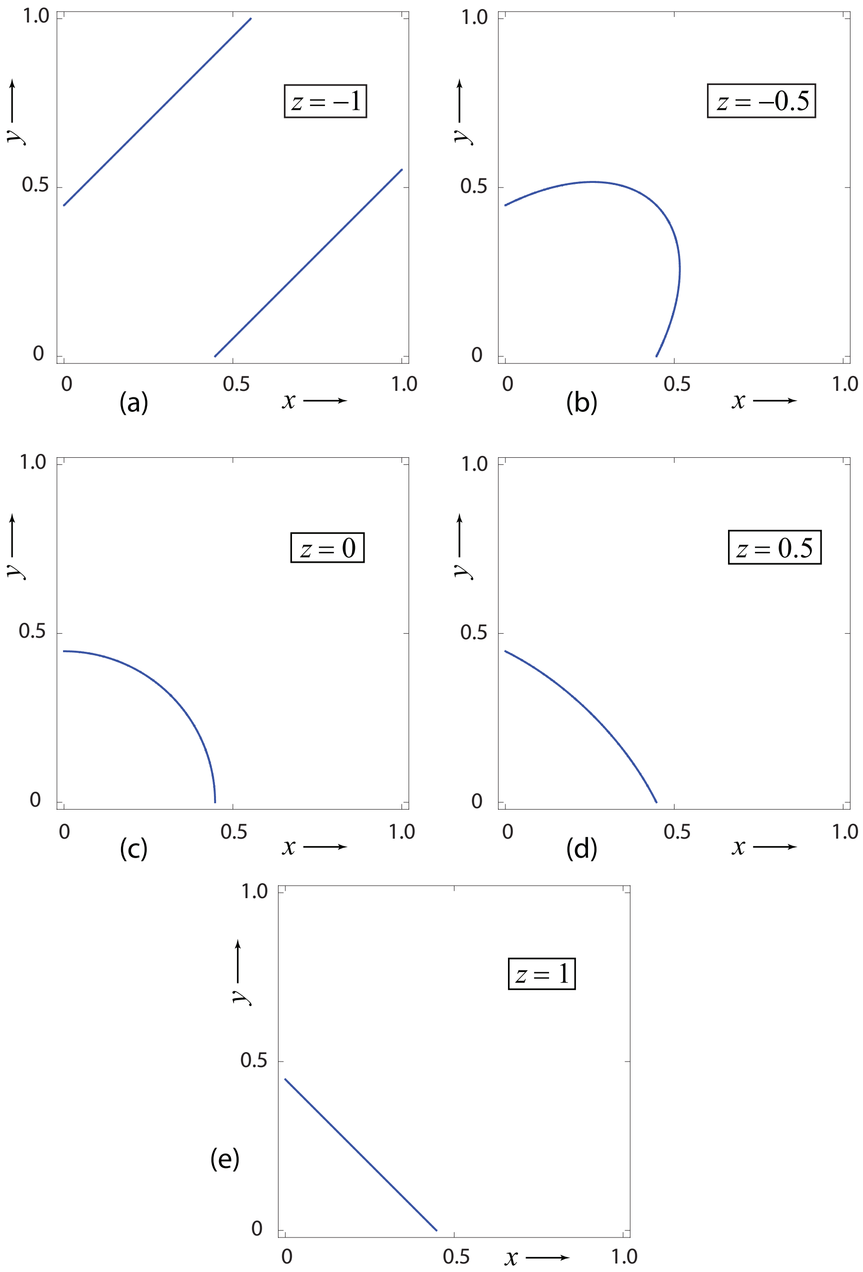

Figure 4.5: Cross-sections of the coherence singularity in the x, y-plane for selected values of z, viz. $z = -1$ (a), $z = -0.5$ (b), $z = 0$ (c), $z = 0.5$ (d), and $z = 1$ (e).

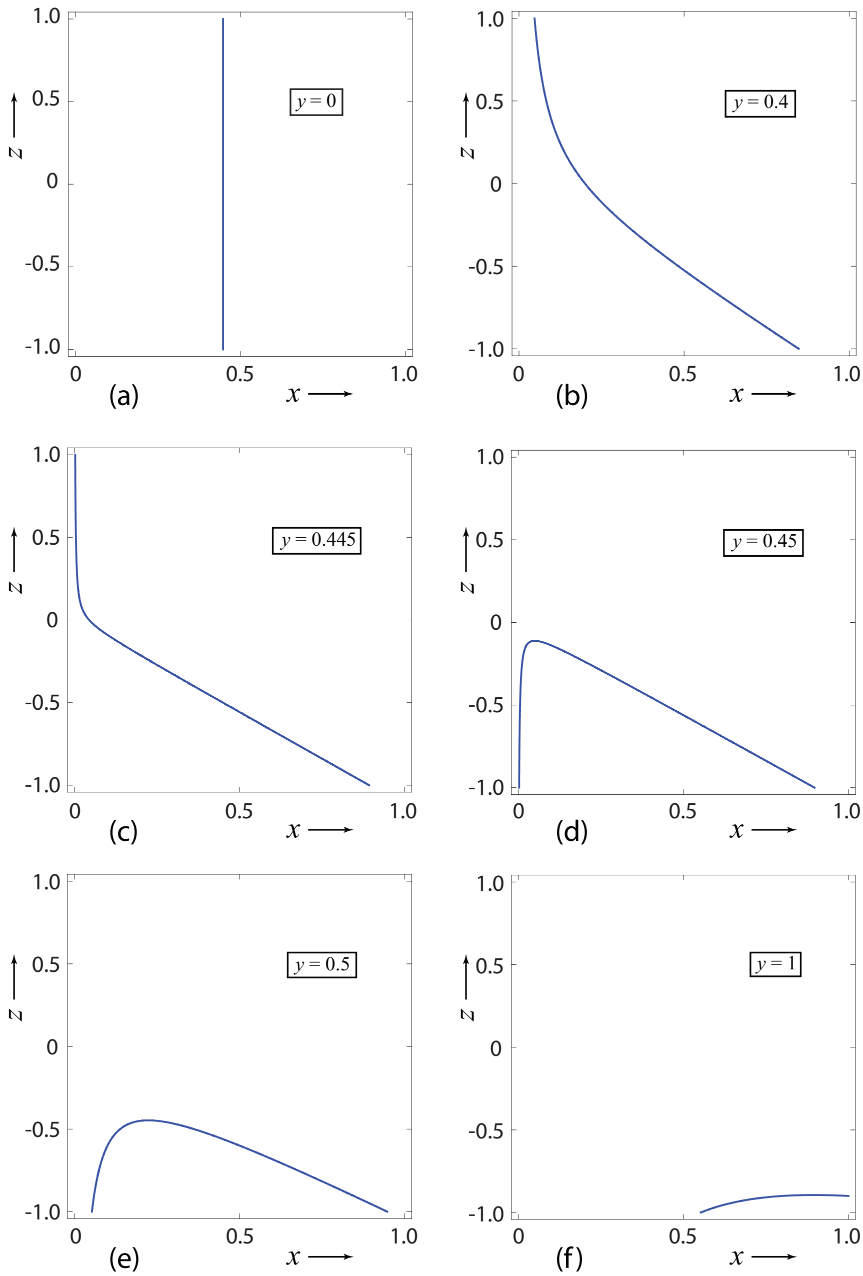

Figure 4.6: Cross-sections of the coherence singularity in the x, z-plane for selected values of y, viz. $y = 0$ (a), $y = 0.4$ (b), $y = 0.445$ (c), $y = 0.45$ (d), $y = 0.5$ (e), and $y = 1$ (f).

Chapter 5

The Pancharatnam-Berry phase for non-cyclic polarization changes

This Chapter is based on the following publication:

- T. van Dijk, H.F. Schouten, W. Ubachs and T.D. Visser "The Pancharatnam-Berry phase for non-cyclic polarization changes",
  Opt. Express, vol. 18, pp. 10796–10804 (2010).

Abstract
We present a novel setup that allows the observation of the geometric phase that accompanies polarization changes in monochromatic light beams for which the initial and final states are different (so-called non-cyclic changes). This Pancharatnam-Berry phase can depend in a linear or in a nonlinear fashion on the orientation of the optical elements, and sometimes the dependence is singular. Experimental results that confirm these three types of behavior are presented. The observed singular behavior may be applied in the design of optical switches.

5.1 Introduction

In a seminal paper Berry [Berry, 1984] showed that when the Hamiltonian of a quantum mechanical system is adiabatically changed in a cyclic manner the system acquires, in addition to the usual dynamic phase, a so-called geometric phase. It was soon realized that such a phase is in fact quite general: it can also occur for non-adiabatic state changes and even in classical systems [Berry, 1990; Samuel and Bhandari, 1988; Jordan, 1988; Shapere and Wilczek, 1989]. One of its manifestations is the Pancharatnam phase in classical optics [Pancharatnam, 1956; Berry, 1987]. The polarization properties of a monochromatic light beam can be represented by a point on the Poincaré sphere [Born and Wolf, 1999]. When, with the help of optical elements such as polarizers and retarders, the state of polarization is made to trace out a closed contour on the sphere, the beam acquires a geometric phase. This *Pancharatnam-Berry phase*, as it is nowadays called, is equal to half the solid angle of the contour subtended at the origin of the sphere [Bhandari, 1997; Hariharan, 2005; Bhandari and Samuel, 1988]. The various kinds of behavior of the geometric phase for cyclic polarization changes have been studied extensively [Chyba et al., 1988; Schmitzer et al., 1993; Bhandari, 1992a,b].

In this paper we study the geometric phase for *non-cyclic* polarization changes, i.e. polarization changes for which the initial state and the final state are different. Such changes correspond to non-closed paths on the Poincaré sphere. The geometric phase can depend in a linear, a nonlinear or in a singular fashion on the orientation of the optical elements. Experimental results that confirm these three types of behavior are presented. The observed singular behavior may be applied in the design of fast optical switches.

The states of polarization, A and B, of two monochromatic light beams can be represented by the Jones vectors [Jones, 1941]

$$\mathbf{E}_A = \begin{pmatrix} \cos\alpha_A \\ \sin\alpha_A e^{\mathrm{i}\theta_A} \end{pmatrix}, \qquad (0 \leq \alpha_A \leq \pi/2;\ -\pi \leq \theta_A \leq \pi), \tag{5.1}$$

$$\mathbf{E}_B = e^{\mathrm{i}\gamma} \begin{pmatrix} \cos\alpha_B \\ \sin\alpha_B e^{\mathrm{i}\theta_B} \end{pmatrix}, \qquad (0 \leq \alpha_B \leq \pi/2;\ -\pi \leq \theta_B \leq \pi). \tag{5.2}$$

Since only relative phase differences are of concern, the overall phase of $\mathbf{E}_A$ in Eq. (5.1) is taken to be zero. According to Pancharatnam's connection [Berry, 1987; van Dijk et al., 2010b] the two states are in phase when their superposition yields a maximal intensity, i.e., when

$$|\mathbf{E}_A + \mathbf{E}_B|^2 = |\mathbf{E}_A|^2 + |\mathbf{E}_B|^2 + 2\,\mathrm{Re}(\mathbf{E}_A \cdot \mathbf{E}_B^*) \tag{5.3}$$

reaches its greatest value, and hence

$$\mathrm{Im}\,(\mathbf{E}_A \cdot \mathbf{E}_B^*) = 0, \tag{5.4}$$

$$\mathrm{Re}\,(\mathbf{E}_A \cdot \mathbf{E}_B^*) > 0. \tag{5.5}$$

These two conditions uniquely determine the phase γ, except when A and B are orthogonal.

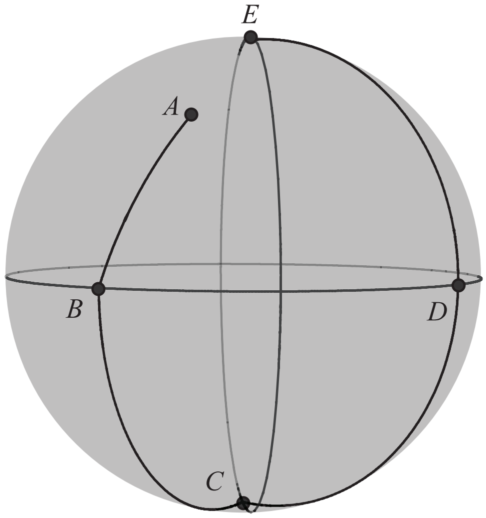

Figure 5.1: Non-closed path $ABCDE$ on the Poincaré sphere for a monochromatic light beam that passes through a sequence of polarizers and compensators.

5.2 Non-cyclic polarization changes

We study a series of polarization changes for which the successive states are assumed to be in phase. To illustrate the rich behavior of the geometric phase, consider a beam in an arbitrary initial state A, that passes through a linear polarizer whose transmission axis is under an angle ϕ_1 with the positive x-axis. This results in a second state B that lies on the equator of the Poincaré sphere (see Fig. 5.1). Next the beam passes through a suitably oriented compensator, which produces a third, left-handed circularly polarized state C on the south pole. The action of a second linear polarizer, with orientation angle ϕ_2, creates state D on the equator. Finally, a second compensator causes the polarization to become right-handed circular, corresponding to the state E on the north pole. These successive manipulations can be described with the help of Jones calculus [Jones, 1941; Brosseau, 1998]. The matrix for a linear polarizer whose transmission axis is under an angle ϕ with the positive x-axis equals

$$\mathbf{P}(\phi) = \begin{pmatrix} \cos^2\phi & \cos\phi\sin\phi \\ \cos\phi\sin\phi & \sin^2\phi \end{pmatrix}, \tag{5.6}$$

whereas the matrix for a compensator ("retarder") with a fast axis under an angle

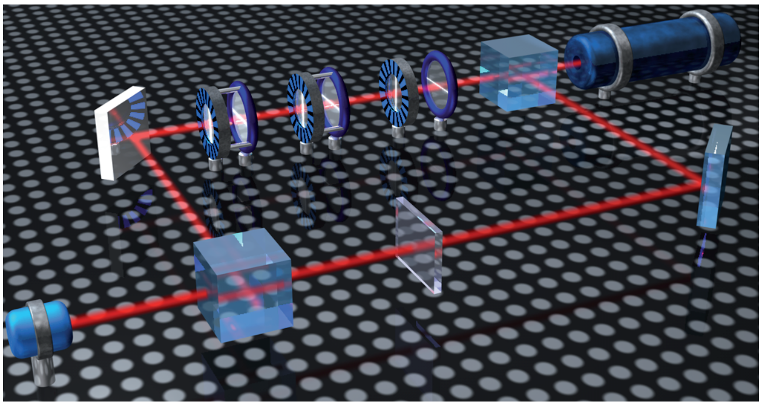

Figure 5.2: Sketch of the Mach-Zehnder setup. The light from a He-Ne laser (right-hand top) is split into two beams. All polarizing elements are placed in the upper arm, the lower arm only contains a gray filter. The compensators are depicted with striped holders, the linear polarizers with non-striped holders. The last two pairs of elements are mounted together. The interference pattern of the recombined beams is recorded with either a photo diode or a CCD camera (left-hand bottom).

θ with the positive x-axis, which introduces a phase change δ between the two field components is

$$\mathbf{C}(\delta,\theta) = \begin{pmatrix} \cos(\delta/2) + \mathrm{i}\sin(\delta/2)\cos(2\theta) & \mathrm{i}\sin(\delta/2)\sin(2\theta) \\ \mathrm{i}\sin(\delta/2)\sin(2\theta) & \cos(\delta/2) - \mathrm{i}\sin(\delta/2)\cos(2\theta) \end{pmatrix}. \tag{5.7}$$

The (unnormalized) Jones vector for the final state E thus equals

$$\mathbf{E}_E = \mathbf{C}(\pi/2, \phi_2 - \pi/4)\cdot\mathbf{P}(\phi_2)\cdot\mathbf{C}(-\pi/2, \phi_1 - \pi/4)\cdot\mathbf{P}(\phi_1)\cdot\mathbf{E}_A. \tag{5.8}$$

Hence we find for the normalized states the expressions

$$\mathbf{E}_B = \mathbf{P}(\phi_1)\cdot\mathbf{E}_A = T(A,\phi_1)\begin{pmatrix}\cos\phi_1\\ \sin\phi_1\end{pmatrix}, \tag{5.9}$$

$$\mathbf{E}_C = \mathbf{C}(-\pi/2, \phi_1 - \pi/4)\cdot\mathbf{E}_B = T(A,\phi_1)e^{-\mathrm{i}\phi_1}\begin{pmatrix}1/\sqrt{2}\\ \mathrm{i}/\sqrt{2}\end{pmatrix}, \tag{5.10}$$

$$\mathbf{E}_D = \mathbf{P}(\phi_2)\cdot\mathbf{E}_C = T(A,\phi_1)e^{\mathrm{i}(\phi_2-\phi_1)}\begin{pmatrix}\cos\phi_2\\ \sin\phi_2\end{pmatrix}, \tag{5.11}$$

$$\mathbf{E}_E = \mathbf{C}(\pi/2, \phi_2 - \pi/4)\cdot\mathbf{E}_D = T(A,\phi_1)e^{\mathrm{i}(2\phi_2-\phi_1)}\begin{pmatrix}1/\sqrt{2}\\ -\mathrm{i}/\sqrt{2}\end{pmatrix}, \tag{5.12}$$

where

$$T(A,\phi_1) = \frac{\cos\alpha_A\cos\phi_1 + \sin\alpha_A e^{\mathrm{i}\theta_A}\sin\phi_1}{|\cos\alpha_A\cos\phi_1 + \sin\alpha_A e^{\mathrm{i}\theta_A}\sin\phi_1|} \tag{5.13}$$

is the (normalized) projection of the initial state A onto the state $(\cos\phi_1, \sin\phi_1)^T$. Although in general the output produced by a compensator is not in phase with the input, it is easily verified with the help of Eqs. (5.4) and (5.5) that in this example all consecutive states are indeed in phase. Hence it follows from Eq. (5.12), that we can identify the quantity

$$\Psi = \arg[T(A,\phi_1)e^{\mathrm{i}(2\phi_2-\phi_1)}] \tag{5.14}$$

as the geometric phase of the final state E. When a beam in this state is combined with a beam in state A, the intensity equals [cf. Eq. (5.3)]

$$\begin{aligned} |\mathbf{E}_A|^2 + |\mathbf{E}_E|^2 + 2\,\mathrm{Re}(\mathbf{E}_A \cdot \mathbf{E}_E^*) = 1 + |T(A,\phi_1)|^2 \\ + 2H(A,\phi_1)\cos(2\phi_2 - \phi_1 + \phi_H), \end{aligned} \tag{5.15}$$

where

$$H(A,\phi_1)e^{\mathrm{i}\phi_H} = T^*(A,\phi_1)\mathbf{E}_A \cdot \begin{pmatrix} 1/\sqrt{2} \\ \mathrm{i}/\sqrt{2} \end{pmatrix}, \tag{5.16}$$

and with $H(A,\phi_1) \in \mathbb{R}^+$. In the next section we investigate the dependence of the geometric phase of the final state E on the initial state A, and as a function of the two orientation angles ϕ_1 and ϕ_2, and experimentally test our predictions.

5.3 Experimental method

The above sequence of polarization changes can be realized with a Mach-Zehnder interferometer (see Fig. 5.2). The output of a He-Ne laser operating at 632.8 nm is divided into two beams. The beam in one arm passes through a linear polarizer and a quarter-wave plate. This produces state A. By rotating the plate, this initial polarization state can be varied. Next the field passes through a polarizer $P(\phi_1)$ that creates state B, and a compensator C_1, resulting in state C. A polarizer $P(\phi_2)$ produces state D, and a compensator C_2 creates the final state E. The elements $P(\phi_1), C_1$ and $P(\phi_2), C_2$ are joined pairwise to ensure that their relative orientation remains fixed when the angles ϕ_1 and ϕ_2 are varied, and the resulting states are circularly polarized. The field in the other arm is attenuated by a gray filter in order to increase the sharpness of the fringes. The fields in both arms are combined, and the ensuing interference pattern is detected with the help of a detector. Both a photodiode and a CCD camera are used.

On varying the angle ϕ_2, the intensity in the upper arm of Fig. 5.2 remains unchanged and the changes in the diffraction pattern can be recorded with a photodiode. However, when the angle ϕ_1 is varied, the intensity in that arm changes. The shape of the interference pattern then changes as well, and the geometric phase can only be observed by measuring a shift of the *entire* pattern with a CCD camera [Wagh and Rakhecha, 1995].

One has to make sure that rotating the optical elements does not affect the optical path length and introduces an additional dynamic phase. This was achieved by an alignment procedure in which the invariance of the interference pattern for 180° rotations of the linear polarizers was exploited. Mechanical vibrations were minimized by remotely controlling the optical elements.

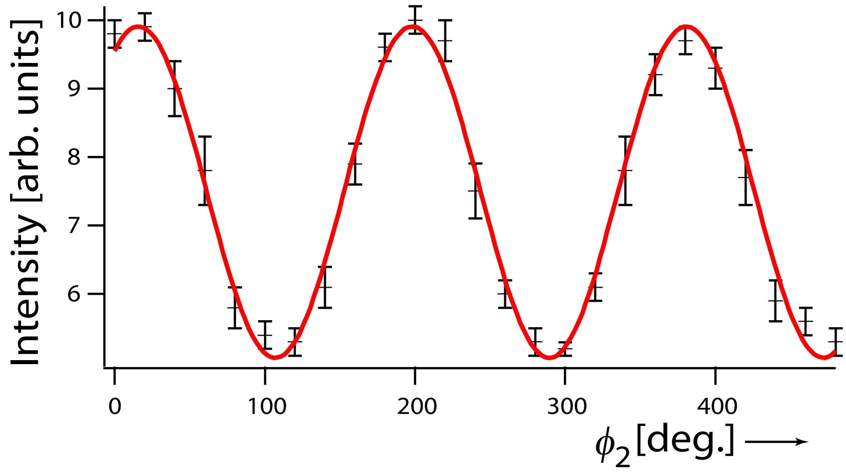

Figure 5.3: Measured intensity as a function of the orientation angle ϕ_2. The solid curve is a fit of the measured data to the function $C_1 + C_2 \cos(2\phi_2 + C_3)$. The vertical symbols indicate error bars.

5.4 Experimental results

The dependence of the geometric phase of the final state E on the orientation angles ϕ_1 and ϕ_2 of the two polarizers is markedly different. It is seen from Eq. (5.14) that the phase is proportional to ϕ_2. This linear behavior is illustrated in Fig. 5.3 in which the intensity observed with a photodiode is plotted as a function of the angle ϕ_2. The solid curve is a fit of the data to the function $C_1 + C_2 \cos(2\phi_2 + C_3)$, with C_1, C_2 and C_3 all constants [cf. Eq. (5.15)]. The excellent agreement between the measurements and the fitted curve show that the geometric phase Ψ indeed increases twice as fast as the angle ϕ_2.

In order to investigate the change $\Delta\Psi$ when the angle ϕ_1 is varied from 0° to 180° (after which the polarizer returns to its original state), let us first assume that the initial state A coincides with the north pole (i.e., $\alpha_A = \pi/4, \theta_A = -\pi/2$). In that case the path on the Poincaré sphere is closed and we find from Eq. (5.14) that $\Psi = 2(\phi_2 - \phi_1)$. The solid angle of the traversed path is now $4(\phi_2 - \phi_1)$. Thus we see that in that case we retrieve Pancharatnam's result that the acquired geometric

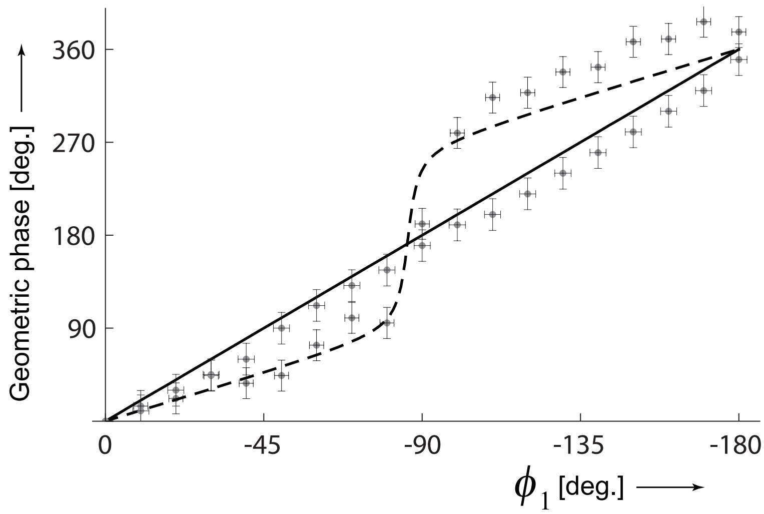

Figure 5.4: Geometric phase of the final state E when the initial state A coincides with the north pole (solid curve), and when A lies between the equator and the north pole (dashed curve), both as a function of the orientation angle ϕ_1. The curves are theoretical predictions [Eq. (5.14)], the dots and error bars represent measurements. In this example $\phi_2 = 0$.

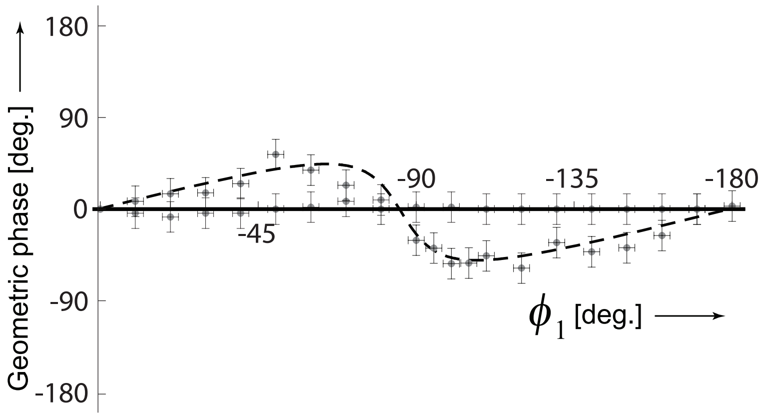

Figure 5.5: Geometric phase of the final state E when the initial state A coincides with the south pole (solid curve), and when A lies between the equator and the south pole (dashed curve), both as a function of the orientation angle ϕ_1. The curves are theoretical predictions [Eq. (5.14)], the dots and error bars represent measurements. In this example $\phi_2 = 0$.

phase for a closed circuit equals half the solid angle of the circuit subtended at the sphere's origin. Hence, on rotating ϕ_1 over 180°, the accrued geometric phase $\Delta\Psi$ equals 360°. This predicted behavior is indeed observed, see Fig. 5.4 (blue curve). For an arbitrary initial state on the northern hemisphere [in this example, with Stokes vector $(0.99, -0.14, 0.07)$] the behavior is nonlinear, but again we find that $\Delta\Psi = 360°$ after the first polarizer has been rotated over 180°, see Fig. 5.4 (red curve).

Let us next assume that the initial state A coincides with the south pole ($\alpha_A = \pi/4, \theta_A = \pi/2$). In that case, Eq. (5.14) yields $\Psi = 2\phi_2$. Since this is independent of ϕ_1, a rotation of ϕ_1 over 180° results in $\Delta\Psi = 0°$. This corresponds to the blue curve in Fig. 5.5. For an arbitrary initial state on the southern hemisphere [in this example, with Stokes vector $(0.93, 0.23, -0.28)$] the geometric phase does vary with ϕ_1, but again $\Delta\Psi = 0°$ after a 180° rotation of the polarizer $P(\phi_1)$, see Fig. 5.5 (red curve). So, depending on the initial polarization state A, topologically different types of behavior can occur, with either $\Delta\Psi = 0°$ or $\Delta\Psi = 360°$ after half a rotation of the polarizer $P(\phi_1)$. This implies that on moving the state A across the Poincaré sphere a continuous change from one type of behavior to another is not possible. A discontinuous change in behavior can only occur when the geometric phase Ψ is singular. This happens when the first state A and the second state B are directly opposite to each other on the Poincaré sphere (and form a pair of "anti-podal points"). They are then orthogonal and the phase of the final state E is singular [Nye, 1999]. Indeed, when the state A lies on the equator ($\theta_A = 0$) then $\Psi = 2\phi_2 - \phi_1$, or $\Psi = 2\phi_2 - \phi_1 + \pi$, except when A and B are

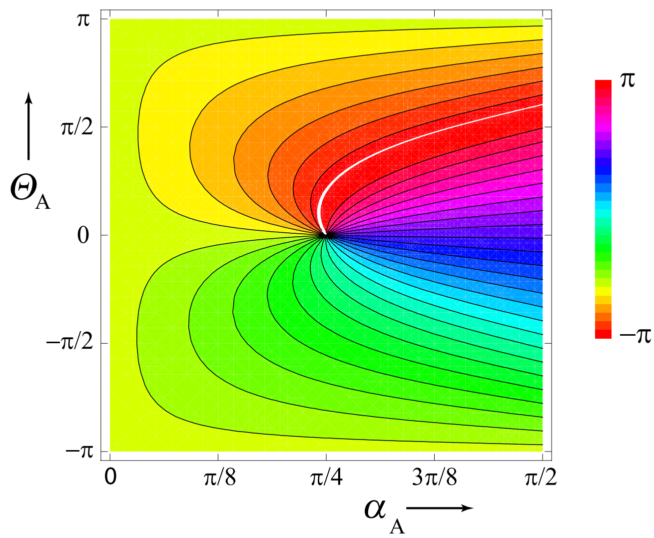

Figure 5.6: Color-coded plot of the phase of the final state E as a function of the initial state A as described by the two parameters α_A and θ_A [cf. Eq. (5.1)]. In this example $\phi_1 = 3\pi/4$, and $\phi_2 = 1.8$.

opposite. In that case Ψ is singular and undergoes a π phase jump. In Fig. 5.6 this occurs for the point ($\alpha_A = \pi/4, \theta_A = 0$) at which all the different phase contours intersect. In other words, when A moves across the equator, the geometric phase as a function of the angle ϕ_1 is singular and a transition from one type of behavior (with $\Delta\Psi = 360°$) to another type (with $\Delta\Psi = 0°$) occurs. This singular behavior, resulting in a 180° discontinuity of the geometric phase was indeed observed, see Fig. 5.7. Notice that although the depicted jump equals 180°, in our experiment it cannot be discerned from a −180° discontinuity. Whereas a positive jump results in $\Delta\Psi = 360°$ after a 180° rotation of the first polarizer, a negative jump yields $\Delta\Psi = 0°$. In that sense the singular behavior forms an intermediate step between the two dependencies shown in Figs. 5.4 and 5.5.

The ability to produce a 180° phase jump by means of a much smaller variation in ϕ_1 can be employed to cause a change from constructive interference to deconstructive interference when the beam is combined with a reference beam. Clearly, such a scheme can be used for fast optical switching [Papadimitriou et al., 2007].

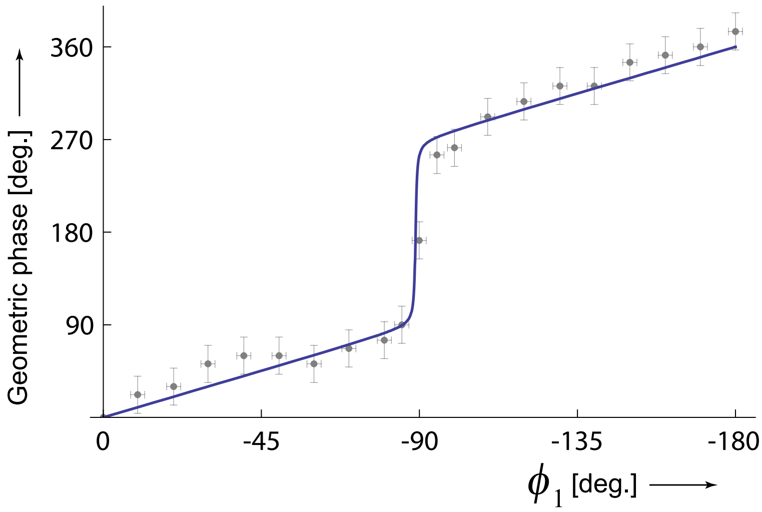

Figure 5.7: Singular behavior of the geometric phase of the final state E when the initial state A lies on the equator, as a function of the orientation angle ϕ_1. The solid curve is a theoretical prediction [Eq. (5.14)], the dots and error bars represent measurements. In this example $\theta_A = 0.27$, $\alpha_A = 0.0$ and $\phi_2 = 0$.

5.5 Conclusions

In summary, we have presented a new Mach-Zehnder type setup with which the geometric phase that accompanies non-cyclic polarization changes can be observed. The geometric phase can exhibit linear, nonlinear or singular behavior. Excellent agreement between the predicted and observed behavior was obtained.

Chapter 6

Geometric interpretation of the Pancharatnam connection and non-cyclic polarization changes

This Chapter is based on the following publication:

- T. van Dijk, H.F. Schouten and T.D. Visser "Geometric interpretation of the Pancharatnam connection and non-cyclic polarization changes", J. Opt. Soc. Am. A vol. 27, 1972–1976 (2010).

Abstract
If the state of polarization of a monochromatic light beam is changed in a cyclical manner, the beam acquires–in addition to the usual dynamic phase–a *geometric phase*. This geometric or *Pancharatnam-Berry phase*, equals half the solid angle of the contour traced out on the Poincaré sphere. We show that such a geometric interpretation also exists for the *Pancharatnam connection*, the criterion according to which two beams with different polarization states are said to be in phase. This interpretation offers a new and intuitive method to calculate the geometric phase that accompanies non-cyclic polarization changes.

In 1984 Berry pointed out that a quantum system whose parameters are cyclically altered does not return to its original state but acquires, in addition to the usual dynamic phase, a so-called geometric phase [Berry, 1984]. It was soon realized that such a phase is not just restricted to quantum systems, but also occurs in contexts such as Foucault's pendulum [Berry, 1990]. Also the polarization phenomena described by Pancharatnam [1956] represent one of its manifestations. The polarization properties of a monochromatic light beam can be represented by a point on the Poincaré sphere [Born and Wolf, 1999]. When, with the help of optical elements such as polarizers and retarders, the state of polarization is made to trace out a closed contour on the sphere, the beam acquires a geometric phase. This *Pancharatnam-Berry phase*, as it is nowadays called, is equal to half the solid angle of the contour subtended at the origin of the sphere [Berry, 1987; Bhandari, 1997; Hariharan, 2005; Bhandari and Samuel, 1988; Bomzon et al., 2002; Biener et al., 2006].

In this work we show that such a geometric relation also exists for the so-called *Pancharatnam connection*, the criterion according to which two beams with different polarization states are in phase, i.e., their superposition produces a maximal intensity. This relation can be extended to arbitrary (e.g., non-closed) paths on the Poincaré sphere, and allows us to study how the phase builds up for such non-cyclic polarization changes. Our work offers an geometry-based alternative, to the algebraic work presented in Refs. [Samuel and Bhandari, 1988; Jordan, 1988].

The state of polarization of a monochromatic beam can be represented as a two-dimensional Jones vector [Jones, 1941] with respect to an orthonormal basis $\{\hat{\mathbf{e}}_1, \hat{\mathbf{e}}_2\}$, as

$$\mathbf{E} = \cos\alpha\,\hat{\mathbf{e}}_1 + \sin\alpha\exp(\mathrm{i}\theta)\,\hat{\mathbf{e}}_2, \tag{6.1}$$

with $0 \leq \alpha \leq \pi/2$; $-\pi \leq \theta \leq \pi$, and $\hat{\mathbf{e}}_i \cdot \hat{\mathbf{e}}_j = \delta_{ij}, (i,j = 1,2)$. The angle α is a measure of the relative amplitudes of the two components of the electric vector $\mathbf{E}$, and the angle θ denotes their phase difference. Two different states of polarization, A and B, can hence be written as

$$\mathbf{E}_A = \left(\cos\alpha_A, \sin\alpha_A e^{\mathrm{i}\theta_A}\right)^T, \tag{6.2}$$

$$\mathbf{E}_B = e^{\mathrm{i}\gamma_{AB}}\left(\cos\alpha_B, \sin\alpha_B e^{\mathrm{i}\theta_B}\right)^T. \tag{6.3}$$

Since only relative phase differences are of concern, the overall phase of $\mathbf{E}_A$ in Eq. (6.2) is taken to be zero. According to Pancharatnam's connection [Berry, 1987] these two states are in phase when their superposition yields a maximal intensity, i.e., when

$$|\mathbf{E}_A + \mathbf{E}_B|^2 = |\mathbf{E}_A|^2 + |\mathbf{E}_B|^2 + 2\,\mathrm{Re}(\mathbf{E}_A \cdot \mathbf{E}_B^*) \tag{6.4}$$

reaches its greatest value, implying that

$$\mathrm{Im}\,(\mathbf{E}_A \cdot \mathbf{E}_B^*) = 0, \tag{6.5}$$

$$\mathrm{Re}\,(\mathbf{E}_A \cdot \mathbf{E}_B^*) > 0. \tag{6.6}$$

These two conditions uniquely determine the phase γ_{AB}, except when the states A and B are orthogonal.

Let us now consider a sequence of three polarization states with each succesive state being in phase with its predecessor. As the initial state we take the basis-state X with Jones vector $\mathbf{E}_X = (1,0)^T$. It follows immediately that *any polarization state A with Jones vector $\mathbf{E}_A$ as defined by Eq. (6.2) is in phase with X.* Consider now a third state B. This state is in phase with A provided that the angle γ_{AB} in Eq. (6.3) satifies the relations (6.5) and (6.6). Clearly, B is not in phase with X, but rather with $e^{i\gamma_{AB}}X$. Apparently the total geometric phase that is accrued by following the closed circuit XAB equals γ_{AB}. This observation allows us to make use of Pancharatnam's classic result which relates the accumulated geometric phase to the solid angle of the geodesic triangle XAB [Pancharatnam, 1956]. According to this result then, the angle (phase) γ_{AB} between the states A and B for which they are in phase is given by half the solid angle Ω_{XAB} of the triangle XAB subtended at the center of the Poincaré sphere, i.e.,

$$\gamma_{AB} = \Omega_{XAB}/2. \tag{6.7}$$

The solid angle Ω_{XAB} is taken to be positive (negative) when the the circuit XAB is traversed in a counter-clockwise (clockwise) manner. Thus we have $-2\pi \leq \Omega_{XAB} \leq 2\pi$, and hence $-\pi \leq \gamma_{AB} \leq \pi$. Hence we arrive at the following geometric interpretation of Pancharatnam's connection: *The phase γ_{AB} for which the superposition of two beams with polarization states A and B yields a maximum intensity, equals half the solid angle subtended by their respective Stokes vectors and the Stokes vector corresponding to the basis-state X.* We emphasize that γ_{AB} is defined with respect to a certain basis. We return to this point later.

Several consequences follow from the geometric interpretation. First, consider a state B that lies on the great circle through the points A and X. As illustrated in Fig. 6.1, two cases can be distinguished. If B is not on the geodesic that connects $-A$ and $-X$, then the curves XA, AB and BX cancel each other [see panel (a)], i.e., $\gamma_{AB} = \Omega_{XAB}/2 = 0$. If B does lie on the geodesic connecting $-A$ and $-X$ [see panel (b)], then these three curves together constitute the entire great circle and hence $\gamma_{AB} = \Omega_{XAB}/2 = \pi$. Consequently, we arrive at

Corollary 1 *All polarization states that lie on the great circle that runs through A and X and which are not part of the geodesic curve that connects $-A$ and $-X$ are in phase with state A. All other states on the great circle are out of phase with state A.*

(We exlude the pathological case $A = \pm X$.)

The great circle through A and X divides the Poincaré sphere into two hemispheres. For all states B on one hemisphere, the path XAB runs clockwise. For B on the other hemisphere, the path XAB runs counter-clockwise. Thus we find

Corollary 2 *The great circle that runs through A and X divides the Poincaré sphere into two halves, one on which all states have a positive phase with respect to A, and one on which all states have a negative phase with respect to A.*

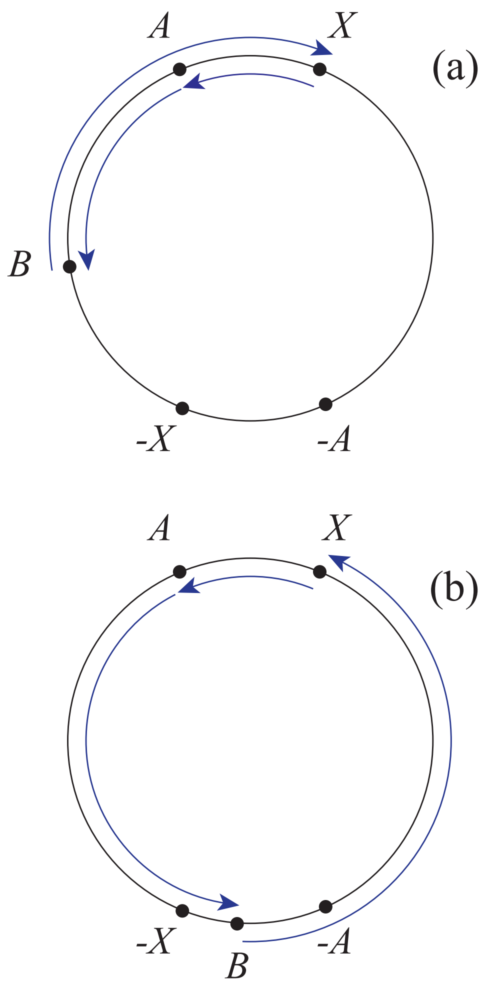

Figure 6.1: The great circle through A, B and basis state X. If state B does not lie on the segment between $-A$ and $-X$ [panel (a)], then the sum of the three geodesics XA, AB and BX is zero. If B lies on the segment between $-A$ and $-X$ [panel (b)], then the sum of the three geodesics equals the great circle.

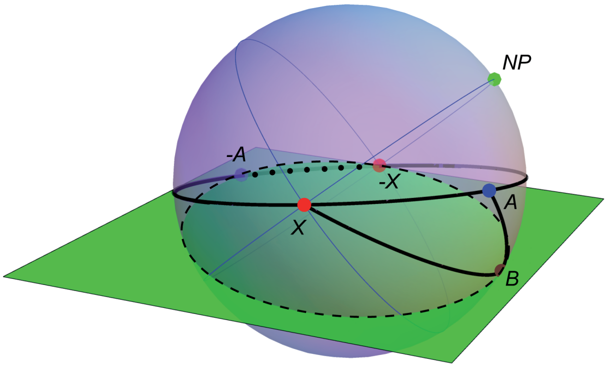

Figure 6.2: Illustrating the intersection of the plane given by Eq. (6.10) and the Poincaré sphere. This intersection is a circle (indicated by the dashed curve) that runs through the points $-A$, $-X$ and B. All points on the circle segment that runs from $-A$ to B to $-X$ constitute the set $\{B'\}$ of states that have the same phase difference γ_{AB} with respect to A as the state B. The great circle through A and X is shown solid-dotted. The point NP indicates the North Pole.

Thus far we not specified the basis vectors in which the Jones vectors are expressed. The two most commonly used are the cartesian representation and the helicity representation. The Stokes vector corresponding to the basis-state X is $(1, 0, 0)$ and $(0, 0, 1)$ in these two bases, respectively. Our results so far are valid for any choice of representation. For computational ease, however, we will from now on make use of the cartesian basis.

Given two different polarization states A and B, we may enquire about the set $\{B'\}$ of all states which have the same phase difference γ_{AB} with respect to A as B has. We begin by noticing that the solid angle Ω_{ABC} subtended at the origin of the Poincaré sphere by three unit vectors **A**, **B** and **C** satisfies the equation [Eriksson, 1990]

$$\tan\left(\frac{\Omega_{ABC}}{2}\right) = \frac{\mathbf{A}\cdot(\mathbf{B}\times\mathbf{C})}{1+\mathbf{B}\cdot\mathbf{C}+\mathbf{A}\cdot\mathbf{C}+\mathbf{A}\cdot\mathbf{B}}. \tag{6.8}$$

On taking **A**, **B** and **C** as the Stokes vectors corresponding to states A, B, and X, i.e., $\mathbf{C} = (1, 0, 0)$, Eqs. (6.7) and (6.8) yield

$$\tan\gamma_{AB} = \frac{A_yB_z - A_zB_y}{1+B_x+A_x+A_xB_x+A_yB_y+A_zB_z}. \tag{6.9}$$

For γ_{AB} and **A** fixed, we thus find that the three components of **B** must satisfy the relation

$$c_xB_x + c_yB_y + c_zB_z + D = 0, \tag{6.10}$$

with the coefficients c_x, c_y, c_z and D given by

$$c_x = \tan\gamma_{AB}(1 + A_x), \tag{6.11}$$

$$c_y = \tan\gamma_{AB}A_y + A_z, \tag{6.12}$$

$$c_z = \tan\gamma_{AB}A_z - A_y, \tag{6.13}$$

$$D = c_x. \tag{6.14}$$

The solutions of Eq. (6.10) form a plane. In addition, the vector $\mathbf{B}$ must be of unit length, ensuring that it lies on the Poincaré sphere. The intersection of the plane and the sphere is a circle that runs through B. Finding two other point on this circle defines it uniquely. It can be verified by substitution that the Stokes vectors $-\mathbf{A}$ and $-\mathbf{X}$ both satisfy Eq. (6.10). Hence, for all states on the circle that runs through B, $-A$ and $-X$, the phase γ_{AB} has the same value, mod π. Since the plane defined by Eq. (6.10) does, in general, not include the origin of the Poincaré sphere, this circle is not a great circle. This is illustrated in Fig. 6.2, where the circle through B is drawn dashed. The dashed circle intersects the great circle through A and X at the points $-A$ and $-X$. According to Corollary 2, γ_{AB} changes sign at these points. Since Eq. (6.9) defines the phase modulo π, it follows that γ_{AB} undergoes a π phase jump at these points. We thus arrive at

Corollary 3 *Consider the circle through $-A$, $-X$ and B. It consists of two segments, both with endpoints $-A$ and $-X$. The segment which includes B equals the set $\{B'\}$ of states such that $\gamma_{AB'} = \gamma_{AB}$. The other segment represents states for which $\gamma_{AB'} = \gamma_{AB} \pm \pi$.*

It can be shown that the plane-sphere intersection is always a circle, and not just a single point, if the pathological case $A = \pm X$ is excluded. If, for a fixed state A, the state B is being varied, the plane given by Eq. (6.10) rotates along the line connecting $-A$ and $-X$.

We now demonstrate how our geometric interpretation implies that for a fixed state A the phase γ_{AB} may vary in different ways when the state B is moved across the Poincaré sphere. We specify the position of B by spherical coordinates (ϕ, θ), where $0 \leq \phi \leq 2\pi$ and $0 \leq \theta \leq \pi$ represent the azimuthal angle and the angle of inclination, respectively. If A is taken to be at the south pole and $B = B(\phi)$ lies on the equator, then

$$\gamma_{AB} = \frac{\Omega_{XAB}}{2} = \frac{1}{2}\int_{\pi/2}^{\pi}\int_{0}^{\phi} \sin\theta \, \mathrm{d}\phi' \mathrm{d}\theta = \frac{1}{2}\phi. \tag{6.15}$$

Clearly, the phase varies linearly with the angle ϕ in this case.

Let us now consider the contours of equal phase γ_{AB} as shown in Fig. 6.3. It is seen that the intersections of the contours with the equator are not equidistant. Hence in this case the phase depends in a non-linear way on the angle ϕ.

The singular behavior, finally, of the phase is a direct consequence of the fact that two anti-podal states A and $-A$ do not interfere with each other [see the

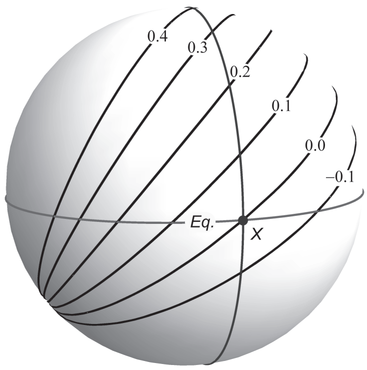

Figure 6.3: Selected contours of the phase γ_{AB} for the case $\mathbf{A} = (0, 0.8, 0.6)$. The basis-state X, the equator ($Eq.$) and the meridian through X are also shown.

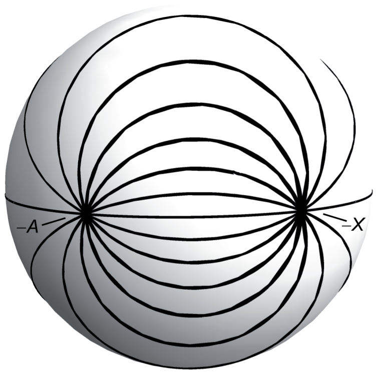

Figure 6.4: Contours of equal phase of γ_{AB} for the case that the state A is taken to be $(0.6, 0, 0.8)$. Two singular points with opposite topological charge can be seen at $-A$ and $-X$.

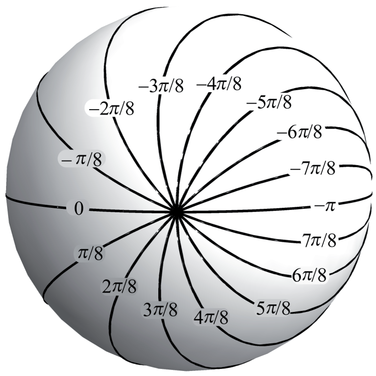

Figure 6.5: Contours of equal phase of γ_{AB} for the case that the state A is taken to be $(0,0,1)$. The singularity at $-A$ is seen to have topological charge $+1$.

remark below Eq. (6.6)]. From Eq. (6.8) it follows that the phase is antisymmetric under the interchange of the points $\mathbf{C} = \mathbf{X}$ and $\mathbf{A}$. Hence we expect two singular points, namely $-A$ and $-X$, with opposite topological charge (± 1). This is illustrated in Figs. 6.4 and 6.5. We note that the existence of singular points is in agreement with the "Hairy Ball Theorem" due to Brouwer [Brouwer, 1912], according to which there is no nonvanishing continuous tangent vector field on a sphere in $\mathbb{R}^3$. This implies that $\nabla\gamma_{AB}$ has at least one zero, in this case at the two singularities.

Let us now apply our results for the Pancharatnam connection to study the geometric phase for an arbitrary, i.e. non-closed, path ABC on the Poincaré sphere. The successive states are assumed to be in phase. Therefore the geometric phase accumulated on this path equals

$$\begin{aligned} \gamma_{ABC} \equiv \gamma_{AB} + \gamma_{BC} &= (\Omega_{XAB} + \Omega_{XBC})/2, \\ &= \Omega_{XABC}/2, \end{aligned} \tag{6.16}$$

where Ω_{XABC} is the *generalized solid angle* of the path $X \to A \to B \to C \to X$. Ω_{XABC} can consist of two triangles (see Fig. 6.6), whose contribution is positive or negative depending on their handedness.

Now we keep states A and C fixed, and study how the geometric phase γ_{ABC} changes when state B is varied. We will show that this change, in contrast to γ_{AB}, is independent of the choice of basis vectors. Consider the phase γ'_{ABC} in a non-cartesian basis (for example, the helicity basis) whose first basis state we call N. We then have, in analogy to Eq. (6.16),

$$\begin{aligned} \gamma'_{ABC} \equiv \gamma'_{AB} + \gamma'_{BC} &= (\Omega_{NAB} + \Omega_{NBC})/2, \\ &= \Omega_{NABC}/2. \end{aligned} \tag{6.17}$$

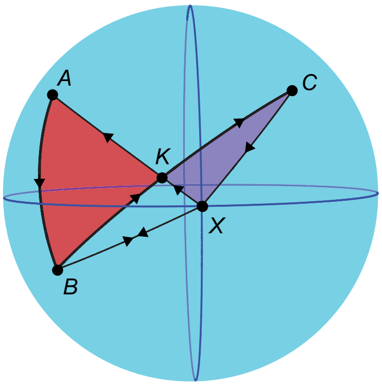

Figure 6.6: Illustrating the generalized solid angle Ω_{XABC}. In going from state A to state B, the beam acquires a geometric phase equal to half the solid angle Ω_{XAB}, which is positive. In going from B to C the acquired phase equals half the solid angle Ω_{XBC}, which is negative. Since the triangle BKX does not contribute, this is equivalent to the generalized solid angle Ω_{XABC}, which equals half the solid angle of the triangle ABK (positive), plus half the solid angle of the triangle XKC (negative).

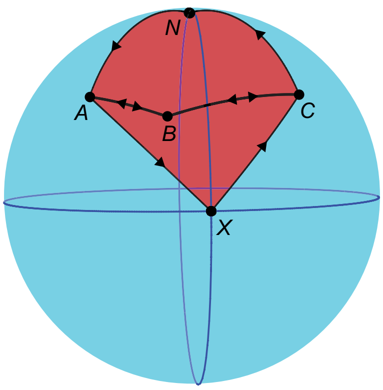

Figure 6.7: Illustrating the equality $\Omega_{NABC} + \Omega_{CBAX} = \Omega_{NAXC}$. Such a construction can be made for any choice of states.

Also,

$$\Omega_{NABC} - \Omega_{XABC} = \Omega_{NABC} + \Omega_{CBAX} = \Omega_{NAXC}. \tag{6.18}$$

The justification of the last step of Eq. (6.18) is illustrated in Fig. 6.7. It follows on using Eqs. (6.16)–(6.18) that

$$\gamma'_{ABC} - \gamma_{ABC} = \Omega_{NAXC}/2. \tag{6.19}$$

The term $\Omega_{NAXC}/2$ is a constant, independent of B, i.e. the geometric phase in both reprensentations differs by a constant only. Hence the variation of the geometric phase with B is independent of the choice of the basis, as it should be for an observable quantity. This is in contrast to γ_{AB}, which explicitly depends on the choice of basis, as is evident from Eqs. (6.2–6.3).

The behavior of γ_{ABC} on varying B can be linear [Chyba et al., 1988], non-linear [Schmitzer et al., 1993] or singular [Bhandari, 1992a,b; van Dijk et al., 2010a], as we have also shown for γ_{AB}. However γ_{AB} has singularities at $B = -A$ and $B = -X$. The first is due to the orthogonality of A and $-A$, while the second is a consequence of the choice of representation. The phase γ_{ABC} is singular only at $B = -A$ and $B = -C$, and not at $B = -X$.

In conclusion, we have shown how the Pancharatnam connection may be interpreted geometrically. Our work offers an geometry-based approach to calculate the Pancharatnam-Berry phase associated with non-cyclic polarization changes. As such it is an alternative to the algebraic treatments presented in [Samuel and Bhandari, 1988] and [Jordan, 1988]. Our approach can be extended to the description of geometric phases in quantum mechanical systems.

Chapter 7

Effects of spatial coherence on the angular distribution of radiant intensity generated by scattering on a sphere

This Chapter is based on the following publication:

- T. van Dijk, D.G. Fischer, T.D. Visser and E. Wolf, "Effects of spatial coherence on the angular distribution of radiant intensity generated by scattering on a sphere",
  Phys. Rev. Lett. vol. 104, 173902 (2010).

Abstract
In the analysis of light scattering on a sphere it is implicitely assumed that the incident field is spatially fully coherent. However, under usual circumstances the field is partially coherent. We generalize the partial waves expansion method to this situation and examine the influence of the degree of coherence of the incident field on the the radiant intensity of the scattered field in the far zone. We show that when the coherence length is comparable to or is smaller than the radius of the sphere, the angular distribution of the radiant intensity depends strongly on the degree of coherence. The results have implications for, for example, scattering in the atmosphere and colloidal suspensions.

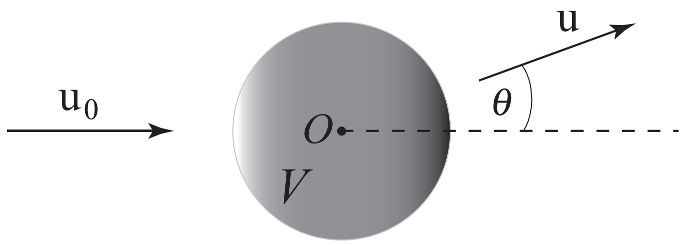

Figure 7.1: Illustrating the notation. The origin O is taken at the center of the sphere.

In the usual description of light scattering by a homogeneous sphere (the scalar analogue of the well-known Mie scattering) it is generally assumed that the incident field is spatially fully coherent [Mie, 1908; van de Hulst, 1957; Born and Wolf, 1999; Nussenzveig, 1992; Grandy Jr., 1992]. In practice, this assumption is not always justified. Examples are fields generated by multi-mode lasers, and fields that have passed through a random medium such as the turbulent atmosphere. Hardly any studies have been devoted to this more general case (see, however [Wolf, 2007]). The extinguished power due to scattering of random fields on a random medium has been analyzed in [Carney et al., 1997] and [Carney and Wolf, 1998], and certain reciprocity relations for cases of this kind were derived in [Visser et al., 2006]. The extinguished power from scattering a random field on deterministic media was discussed in [Cabaret et al., 1998] and [Greffet et al., 2003]. However, the influence of the state of coherence of the incident field on the angular distribution of the scattered field seems to have been studied only in two publications [Jannson et al., 1988; Gori et al., 1990].

In this Letter we analyze the scattering of a wide class of beams of any state of coherence on a homogeneous spherical scatterer, namely beams of the well-known Gaussian Schell-model class (see [Mandel and Wolf, 1995, Sec. 5.6.4]). We present numerical examples that show how the effective spectral coherence length (i.e., the coherence length at a fixed frequency) of the incident beam affects the angular distribution of the radiant intensity of the scattered field.

Let us first consider a plane, monochromatic scalar wave of unit amplitude, propagating in a direction specified by a real unit vector $\mathbf{u}_0$, incident on a deterministic, spherical scatterer occupying a volume V (see Fig. 7.1):

$$V^{(i)}(\mathbf{r}, t) = U^{(i)}(\mathbf{r}, \omega) \exp(-\mathrm{i}\omega t), \tag{7.1}$$

where

$$U^{(i)}(\mathbf{r}, \omega) = \exp(\mathrm{i}k\mathbf{u}_0 \cdot \mathbf{r}). \tag{7.2}$$

Here $\mathbf{r}$ denotes the position vector of a point in space, t the time, and ω the angular frequency. Also, $k = \omega/c = 2\pi/\lambda$ is the wavenumber, c being the speed of light in vacuum and λ denotes the wavelength. The time-independent part $U(\mathbf{r},\omega)$ of the total field that results from scattering of the plane wave on a sphere may be expressed as the sum of the incident field $U^{(i)}(\mathbf{r},\omega)$ and the scattered field $U^{(s)}(\mathbf{r},\omega)$, viz.,

$$U(\mathbf{r},\omega) = U^{(i)}(\mathbf{r},\omega) + U^{(s)}(\mathbf{r},\omega). \tag{7.3}$$

The scattered field in the far-zone of the scatterer, at an observation point $\mathbf{r} = r\mathbf{u}$ ($\mathbf{u}^2 = 1$) is given by the asymptotic formula

$$U^{(s)}(r\mathbf{u},\omega) \sim f(\mathbf{u},\mathbf{u}_0,\omega)\frac{e^{\mathrm{i}kr}}{r}, \qquad (kr \to \infty,\ \mathbf{u} \text{ fixed}), \tag{7.4}$$

where $f(\mathbf{u},\mathbf{u}_0,\omega)$ denotes the *scattering amplitude*.

Next consider the situation where the incident field is not a plane wave but is of a more general form. Such a field may be represented as an *angular spectrum* of plane waves propagating into the half-space $z > 0$, i.e. [Mandel and Wolf, 1995, Sec. 3.2]

$$U^{(i)}(\mathbf{r},\omega) = \int_{|\mathbf{u}'_\perp|^2 \le 1} a(\mathbf{u}'_\perp,\omega)e^{\mathrm{i}k\mathbf{u}'\cdot\mathbf{r}}\,\mathrm{d}^2u'_\perp, \tag{7.5}$$

where $\mathbf{u}'_\perp = (u'_x, u'_y)$ is a real two-dimensional vector, and evanescent waves have been omitted. The scattered field in the far zone can then be expressed in the form

$$U^{(s)}(r\mathbf{u},\omega) = \frac{e^{\mathrm{ikr}}}{r}\int_{|\mathbf{u}'_\perp|^2 \le 1} a(\mathbf{u}'_\perp,\omega)f(\mathbf{u},\mathbf{u}',\omega)\,\mathrm{d}^2u'_\perp. \tag{7.6}$$

Let us next consider the case where the incident field is not deterministic but is stochastic. The *radiant intensity* of the scattered field in a direction specified by a real unit vector $\mathbf{u}$ is given by the formula [Mandel and Wolf, 1995, Eq. (5.2–12)]

$$J_s(\mathbf{u},\omega) \equiv r^2\langle U^{(s)*}(r\mathbf{u},\omega)U^{(s)}(r\mathbf{u},\omega)\rangle \qquad (kr \to \infty), \tag{7.7}$$

which, on using Eq. (7.6) becomes

$$J_s(\mathbf{u},\omega) = \iint \mathcal{A}(\mathbf{u}',\mathbf{u}'',\omega)f^*(\mathbf{u},\mathbf{u}',\omega)f(\mathbf{u},\mathbf{u}'',\omega)\,\mathrm{d}^2u'_\perp\mathrm{d}^2u''_\perp, \tag{7.8}$$

where

$$\mathcal{A}(\mathbf{u}',\mathbf{u}'',\omega) = \langle a^*(\mathbf{u}'_\perp,\omega)a(\mathbf{u}''_\perp,\omega)\rangle \tag{7.9}$$

is the so-called *angular correlation function* [Mandel and Wolf, 1995, Eq. (5.6–48)] of the stochastic field, and the angled brackets denote the ensemble average.

An important class of partially coherent beams (which includes the lowest-order Hermite-Gaussian laser mode) are the so-called *Gaussian Schell-model beams* (see [Mandel and Wolf, 1995, Sec. 5.6.4]). For such beams the *cross-spectral* *density function* in the plane $z = 0$ (the plane which passes through the center of the sphere) has the form

$$W^{(0)}(\boldsymbol{\rho}_1, \boldsymbol{\rho}_2, \omega) = \left[S^{(0)}(\boldsymbol{\rho}_1, \omega)\right]^{1/2} \left[S^{(0)}(\boldsymbol{\rho}_2, \omega)\right]^{1/2} \mu^{(0)}(\boldsymbol{\rho}_1, \boldsymbol{\rho}_2, \omega), \quad (7.10)$$

with

$$S^{(0)}(\boldsymbol{\rho}, \omega) = \langle U^{(0)*}(\boldsymbol{\rho}, \omega) U^{(0)}(\boldsymbol{\rho}, \omega)\rangle, \quad (7.11)$$

representing the *spectral density*, and

$$\mu^{(0)}(\boldsymbol{\rho}_1, \boldsymbol{\rho}_2, \omega) = \frac{\langle U^{(0)*}(\boldsymbol{\rho}_1, \omega) U^{(0)}(\boldsymbol{\rho}_2, \omega)\rangle}{\left[S^{(0)}(\boldsymbol{\rho}_1, \omega) S^{(0)}(\boldsymbol{\rho}_2, \omega)\right]^{1/2}}, \quad (7.12)$$

representing the *spectral degree of coherence* of the field in the plane $z = 0$. Each of the functions on the right-hand side of Eq. (7.10) has a Gaussian form, i.e.

$$S^{(0)}(\boldsymbol{\rho}, \omega) = A_0^2 \exp(-\rho^2/2\sigma_S^2), \quad (7.13)$$

$$\mu^{(0)}(\boldsymbol{\rho}_1, \boldsymbol{\rho}_2, \omega) = \exp[-(\boldsymbol{\rho}_2 - \boldsymbol{\rho}_1)^2]/2\sigma_\mu^2. \quad (7.14)$$

In these formulas $\boldsymbol{\rho}_1 = (x_1, y_1)$ and $\boldsymbol{\rho}_2 = (x_2, y_2)$ are two-dimensional position vectors of points in the $z = 0$ plane, and A_0, σ_S and σ_μ are positive constants that are taken to be independent of position, but may depend on frequency.

The angular correlation function of such a beam may be expressed as a four-dimensional Fourier transform of its cross-spectral density in the plane $z = 0$, viz. [Mandel and Wolf, 1995, Eq. (5.6–49)]

$$\mathcal{A}(\mathbf{u}', \mathbf{u}'', \omega) = \left(\frac{k}{2\pi}\right)^4 \iint_{-\infty}^{+\infty} W^{(0)}(\boldsymbol{\rho}_1, \boldsymbol{\rho}_2, \omega) \times \exp[-\mathrm{i}k(\mathbf{u}''_\perp \cdot \boldsymbol{\rho}_2 - \mathbf{u}'_\perp \cdot \boldsymbol{\rho}_1)]\, \mathrm{d}^2\rho_1 \mathrm{d}^2\rho_2. \quad (7.15)$$

On substituting from Eqs. (7.13) and (7.14) into Eq. (7.15), one obtains for the angular correlation function of a Gaussian Schell-model beam the expression

$$\mathcal{A}(\mathbf{u}', \mathbf{u}'', \omega) = \left(\frac{k^2 A_0 \sigma_S \sigma_{\mathrm{eff}}}{2\pi}\right)^2 \times \exp\left\{-\frac{k^2}{2}\left[(\mathbf{u}'_\perp - \mathbf{u}''_\perp)^2 \sigma_S^2 + (\mathbf{u}'_\perp + \mathbf{u}''_\perp)^2 \frac{\sigma_{\mathrm{eff}}^2}{4}\right]\right\}, \quad (7.16)$$

where

$$\frac{1}{\sigma_{\mathrm{eff}}^2} = \frac{1}{\sigma_\mu^2} + \frac{1}{4\sigma_S^2}. \quad (7.17)$$

In order for the incident field to be beam-like, the parameters σ_S and σ_μ must satisfy the so-called *beam condition* [Mandel and Wolf, 1995, Eq. 5.6–73]

$$\frac{1}{\sigma_\mu^2} + \frac{1}{4\sigma_S^2} \ll \frac{k^2}{2}. \tag{7.18}$$

The scattering amplitude $f(\mathbf{u}', \mathbf{u}'', \omega)$ of the field arising from scattering on a sphere centered on the axis of the beam has the form

$$f(\mathbf{u}', \mathbf{u}'', \omega) = \text{function } (\mathbf{u}' \cdot \mathbf{u}'', \omega) = \text{function } (\cos\theta, \omega), \tag{7.19}$$

where θ denotes the angle between the directions of incidence and scattering (see Fig. 7.1). For a homogeneous spherical scatterer of radius a and of refractive index n, the scattering amplitude can be expressed as [Joachain, 1975, Eq. (4.66)]

$$f(\cos\theta, \omega) = \frac{1}{k}\sum_{l=0}^{\infty}(2l+1)\exp[\mathrm{i}\delta_l(\omega)]\sin[\delta_l(\omega)]\,P_l(\cos\theta), \tag{7.20}$$

where P_l is a Legendre polynomial, and the phase shifts $\delta_l(\omega)$ are given by the expressions (see Secs. 4.3.2 and 4.4.1 of Ref. [Joachain, 1975])

$$\tan[\delta_l(\omega)] = \frac{\overline{k}j_l(ka)j_l'(\overline{k}a) - kj_l(\overline{k}a)j_l'(ka)}{\overline{k}j_l'(\overline{k}a)n_l(ka) - kj_l(\overline{k}a)n_l'(ka)}. \tag{7.21}$$

Here j_l and n_l denote spherical Bessel functions and spherical Neumann functions, respectively, of order l. Furthermore

$$\overline{k} = nk, \tag{7.22}$$

and

$$j_l'(ka) = \left.\frac{dj_l(x)}{dx}\right\rfloor_{x=ka}, \tag{7.23}$$

$$n_l'(ka) = \left.\frac{dn_l(x)}{dx}\right\rfloor_{x=ka}. \tag{7.24}$$

On substituting from Eqs. (7.20) and (7.16) into Eq. (7.8) we obtain for the radiant intensity of the scattered field the expression

$$\begin{aligned} J_s(\mathbf{u}, \omega) = & \left(\frac{kA_0\sigma_S\sigma_{\text{eff}}}{2\pi}\right)^2 \sum_{l=0}^{\infty}\sum_{m=0}^{\infty}(2l+1)(2m+1)e^{\mathrm{i}[\delta_m(\omega)-\delta_l(\omega)]}\sin[\delta_l(\omega)] \\ & \times \sin[\delta_m(\omega)]\iint \exp\left\{-\frac{k^2}{2}\left[(\mathbf{u}_\perp' - \mathbf{u}_\perp'')^2\sigma_S^2 + (\mathbf{u}_\perp' + \mathbf{u}_\perp'')^2\frac{\sigma_{\text{eff}}^2}{4}\right]\right\} \\ & \times P_l(\mathbf{u}\cdot\mathbf{u}')P_m(\mathbf{u}\cdot\mathbf{u}'')\,\mathrm{d}^2u_\perp'\mathrm{d}^2u_\perp''. \end{aligned} \tag{7.25}$$

Let us restrict ourselves to the common situation where the beam width is much greater than the transverse spectral coherence length of the beam, i.e., $\sigma_S \gg \sigma_\mu$. One may then use the asymptotic approximation $k\sigma_S \to \infty$ in two of the four integrations (those over $\mathbf{u}''_\perp$), and apply Laplace's method [Born and Wolf, 1999; Wong, 2001; Lopez and Pagola, 2008], which asserts that for two well-behaved functions $h(x, y)$ and $g(x, y)$

$$\iint_\Omega e^{-ph(x,y)} g(x, y)\,\mathrm{d}x\mathrm{d}y \sim \frac{\pi g(x_0, y_0)}{p\sqrt{\mathrm{Det}\{\mathcal{H}[h(x_0, y_0)]\}}} e^{-ph(x_0,y_0)}, \quad \text{as} \quad p \to \infty, \tag{7.26}$$

where (x_0, y_0) is the point at which $h(x, y)$ attains its smallest value, and $\mathcal{H}[h(x_0, y_0)]$ is the Hessian matrix of $h(x, y)$, evaluated at the point (x_0, y_0), i.e.

$$\mathcal{H}[h(x_0, y_0)] = \begin{pmatrix} \dfrac{\partial^2 h(x,y)}{\partial x^2} & \dfrac{\partial^2 h(x,y)}{\partial x \partial y} \\ \dfrac{\partial^2 h(x,y)}{\partial y \partial x} & \dfrac{\partial^2 h(x,y)}{\partial y^2} \end{pmatrix}_{x=x_0, y=y_0} \tag{7.27}$$

Let us make use of Eq. (7.26) with the choices

$$\begin{aligned} g(\mathbf{u}, \mathbf{u}'_\perp, \mathbf{u}''_\perp) \; &= \; \left(\frac{kA_0\sigma_S\sigma_{\mathrm{eff}}}{2\pi}\right)^2 \sum_{l=0}^{\infty}\sum_{m=0}^{\infty} (2l+1)(2m+1)e^{\mathrm{i}[\delta_\mathrm{m}(\omega)-\delta_\mathrm{l}(\omega)]} \\ &\quad \times \sin[\delta_l(\omega)] \sin[\delta_m(\omega)] \exp\left\{-\frac{k^2\sigma_{\mathrm{eff}}^2}{8}(\mathbf{u}'_\perp + \mathbf{u}''_\perp)^2\right\} \\ &\quad \times P_l(\mathbf{u}\cdot\mathbf{u}')P_m(\mathbf{u}\cdot\mathbf{u}''), \end{aligned} \tag{7.28}$$

$$h(\mathbf{u}'_\perp, \mathbf{u}''_\perp) \; = \; \frac{1}{2}(\mathbf{u}'_\perp - \mathbf{u}''_\perp)^2, \tag{7.29}$$

$$p \; = \; (k\sigma_s)^2. \tag{7.30}$$

The minimum of $h(\mathbf{u}'_\perp, \mathbf{u}''_\perp)$ as a function of $\mathbf{u}''_\perp$ occurs at $u''_x = u'_x$ and $u''_y = u'_y$. The determinant of the Hessian matrix evaluated at this point is readily found to have the value unity. Expression (7.25) for the radiant intensity then reduces to

$$\begin{aligned} J_s(\mathbf{u}, \omega) \; &= \; \frac{A_0^2\sigma_{\mathrm{eff}}^2}{4\pi} \sum_{l=0}^{\infty}\sum_{m=0}^{\infty} (2l+1)(2m+1)e^{\mathrm{i}(\delta_\mathrm{m}-\delta_\mathrm{l})} \sin\delta_l \sin\delta_m \\ &\quad \times \int P_l(\mathbf{u}\cdot\mathbf{u}')P_m(\mathbf{u}\cdot\mathbf{u}')e^{-k^2\sigma_{\mathrm{eff}}^2 u'^2_\perp/2}\,\mathrm{d}^2u'_\perp, \end{aligned} \tag{7.31}$$

where $\mathbf{u}\cdot\mathbf{u}' = \sin\theta\sin\theta'\cos\phi' + \cos\theta\cos\theta'$ in spherical coordinates, and we have made use of the fact that the radiant intensity is rotationally symmetric about the beam axis.

In Fig. 7.2 the radiant intensity (normalized to the radiant intensity in the forward direction), calculated from Eq. (7.31), as a function of the angle of scattering

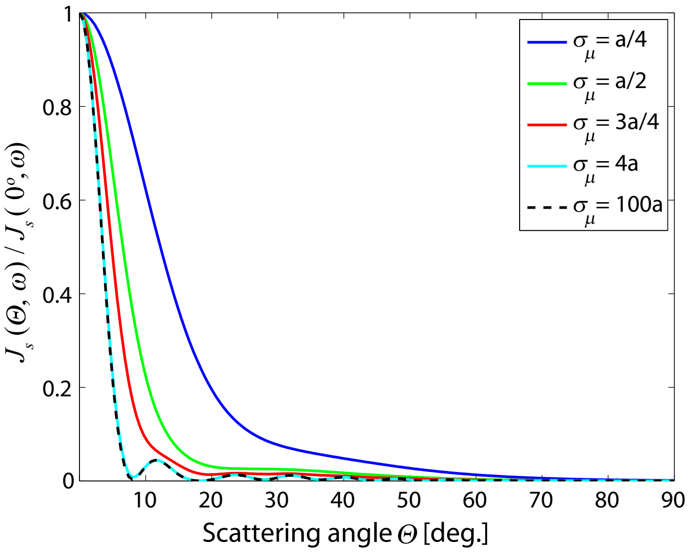

Figure 7.2: (Color on-line) The angular distribution of the normalized radiant intensity $J_s(\theta, \omega)/J_s(0^\circ, \omega)$ of the scattered field for selected values of the transverse spectral coherence length σ_μ of the incident beam, with the choices $a = 4\lambda$ and $n = 1.5$.

θ is shown for selected values of the spectral coherence length σ_μ of the incident field. (For a method to determine σ_μ, see Sec. 4.3.2 of [Mandel and Wolf, 1995]). It is seen that the scattered field becomes less diffuse as the parameter σ_μ increases. If the coherence length of the incident beam is comparable to or is larger than the radius of the sphere (i.e., when $\sigma_\mu > a$), secondary maxima occur. For $\sigma_\mu = 4a$ the radiant intensity can hardly be distinguished from that generated by an almost spectrally fully coherent beam with $\sigma_\mu = 100a$. The displayed scattering angle θ is restricted to the range $0^\circ \leq \theta \leq 90^\circ$, because for larger values the curves essentially coincide with the horizontal axis. In Fig. 7.3 the results are shown on a logarithmic scale, for the full range of the scattering angle, i.e., $0^\circ \leq \theta \leq 180^\circ$. It is seen that in all cases there is some backscattering, i.e., $J_s(\theta = 180^\circ, \omega) > 0$, with the largest amount occurring when $\sigma_\mu = a/4$.

We can summarize our results by saying that we have studied the effects of spatial coherence of the incident beam on the angular distribution of the field scattered by a small homogeneous sphere; and we found that when the transverse spectral coherence length of the incident beam is smaller than the radius of the scatterer, the radiant intensity is rather diffuse and exhibits no secondary maxima.

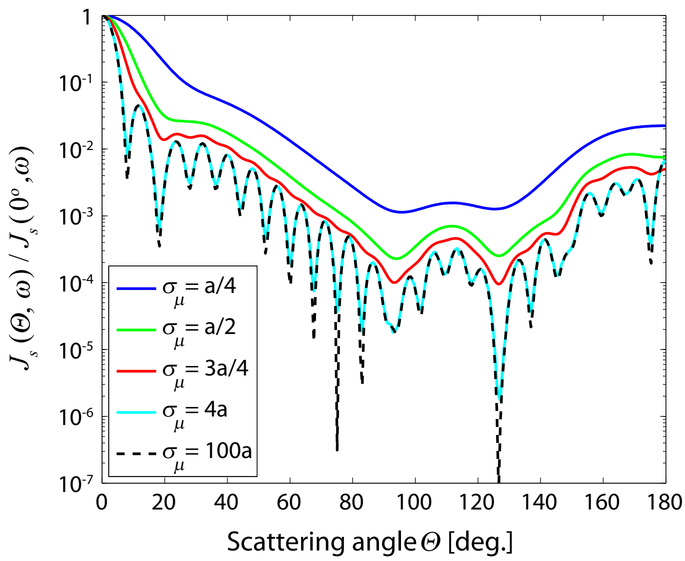

Figure 7.3: (Color on-line) The normalized radiant intensity $J(\theta, \omega)/J_s(0^\circ, \omega)$ of the scattered field for selected values of the transverse spectral coherence length σ_μ, plotted on a logarithmic scale. The sphere radius a has been taken to be 4λ, and the refractive index $n = 1.5$.

Our results may find useful application in, for example, determining scattering effects in the atmosphere and colloidal suspensions.

Bibliography

ANDERSON, M., editor *The Book of the Mirror: An Interdisciplinary Collection exploring the Cultural Story of the Mirror* Cambridge Scholars Publishing, Newcastle (2007).

ANDREWS, L. C. AND PHILLIPS, R. L. *Laser Beam Propagation through Random Media* SPIE Press 2nd edition (2005).

ARFKEN, G. B. AND WEBER, H. J. *Mathematical Methods for Physicists* Hartcourt/Academic Press, San Diego, Calif. 5th edition (2001).

ARLT, J. AND PADGETT, M. J. Generation of a beam with a dark focus surrounded by regions of higher intensity: the optical bottle beam *Opt. Lett.* **25** pp. 191–193 (2000).

BERRY, M. Anticipations of the geometric phase *Physics Today* **43** pp. 34–40 (1990).

BERRY, M. V. Quantal phase-factors accompanying adiabatic changes *Proc. R. Soc. Lond. A* **392** pp. 45–57 (1984).

BERRY, M. V. The adiabatic phase and Pancharatnam phase for polarized light *J. Mod. Opt.* **34** pp. 1401–1407 (1987).

BERRY, M. V. AND DENNIS, M. R. Polarization singularities in isotropic random vector waves *Proc. R. Soc. Lond. A* **457** pp. 141–155 (2001).

BEYER, W. H., editor *CRC Standard Mathematical Tables* CRC Press, Boca Raton 25th edition (1980).

BHANDARI, R. Observation of Dirac singularities with light polarization .1 *Phys. Lett. A* **171** pp. 262–266 (1992a).

BHANDARI, R. Observation of Dirac singularities with light polarization .2 *Phys. Lett. A* **171** pp. 267–270 (1992b).

BHANDARI, R. Polarization of light and topological phases *Phys. Rep.* **281** pp. 2–64 (1997).

BHANDARI, R. AND SAMUEL, J. Observation of topological phase by use of a laser interferometer *Phys. Rev. Lett.* **60** pp. 1211–1213 (1988).

Biener, G., Gorodetski, Y., Niv, A., Kleiner, V., and Hasman, E. Manipulation of polarization-dependent multivortices with quasi-periodic subwavelength structures *Opt. Lett.* **31** pp. 1594–1596 (2006).

Bogatyryova, G. V., Fel'de, C. V., Polyanskii, P. V., Ponomarenko, S. A., Soskin, M. S., and Wolf, E. Partially coherent vortex beams with a separable phase *Opt. Lett.* **28** pp. 878–880 (2003).

Boivin, A., Dow, J., and Wolf, E. Energy flow in the neighborhood of the focus of a coherent beam *J. Opt. Soc. Am.* **57** pp. 1171–1175 (1967).

Bomzon, Z., Biener, G., Kleiner, V., and Hasman, E. Space-variant Pancharatnam-Berry phase optical elements with computer-generated subwavelength gratings *Opt. Lett.* **27** pp. 1141–1143 (2002).

Born, M. and Wolf, E. *Principles of Optics: Electromagnetic Theory of Propagation, Interference and Diffraction of Light* Cambridge University Press, Cambridge 7th edition (1999).

Boyle, R. *The Philosophical Works of the Honourable Robert Boyle Esq* Innys, W. and Manby, R. and Longman, T., London 2nd edition (1738).

Bracewell, R. N. *The Fourier Transform and its Applications* McGraw-Hill electrical and electronic engineering series McGraw-Hill, New York (1965).

Braunbek, W. and Laukien, G. Einzelheiten zur Halbebenen-Beugung *Optik* **9** pp. 174–179 (1952).

Brosseau, C. *Fundamentals of Polarized Light: a Statistical Optics Approach* Wiley, New York, N.Y. (1998).

Brouwer, L. E. J. The mapping of manifold qualities *Math. Ann.* **71** pp. 97–115 (1912).

Cabaret, D., Rossano, S., and Brouder, C. Mie scattering of a partially coherent beam *Opt. Commun.* **150** pp. 239–250 (1998).

Carney, P. S. and Wolf, E. An energy theorem for scattering of partially coherent beams *Opt. Commun.* **155** pp. 1–6 (1998).

Carney, P. S., Wolf, E., and Agarwal, G. S. Statistical generalizations of the optical cross-section theorem with application to inverse scattering *J. Opt. Soc. Am. A* **14** pp. 3366–3371 (1997).

Carter, W. H. Electromagnetic beam fields *Optica Acta* **21** pp. 871–892 (1974).

Chyba, T. H., Wang, L. J., Mandel, L., and Simon, R. Measurement of the Pancharatnam phase for a light-beam *Opt. Lett.* **13** pp. 562–564 (1988).

Dayton, D. C., Browne, S. L., Sandven, S. P., Gonglewski, J. D., and Kudryashov, A. V. Theory and laboratory demonstrations on the use of a nematic liquid-crystal phase modulator for controlled turbulence generation and adaptive optics *Appl. Opt.* **37** pp. 5579–5589 (1998).

Dennis, M. R. Polarization singularities in paraxial vector fields: morphology and statistics *Opt. Commun.* **213** pp. 201–221 (2002).

van Dijk, T., Gbur, G., and Visser, T. D. Shaping the focal intensity distribution using spatial coherence *J. Opt. Soc. Am. A* **25** pp. 575–581 (2008).

van Dijk, T., Schouten, H. F., Ubachs, W., and Visser, T. D. The Pancharatnam-Berry phase for non-cyclic polarization changes *Opt. Express* **18** pp. 10796–10804 (2010a).

van Dijk, T., Schouten, H. F., and Visser, T. D. Geometric interpretation of the Pancharatnam connection and non-cyclic polarization changes *J. Opt. Soc. Am. A* **27** pp. 1972–1976 (2010b).

Einstein, A. Méthode pour la détermination de valeurs statistiques d'observation concernant des grandeurs soumises a des fluctuations irrégulière *Arch. Sci. Phys. et Natur.* **37** pp. 254–256 (1914).

Eriksson, F. On the measure of solid angles *Math. Mag.* **63** pp. 184–187 (1990).

Fischer, D. G. and Visser, T. D. Spatial correlation properties of focused partially coherent light *J. Opt. Soc. Am. A* **21** pp. 2097–2102 (2004).

Flossmann, F., Schwarz, U. T., Maier, M., and Dennis, M. R. Polarization singularities from unfolding an optical vortex through a birefringent crystal *Phys. Rev. Lett.* **95** p. 253901 (2005).

Flossmann, F., Schwarz, U. T., Maier, M., and Dennis, M. R. Stokes parameters in the unfolding of an optical vortex through a birefringent crystal *Opt. Express* **14** pp. 11402–11411 (2006).

Foley, J. T. Effect of an aperture on the spectrum of partially coherent-light *J. Opt. Soc. Am. A* **8** pp. 1099–1105 (1991).

Fresnel, A. *Oeuvres Complètes d'Augustin Fresnel* volume 1 Imprimière Imperiale, Paris (1870).

Freund, I. Polarization singularity indices in Gaussian laser beams *Opt. Commun.* **201** pp. 251–270 (2002).

Freund, I., Mokhun, A. I., Soskin, M. S., Angelsky, O. V., and Mokhun, I. Stokes singularity relations *Opt. Lett.* **27** pp. 545–547 (2002).

Friberg, A. T., Visser, T. D., Wang, W., and Wolf, E. Focal shifts of converging diffracted waves of any state of spatial coherence *Opt. Commun.* **196** pp. 1–7 (2001).

Gahagan, K. T. and Swartzlander, G. A. Simultaneous trapping of low-index and high-index microparticles observed with an optical-vortex trap *J. Opt. Soc. Am. B* **16** pp. 533–537 (1999).

Gbur, G. and Swartzlander, G. A. Complete transverse representation of a correlation singularity of a partially coherent field *J. Opt. Soc. Am. B* **25** pp. 1422–1429 (2008).

Gbur, G. and Tyson, R. K. Vortex beam propagation through atmospheric turbulence and topological charge conservation *J. Opt. Soc. Am. A* **25** pp. 225–230 (2008).

GBUR, G. AND VISSER, T. D. Can spatial coherence effects produce a local minimum of intensity at focus? *Opt. Lett.* **28** pp. 1627–1629 (2003a).

GBUR, G. AND VISSER, T. D. Coherence vortices in partially coherent beams *Opt. Commun.* **222** pp. 117–125 (2003b).

GBUR, G. AND VISSER, T. D. Phase singularities and coherence vortices in linear optical systems *Opt. Commun.* **259** pp. 428–435 (2006).

GBUR, G., VISSER, T. D., AND WOLF, E. 'Hidden' singularities in partially coherent wavefields *J. Opt. A, Pure Appl. Opt.* **6** pp. S239–S242 (2004).

GOODMAN, J. W. *Statistical Optics* Wiley, New York (2000).

GORI, F., GUATTARI, G., AND PADOVANI, C. Modal expansion for j0-correlated Schell-model sources *Opt. Commun.* **64** pp. 311–316 (1987).

GORI, F., PALMA, C., AND SANTARSIERO, M. A scattering experiment with partially coherent-light *Opt. Commun.* **74** pp. 353–356 (1990).

GRANDY JR., W. T. *Scattering of Waves from Large Spheres* Cambridge University Press, Cambridge (1992).

GREFFET, J. J., DE LA CRUZ-GUTIERREZ, M., IGNATOVICH, P. V., AND RADUNSKY, A. Influence of spatial coherence on scattering by a particle *J. Opt. Soc. Am. A* **20** pp. 2315–2320 (2003).

HANNAY, J. H. The Majorana representation of polarization, and the Berry phase of light *J. Mod. Opt.* **45** pp. 1001–1008 (1998).

HARIHARAN, P. The geometric phases in E. Wolf, editor, *Progress in Optics* volume 48 pp. 149–201 Elsevier, Amsterdam (2005).

HOOKE, R. *Micrographia, or, Some Physiological Descriptions of Minute Bodies Made by Magnifying Glasses* Martyn, J. and Allestry, J., London (1665).

VAN DE HULST, H. C. *Light Scattering by Small Particles* Structure of matter series John Wiley, New York, NY (1957).

HUYGHENS, C. *Traité de la Lumière* Gauthier-Villars, Leiden (1690).

JAMES, D. F. V. Change of polarization of light beams on propagation in free space *J. Opt. Soc. Am. A* **11** pp. 1641–1643 (1994).

JANNSON, J., JANNSON, T., AND WOLF, E. Spatial coherence discrimination in scattering *Opt. Lett.* **13** pp. 1060–1062 (1988).

JOACHAIN, C. J. *Quantum Collision Theory* North-Holland Publishing Company, Amsterdam etc. (1975).

JONES, R. C. A new calculus for the treatment of optical systems *J. Opt. Soc. Am.* **31** pp. 488–493 (1941).

JORDAN, T. F. Berry phases for partial cycles *Phys. Rev. A* **38** pp. 1590–1592 (1988).

KHINTCHINE, A. Korrelationstheorie der stationären stochastischen Prozesse *Math. Ann.* **109** pp. 604–615 (1934).

Knorr, W. The geometry of burning-mirrors in antiquity *Isis* **74** pp. 53–73 (1983).

Korotkova, O., Visser, T. D., and Wolf, E. Polarization properties of stochastic electromagnet beams *Opt. Commun.* **281** pp. 515–520 (2008).

Korotkova, O. and Wolf, E. Changes in the state of polarization of a random electromagnetic beam on propagation *Opt. Commun.* **246** pp. 35–43 (2005).

Kuga, T., Torii, Y., Shiokawa, N., Hirano, T., Shimizu, Y., and Sasada, H. Novel optical trap of atoms with a doughnut beam *Phys. Rev. Lett.* **78** pp. 4713–4716 (1997).

Linfoot, E. H. and Wolf, E. Phase distribution near focus in an aberration-free diffraction image *Proc. Phys. Soc. Lond. Sect. B* **69** pp. 823–832 (1956).

Lopez, J. L. and Pagola, P. J. A simplification of the Laplace method for double integrals. Application to the second Appell function *Electronic Transactions on Numerical Analysis* **30** pp. 224–236 (2008).

Lu, B. D., Zhang, B., and Cai, B. W. Focusing of a Gaussian Schell-model beam through a circular lens *J. Mod. Opt.* **42** pp. 289–298 (1995).

Maleev, I. D. and Swartzlander, G. A. Propagation of spatial correlation vortices *J. Opt. Soc. Am. B* **25** pp. 915–922 (2008).

Mandel, L. and Wolf, E. *Optical Coherence and Quantum Optics* Cambridge University Press, Cambridge (1995).

Maxwell, J. C. *A Treatise on Electricity and Magnetism* Clarendon, Oxford (1873).

Mie, G. Articles on the optical characteristics of turbid tubes, especially colloidal metal solutions *Ann. Phys.* **25** pp. 377–445 (1908).

Mokhun, A. I., Soskin, M. S., and Freund, I. Elliptic critical points: C-points, a-lines, and the sign rule *Opt. Lett.* **27** pp. 995–997 (2002).

Nussenzveig, H. M. *Diffraction Effects in Semiclassical Scattering* Montroll memorial lecture series in mathematical physics Cambridge University Press, Cambridge (1992).

Nye, J. F. *Natural Focusing and Fine Structure of Light: Caustics and Wave Dislocations* Institute of Physics Publishing, Bristol (1999).

Nye, J. F. and Berry, M. V. Dislocations in wave trains *Proc. R. Soc. Lond. A* **336** pp. 165–190 (1974).

Nye, J. F., Hajnal, J. V., and Hannay, J. H. Phase saddles and dislocations in two-dimensional waves such as tides *Proc. R. Soc. Lond. A* **417** pp. 7–20 (1988).

Palacios, D. M., Maleev, I. D., Marathay, A. S., and Swartzlander, G. A. Spatial correlation singularity of a vortex field *Phys. Rev. Lett.* **92** p. 143905 (2004).

Pancharatnam, S. Generalized theory of interference, and its applications *Proc. Indian Acad. Sci. A* **44** pp. 247–262 (1956).

Papadimitriou, G. I., Papazoglou, C., and Pomportsis, A. S. *Optical Switching* Wiley, Hoboken (2007).

Ponomarenko, S. A. A class of partially coherent beams carrying optical vortices *J. Opt. Soc. Am. A* **18** pp. 150–156 (2001).

Ponomarenko, S. A. and Wolf, E. The spectral degree of coherence of fully spatially coherent electromagnetic beams *Opt. Commun.* **227** pp. 73–74 (2003).

Raghunathan, S. B., van Dijk, T., Peterman, E. J. G., and Visser, T. D. Experimental demonstration of an intensity minimum at the focus of a laser beam created by spatial coherence: Application to optical trapping of dielectric particles *Opt. Lett.* **35** pp. 4166–4168 (2011).

Rao, L. Z. and Pu, J. X. Spatial correlation properties of focused partially coherent vortex beams *J. Opt. Soc. Am. A* **24** pp. 2242–2247 (2007).

Roslund, C. and Beckman, C. Disputing Viking navigation by polarized skylight *Appl. Opt* **33** pp. 4754–4755 (1994).

Samuel, J. and Bhandari, R. General setting for Berry's phase *Phys. Rev. Lett.* **60** pp. 2339–2342 (1988).

Schmitzer, H., Klein, S., and Dultz, W. Nonlinearity of Pancharatnams topological phase *Phys. Rev. Lett.* **71** pp. 1530–1533 (1993).

Schoonover, R. W. and Visser, T. D. Polarization singularities of focused, radially polarized fields *Opt. Express* **14** pp. 5733–5745 (2006).

Schouten, H. F., Gbur, G., Visser, T. D., and Wolf, E. Phase singularities of the coherence functions in Young's interference pattern *Opt. Lett.* **28** pp. 968–970 (2003a).

Schouten, H. F. and Visser, T. D. The role of correlation functions in the theory of optical wave fields *Am. J. Phys.* **76** pp. 867–871 (2008).

Schouten, H. F., Visser, T. D., Gbur, G., Lenstra, D., and Blok, H. Creation and annihilation of phase singularities near a sub-wavelength slit *Opt. Express* **11** pp. 371–380 (2003b).

Schouten, H. F., Visser, T. D., Gbur, G., Lenstra, D., and Blok, H. Connection between phase singularities and the radiation pattern of a slit in a metal plate *Phys. Rev. Lett.* **93** p. 173901 (2004).

Shapere, A. and Wilczek, F. *Geometric Phases in Physics* Advanced series in mathematical physics World Scientific, Singapore (1989).

Siegman, A. E. *Lasers* University Science Books (1986).

Sines, G. and Sakellarakis, Y. A. Lenses in antiquity *AJA* **91** pp. 191–196 (1987).

SOSKIN, M. S., DENISENKO, V., AND FREUND, I. Optical polarization singularities and elliptic stationary points *Opt. Lett.* **28** pp. 1475–1477 (2003).

SOSKIN, M. S. AND VASNETSOV, M. V. Singular optics in E. Wolf, editor, *Progress in Optics* volume 42 pp. 219–276 North Holland, Amsterdam (2001).

STOKES, G. G. On the composition and resolution of streams of polarized light from different sources *Trans. Cambr. Phil. Soc.* **9** pp. 399–416 (1852).

SWARTZLANDER, G. A. AND SCHMIT, J. Temporal correlation vortices and topological dispersion *Phys. Rev. Lett.* **93** p. 093901 (2004).

VERDET, E. Étude sur la constitution de la lumière non polarisée et de la lumière partiellement polarisée *Ann. Sci. Ecole. Norm. Supér.* **2** pp. 291–316 (1865).

VISSER, T. D., FISCHER, D. G., AND WOLF, E. Scattering of light from quasi-homogeneous sources by quasi-homogeneous media *J. Opt. Soc. Am. A* **23** pp. 1631–1638 (2006).

VISSER, T. D., GBUR, G., AND WOLF, E. Effect of the state of coherence on the three-dimensional spectral intensity distribution near focus *Opt. Commun.* **213** pp. 13–19 (2002).

VISSER, T. D. AND SCHOONOVER, R. W. A cascade of singular field patterns in Young's interference experiment *Opt. Commun.* **281** pp. 1–6 (2008).

WAGH, A. G. AND RAKHECHA, V. C. On measuring the Pancharatnam phase. I. Interferometry *Phys. Lett. A* **197** pp. 107–111 (1995).

WANG, L. AND LU, B. Propagation and focal shift of J(0)-correlated Schell-model beams *Optik* **117** pp. 167–172 (2006).

WANG, W., DUAN, Z. H., HANSON, S. G., MIYAMOTO, Y., AND TAKEDA, M. Experimental study of coherence vortices: Local properties of phase singularities in a spatial coherence function *Phys. Rev. Lett.* **96** p. 073902 (2006).

WANG, W. J., FRIBERG, A. T., AND WOLF, E. Focusing of partially coherent light in systems of large Fresnel numbers *J. Opt. Soc. Am. A* **14** pp. 491–496 (1997).

WANG, Z. L., DAI, M., AND YIN, J. P. Atomic (or molecular) guiding using a blue-detuned doughnut mode in a hollow metallic waveguide *Opt. Express* **13** pp. 8406–8423 (2005).

WIENER, N. Generalized harmonic analyses *Acta Math.* **55** pp. 117–258 (1930).

WOLF, E. Optics in terms of observable quantities *Nuovo Cimento* **XII** pp. 884–888 (1954).

WOLF, E. A macroscopic theory of interference and diffraction of light from finite sources. II. Fields with a spectral range of arbitrary width *Proc. R. Soc. Lond. A* **230** pp. 246–265 (1955).

WOLF, E. New theory of partial coherence in the space-frequency domain. I. Spectra and cross spectra of steady-state sources *J. Opt. Soc. Am.* **72** pp. 343–351 (1982).

WOLF, E. Correlation-induced changes in the degree of polarization, the degree of coherence, and the spectrum of random electromagnetic beams on propagation *Opt. Lett.* **28** pp. 1078–1080 (2003a).

WOLF, E. Unified theory of coherence and polarization of random electromagnetic beams *Phys. Lett. A* **312** pp. 263–267 (2003b).

WOLF, E. *Introduction to the Theory of Coherence and Polarization of Light* Cambridge University Press, Cambridge (2007).

WOLF, E. AND JAMES, D. F. V. Correlation-induced spectral changes *Rep. Prog. Phys.* **59** pp. 771–818 (1996).

WONG, R. *Asymptotic Approximations of Integrals* SIAM, Philadelphia (2001).

YIN, J. P., GAO, W. J., AND ZHU, Y. F. Generation of dark hollow beams and their applications in E. Wolf, editor, *Progress in Optics* volume 45 pp. 119–204 North Holland (2003).

YOUNG, T. The Bakerian lecture: On the theory of light and colours *Phil. Trans. R. Soc. Lond.* **92** pp. 12–48 (1802).

YOUNG, T. *A Course of Lectures on Natural Philosophy and the Mechanical Arts* J. Johnson, London (1807).

ZERNIKE, F. The concept of degree of coherence and its application to optical problems *Physica* **5** pp. 785–795 (1938).

Samenvatting

De Nederlandse titel van dit proefschrift luidt: "Experimentele en theoretische studies in optische coherentie." Optische coherentie theorie is de statistische beschrijving van licht. Doordat de toestand van een lichtbron of die van een medium nooit volledig bekend is moet het systeem beschreven worden met een reeks van correlatiefuncties. Deze beschrijven in welke mate het licht op twee verschillende punten statistisch gezien overeenkomt. Als het licht volledig coherent is dan zijn de velden volledig 'in harmonie' met elkaar. Als de velden volledig ongecorreleerd zijn, dan is er geen relatie tussen de velden. Het licht is dan incoherent. Tussen deze twee extremen in wordt licht partieel coherent genoemd. Uit de correlatiefuncties volgen de eigenschappen van licht, zoals bijvoorbeeld het spectrum, waarin we geïnteresseerd zijn. Net als lichtvelden zelf voldoen deze correlaties aan precies gedefinieerde propagatiewetten. Belangrijk om op te merken is dat de correlatiefuncties in het algemeen zullen veranderen tijdens propagatie, ook bij propagatie door vacuüm. Hieruit volgt dat in principe ook alle eigenschappen van licht, zoals het spectrum en zoals we straks zullen zien ook de polarisatie, veranderen. Voor het beschrijven van polarisatie-eigenschappen is het nodig om naar correlaties van verschillende componenten van het elektromagnetische veld te kijken op één punt, in plaats van naar correlaties van het veld op twee punten. Alle onderwerpen die worden besproken in dit proefschrift kunnen beschreven worden met het formalisme van de optische coherentie theorie, de geünificeerde theorie van coherentie en polarisatie.

In het tweede hoofdstuk wordt onderzocht wat de invloed is van de mate van coherentie op het focuseren van licht. De intensiteitsverdeling in de buurt van het brandpunt is in kaart gebracht als functie van de coherentielengte. In het bijzonder worden zogenaamde Bessel-gecorreleerde velden onderzocht. In voorafgaande studies wordt vrijwel altijd aangenomen dat het verlagen van de coherentielengte leidt tot het uitsmeren van de intensiteit. In dit hoofdstuk wordt theoretisch aangetoond dat de effecten veel subtieler kunnen zijn. In het geval van een Bessel-gecorreleerd veld is het mogelijk om een minimum te creëren op de plaats van het brandpunt. Het is zelfs mogelijk om op een continue wijze de intensiteit te veranderen van een maximum naar een minimum door eenvoudig de coherentielengte te veranderen. Deze voorspelling is ondertussen experimenteel bevestigd. De behaalde resultaten kunnen mogelijk toepassing krijgen in het optisch vastpakken en manipuleren van deeltjes.

Het onderwerp van het derde hoofdstuk is singuliere optica, in het bijzonder wordt de relatie tussen coherentiesingulariteiten en fasesingulariteiten onderzocht. Fasesingulariteiten zijn punten in de ruimte waar de amplitude van het veld nul is, daardoor is de fase van het veld ongedefinieerd of 'singulier'. Als twee punten in een veld volledig ongecorreleerd zijn, dan is de fase van de correlatiefunctie singulier. Als het licht van deze twee punten wordt gecombineerd in een zogenaamd twee spleten experiment zal er geen interferentiepatroon zichtbaar zijn. Men spreekt dan van een correlatiesingulariteit. Gekeken wordt hoe deze singuliere punten zich ontwikkelen als een bundel propageert. De bundel die onderzocht wordt is een partieel-coherente vortex bundel. Deze begint met een fasesingulariteit die onmiddellijk verdwijnt als de bundel zich voortplant en tegelijkertijd ontstaat er een correlatiesingulariteit. Als de observatiehoek in het verre veld wordt vergroot ontvouwt deze singulariteit zich in een doublet, met andere woorden; er ontstaan twee paren van singuliere punten.

Coherentiesingulariteiten zijn ook het onderwerp van het vierde hoofdstuk. De topologie van een brede klasse partieel coherente velden wordt geanalyseerd. Voor rotatie-symmetrische quasi-homogene bronnen vormen de coherentiesingulariteiten een twee-dimensionaal oppervlak. Dit wordt geïllustreerd met een partieel-coherente vortex bundel. In dit geval vormen de doorsnedes van het oppervlak van de singulariteiten kegelsneden, namelijk ellipsen, rechte lijnen en hyperbolen.

In het vijfde hoofdstuk wordt een nieuwe opstelling beschreven om de geometrische fase te meten die gerelateerd is aan polarisatieveranderingen in een monochromatische bundel. De polarisatietoestand wordt veranderd door het verdraaien van optische elementen zoals lineaire polarizatoren en kwart-golflengte platen. Eerst wordt theoretisch beschreven wat de faseverandering is die een bundel uiteindelijk oploopt na de reis door een aantal optische elementen. Het gedrag dat hieruit volgt blijkt op verschillende manieren van de experimentele parameters te kunnen afhangen, namelijk op een lineaire, niet-lineaire en singuliere wijze. Deze voorspelling zijn experimenteel geverifieerd, en de resultaten van het experiment worden gepresenteerd in het laatste deel van hoofdstuk vijf.

Geometrische fases zijn ook het onderwerp van hoofdstuk zes. De polarisatietoestand van licht kan gevisualiseerd worden als een punt op de zogenaamde Poincaré bol. Als een reeks opeenvolgende polarisatieveranderingen ervoor zorgen dat de polarisatietoestand een gesloten pad beschrijft op deze bol, dan is de bijbehorende geometrische fase gerelateerd aan het omsloten oppervlak. Dit is een beroemd resultaat van Pancharatnam. Deze geometrische fase is naar hem vernoemd. Aangetoond wordt dat er voor een niet-gesloten pad ook een geometrische interpretatie bestaat. Dit maakt het mogelijk om op een nieuwe en meer intuïtieve manier de geometrische fase te bepalen die de bundel oploopt bij een niet-gesloten pad.

Als licht op een deeltje botst kan het van richting veranderen. Zo wordt licht in de atmosfeer bijvoorbeeld verstrooid aan luchtmoleculen. Hierdoor krijgt de lucht zijn blauwe kleur. Dit proces is voor het eerst beschreven door Lord Rayleigh.

Zijn beschrijving is alleen geldig als de deeltjes veel kleiner zijn dan de golflengte. Voor grotere bolletjes is het nodig om een lastigere, maar exacte oplossing te gebruiken. De zogenaamde Mie theorie is een analytische oplossing van de Maxwell vergelijkingen voor het verstrooien van licht aan bolletjes met een willekeurige grootte. Impliciet wordt in deze beschrijving aangenomen dat het inkomende veld ruimtelijk volledig coherent is. Dit is echter in het algemeen niet het geval. In hoofdstuk zeven wordt de Mie theorie gegeneraliseerd voor partieel coherente velden. De invloed van de mate van coherentie op de intensiteitsverdeling van het verstrooide licht wordt onderzocht. Het blijkt dat de correlatielengte van groot belang is zo gauw deze vergelijkbaar is met of kleiner is dan de grootte van het bolletje.

List of publications

- *Shaping the focal intensity distribution using spatial coherence*,
  T. van Dijk, G. Gbur and T.D. Visser,
  J. Opt. Soc. Am. A **25**, 575 (2008).
- *Evolution of singularities in a partially coherent vortex beam*,
  T. van Dijk and T.D. Visser,
  J. Opt. Soc. Am. A **26**, 741 (2009).
- *Coherence singularities in the far field generated by partially coherent sources*,
  T. van Dijk, H.F. Schouten and T.D. Visser,
  Phys. Rev. A **79**, 033805 (2009).
- *The Pancharatnam-Berry phase for non-cyclic polarization changes*,
  T. van Dijk, H.F. Schouten, W. Ubachs and T.D. Visser,
  Opt. Express, **18**, 10796 (2010).
- *Geometric interpretation of the Pancharatnam connection and non-cyclic polarization changes*,
  T. van Dijk, H.F. Schouten and T.D. Visser
  J. Opt. Soc. Am. A **27**, 1972 (2010).
- *Effects of spatial coherence on the angular distribution of radiant intensity generated by scattering on a sphere*,
  T. van Dijk, D.G. Fischer, T.D. Visser and E. Wolf,
  Phys. Rev. Lett. **104**, 173902 (2010).
- *Experimental demonstration of an intensity minimum at the focus of a laser beam created by spatial coherence: Application to optical trapping of dielectric particles*,
  S.B. Raghunathan, T. van Dijk, E.J.G. Peterman and T.D. Visser,
  Optics Letters, **35**, 4166 (2010).
- *Coherence effects in Mie scattering*,
  D.G. Fischer, T. van Dijk, T.D. Visser and E. Wolf,
  to be submitted.

- *Inverse scattering with random media*,
  D.G. Fischer, T. van Dijk and P.S. Carney,
  to be submitted.

Dankwoord

Graag zou ik allereerst mijn promoter Taco Visser willen bedanken voor zijn enthousiaste begeleiding. Ik ben je erg dankbaar dat je me tijdens conferenties in contact hebt gebracht met verschillende wetenschappers met wie we vervolgens ook nog gezellig gingen eten. Conferenties en andere buitenlandse reisjes waren daardoor altijd niet alleen interessant maar ook heel leuk. Daarnaast ben ik blij met de intensieve samenwerking en de tijd die je altijd had voor het voeren van discussies. Daarnaast gaat mijn dank natuurlijk ook uit naar mijn promoter Wim Ubachs, voor de geboden ondersteuning en enthousiasme. Het was erg interessant om ook de kans te krijgen ervaring op te doen in experimenteel onderzoek.

Uiteraard wil ik ook alle leden van de leescommissie, Han Woerdman, Kobus Kuipers, Johannes de Boer, Fred Mackintosh en Hugo Schouten, hartelijk bedanken voor de tijd en moeite die zij gestoken hebben in het lezen van mijn proefschrift.

Verder wil ik graag Mathieu Blom, Wilco den Dunnen, Thijs Stegeman, Jorn Boomsma, Erik Wessels en Tomas Jezo bedanken voor de gezelligheid binnen en buiten de VU. Jorn het waren gezellige jaren en ik ben blij dat je er altijd was. Ik denk dat we veel aan elkaar gehad hebben en ben je ook erg dankbaar voor de ontelbare keren dat je me heb bijgestaan met computerproblemen. Thijs en Wilco wil ik in het bijzonder nog bedanken voor de goede sfeer op onze gedeelde kamer. Dat was een van de belangrijkste ingrediënten voor een succesvolle promotieperiode. Ik wil ook nog Shreyas Raghunathan bedanken met wie ik het afgelopen jaar intensief heb samengewerkt met als resultaat een mooie publicatie en hopelijk binnenkort nog eentje.

Verder zijn er natuurlijk nog veel meer collega's die hebben bijgedragen aan een goede sfeer: Klaas Allaart, Piet Mulders, Elmar Biernat, Chase Broedersz, Kirk Green, Cedran Bomhof, Paul McCullough, Christian Pisano en Marja Herronen.

Tot slot wil ik mijn ouders bedanken voor hun onvoorwaardelijke steun waarop ik altijd heb kunnen rekenen.

Maar natuurlijk ben ik vooral Laura dankbaar.